HOST CELLULAR CHOLESTEROL DISTRIBUTION AND DYNAMICS DURING ENTEROVIRAL INFECTION

by

MARIANITA SANTIANA

A Dissertation submitted to the

Graduate School-Newark

Rutgers, The State University of New Jersey

in partial fulfillment of the requirements

for the degree of

Doctor of Philosophy

Graduate Program in Biological Sciences

written under the direction of

Nihal Altan-Bonnet, Ph.D.

and approved by

_____

_____

_____

_____

_____

Newark, New Jersey

May 2015

©[2015]

Marianita Santiana

ALL RIGHTS RESERVED

ABSTRACT OF THE DISSERTATION

HOST CELLULAR CHOLESTEROL DISTRIBUTION AND DYNAMICS DURING ENTEROVIRAL INFECTION

By MARIANITA SANTIANA

Dissertation Director:
Nihal Altan-Bonnet, Ph.D.

Many RNA viruses, including enteroviruses, remodel host ER membranes to form platforms with unique lipid components to assemble replication complexes and synthesize new viral RNA. Cholesterol is a critical component of cellular membranes regulating fluidity and being indispensable for proper assembly and function of membrane based protein-lipid complexes. Here we show that enteroviruses harness the clathrin mediated endocytosis (CME) pathway to transfer free cholesterol from the plasma membrane to the viral replication organelles (VROs). We show that cholesterol is responsible for regulating viral protein processing and facilitates viral RNA synthesis, and disrupting CME causes cellular cholesterol pools to be stored in lipid droplets obstructing the transfer to VROs and inhibiting viral replication. In contrast, we found that the presence of excess intracellular cholesterol, as in cells lacking caveolins or those from patients with Niemann-Pick disease, stimulates viral replication. We demonstrate that, the redistribution of free cellular cholesterol and the cellular recycle dynamics are affected during infection. The CME rate of

uptake does not change during the initial 2 hours of infection while the rate of cellular endosomal recycling is inhibited resulting in a net decrease of free cholesterol at the plasma membrane, and facilitating the access and active transfer of cholesterol from enriched internal cellular compartments to VROs. Our findings indicate that cholesterol is critical for enteroviral replication and that CME has an important role in the enteroviral life cycle and in the host cellular cholesterol homeostasis.

ACKNOWLEDGEMENTS

Culmination of this project is the greatest achievement of my life and my dream come true. But it was only possible with the help of amazing people that have continuously supported me along the way.

First, I want to thank my advisor, Dr. Nihal Altan-Bonnet, for guiding me and sharing her knowledge and love of science. I have learned from her that I should always work hard to achieve the best, to value my self for who I am, to be proud and confident of myself and of my work, and to always stand strong.

Next, I want to thank the members of my committee Dr. Nan Gao, Dr. Tracy Tran, and Dr. Julie Donaldson for their time and valuable advice to complete this work.

To Dr. Ann Cali, there are no words to express my gratitude for all the support that I have received from her over the years. I would not be here if it was not for her, she helped me make the best decision in my life, to stay in school and to first give it try before I say no. So I gave it try and here I am! Thank you so much Dr. Cali, you are my guardian angel!

A special thanks to Dr. Olha Ilnitska who patiently taught me many of the experimental techniques we used in this project; and with whom I worked side by side for endless hours and supported each other in the ups and downs of this project. Also to my friends and lab mates Nai-Yun, Yin-Han, Wen-Li, and Marne your help has been invaluable in completing this work.

To Cyrilla Pau, thank you for teaching me and helping me in the lab. And thank you for being my friend; you will always be in my heart!

To Dr. Takvorian, and the labs of Dr. Kim, Dr. Friedman, Dr. Tamas Balla, Dr. Lois Greene and many others who collaborated with advice, reagents, and equipment to complete some of the experiments in this work.

Finally, I want to dedicate this work to my family: Danny Espinosa, my beloved husband, his love and support has always kept me going during this work. Thank you for being there for me. My children, Steven and Oscar, thank you for the time I took away from you and for your unconditional love. To my Mother, my role model, Marianita Pazmiño, thank you for loving me, believing in me, and for teaching me what love and responsibility really are with actions and not only with words; I saw you sacrificing your life to bring up 3 girls all on your own with love, you worked endless days to keep us well fed, with shelter over our heads, and with a good education, you are the greatest mother of all! Le adoro Mamita linda! To my Father, Raul Santiana, thank you for your love and daily blessings. To my sisters, Monica and Marisol, thank you for your love and support. Finally to my brothers in law Manuel and Houdinis, to my nieces Emily and Maia, and nephews Eddy, Alex, Keven, Sebis, and Alejito thank you for cheering me up with your happiness and good humor.

TABLE OF CONTENTS

Title page..... **i**

Abstract of the Dissertation..... **ii**

Acknowledgments..... **iv**

Table of Contents..... **vi**

List of Illustrations..... **ix**

List of Tables..... **xi**

List of Abbreviations..... **xii**

Chapter 1: Background and Project Introduction..... **1**
Background..... **1**
Enterovirus Classification..... **1**
Human Enterovirus and Disease..... **2**
Enteroviral Life Cycle..... **3**
Coxsackievirus and Poliovirus Selected "Model System"... **4**
Viral Genome Structure **5**
Processing and Viral Protein Function..... **6**
Viral Replication Mechanism..... **8**
Host Secretory Pathway..... **11**
Host Endocytosis..... **12**
Host Recycling..... **15**
Thesis Project Introduction..... **16**

Chapter 2: Materials and Methods..... **18**
Plasmids and Antibodies..... **18**
Chemicals and Reagents..... **19**
Cell Culture and Virus Propagation..... **20**
Cell Viability Quantification..... **21**
Imaging and Analysis..... **21**
Lipid Assays..... **24**
AM4-65 Uptake..... **27**
siRNA Transfection..... **27**
Replicon Assays..... **28**
Drug Treatments and Analysis..... **29**
Western-Blot Analysis **30**
Immunoprecipitation **30**
Rab11A Mutant Constructs..... **31**

Chapter 3: Cholesterol is Part of the Viral Replication Organelles……. **32**
Results…….. **32**
Cholesterol Localizes to Viral Replication Organelles……. **32**
Viral Replication Organelles have Cholesterol Domains… **33**
Conclusion…… **35**

Chapter 4: Free Cholesterol is Necessary for Viral Replication and Viral Protein Processing……. **39**
Results…….. **39**
Cholesterol Removal from Viral Replication Organelles Inhibits Replication…… **39**
High Levels of Cholesterol Stimulates Viral Replication..... **41**
Cholesterol is Critical in Viral Protein Processing…… **42**
Conclusion……... **43**

Chapter 5: Cellular Cholesterol Homeostasis and Dynamics of Plasma Membrane Free Cholesterol Redistribution……..... **52**
Results…….. **52**
Free Cholesterol Levels Increase During Viral Infection…. **52**
Plasma Membrane Cholesterol is Redistributed During Infection by Viral Protein 2BC……..... **53**
Conclusion……... **55**

Chapter 6: The Endocytic Machinery is Required for Cellular Cholesterol Homeostasis and Viral Replication……. **61**
Results…….. **61**
Endocytic Machinery Regulates Viral replication……. **61**
Depletion of Clathrin Mediated Endocytosis, Endosomal Machinery, and Clathrin Independent Endocytosis Proteins Modify Host Cellular Free Cholesterol Pools…….. **62**
Conclusion…… **65**

Chapter 7: CME Uptake and Endosomal Recycling Pathway Dynamics are Essential for Cholesterol Redistribution to Viral Replication Organelles and Viral Replication……. **80**
Results……..... **80**
Clathrin Mediated Endocytosis is Associated with Free Cholesterol uptake and Redistribution to Viral Replication Organelles……. **80**
Uptake Kinetics of Clathrin Mediated Endocytosis is Unaffected During Viral Replication…… **82**
Endosomal Recycling is Inhibited During Viral Infection…. **84**

Viral Protein 3A Recruits and Targets Free Cholesterol-Rich Rab11 Recycling Endosomes to Viral Replication Organelles…….. **86**
Conclusion……... **88**

Chapter 8: Discussion and Future Aims……. **103**
Discussion……..... **103**
Future Aims…….. **108**
Bibliography……..... **115**

Curriculum Vitae…….. **124**

LIST OF ILLUSTRATIONS

Figures		Page
1	Coxsackievirus and Poliovirus Genome Organization……..	6
2	Enteroviral Replication Organelles are Enriched in Cholesterol and PI4P Lipids……..	36
3	Cholesterol Removal from Viral Replication Organelles Inhibits Replication……..	44
4	High Levels of Cholesterol Stimulates Viral Replication……..	47
5	Cholesterol is Critical in Viral Protein Processing…….....	50
6	Free Cholesterol Levels Increase During Viral Infection……..	56
7	Free Plasma Membrane Cholesterol is Redistributed During Infection by Viral Protein 2BC……..	58
8	Endocytic Machinery Regulates Viral Replication ……	66
9	Endocytic Machinery Regulates Viral Replication Organelle Biogenesis……	68
10	Caveolin Depletion Stimulates Viral Replication……	70
11	Depletion of CME, Endosomal Machinery, and CIE Proteins Modify Host Cellular Free Cholesterol Pools Toward Esterification...	74
12	Depletion of Caveolin Proteins Modify Host Cellular Free Cholesterol Toward Enrichment of Internal Pools……	78
13	Clathrin Mediated Endocytosis is Associated with Free Cholesterol Uptake and Redistribution to Viral Replication Organelles……..	90

14 Uptake kinetics of Clathrin Mediated Endocytosis is Unaffected During Viral replication……... **94**

15 Endosomal Recycling is Inhibited During Viral Infection…….. **96**

16 Free cholesterol Colocalizes with Rab11 Recycling Endosomes During Viral Infection…….. **99**

17 Viral Protein 3A Recruits and Targets Free Cholesterol-Rich Rab11 Recycling Endosomes to Viral Replication Organelles……. **101**

18 Model for Cholesterol Redistribution and Dynamics During Enteroviral Infection…… **111**

19 Mutant Rab11 Constructs…….. **113**

LIST OF TABLES

Table		Page
1	Cell Viability Assays for siRNA Treatment Experiments…….....	**72**

LIST OF ABBREVIATIONS

ACAT	Acyl CoA Cholesterol Acyltransferase
AD	Alzheimer's Disease
ADP	Adenosine Diphosphate
ADRP	Adipose Differentiation Related Protein
AP2	Adaptor Protein 2
APP	Amyloid Precursor Protein
Arf	ADP-Ribosylation Factor
ATP	Adenosine Triphosphate
CAR	Coxsackie and Adenovirus Receptor
Cav	Caveolin
CCM	Complete Culture Media
CCP	Clathrin Coated Pits
CCV	Clathrin Coated Vesicles
CDC	Centers for Disease Control
CG	CLIC/GEEC
CI	Clathrin Independent
CICM	Complete Imaging Culture Media
CIE	Clathrin Independent Endocytosis
CLIC	Clathrin Independent Carriers
CME	Clathrin Mediated Endocytosis
CNS	Central Nervous System
COPI	Coat Protein I
COPII	Coat Protein II
CRE	*Cis*-Replicating Element
CRSH	Clathrin RFP Stable Hela
CV	Coxsackievirus
CVB	Coxsackievirus type B
DAB2	Disabled 2
DD-CIE	Dynamin Dependent CIE
DM	Double Mutant
DNA	Deoxyribonucleic Acid
-ssDNA	Negative Single Stranded DNA
+ssDNA	Positive Single Stranded DNA
dsDNA	Double Strand DNA
ECV	Echovirus
EGF	Epidermal Growth Factor
eIF4F	Eukaryotic Initiation Factor 4F
ER	Endoplasmic Reticulum
ERGIC	ER-Golgi Intermediate Compartment
EV	Enterovirus
FAPP	Four Phosphate Adaptor Protein
GAP	GTPase Activating Protein
GBF1	Golgi Specific Brefeldin A Resistant Factor 1

GDP	Guanosine Diphosphate
GEEC	GPI-AP Enriched Early Endosomal Compartment
GEF	Guanine Nucleotide Exchange Factor
GFP	Green Fluorescent Protein
GPI-AP	Glycosylphosphatidylinositol Anchored Protein Aminopeptidase-P
GTP	Guanosine Triphosphate
HD	Huntington Disease
HEPA	Hepatitis A virus
HEPES	4-(2-hydroxyethyl)-1-piperazineethanesulfonic acid
HIP1	Huntington Interacting Protein 1
HMG-CoA	3-hydroxy-3-methylglutaryl-coenzyme A
hTfnR	Human Transferrin Receptor
hTfnR-phl	Human Transferrin Receptor pH Luorin
ICTV	International Committee on Taxonomy of Virus
IL	Interleukin
IRES	Internal Ribosome Recognition Site
kDa	Kilo Dalton
LDL	Low Density Lipoprotein
MβCD	Methyl Beta Cyclodextrin
MHC1	Major Histocompatibility Complex 1
MOI	Multiplicity of Infection
NPC	Niemann Pick type C
NPC1-L1	NPC1 Like 1
ORF	Open Reading Frame
ORP	OSBP Related Protein
OSBP	Oxysterol Binding Protein
PABP1	Poly A Binding Protein 1
PCBP2	Poly (rC) Binding Protein 2
PH	Plekstrin Homology
PI4KIIIα	Phosphatidylinositol 4 Kinase type IIIα
PI4KIIIβ	Phosphatidylinositol 4 Kinase type IIIβ
PI4P	Phosphatidylinositol 4 Phosphate
PM	Plasma Membrane
pol	Polymerase
pro	Protease
PV	Poliovirus
PVR	Poliovirus Receptor
RdRp	RNA Dependent RNA Polymerase
RF	Replicative Form
RFP	Red Fluorescent Protein
RI	Replicative Intermediate
RNA	Ribonucleic Acid
-ssRNA	Negative Single Stranded RNA
+ssRNA	Positive Single Stranded RNA

dsRNA	Double Strand RNA
mRNA	Messenger RNA
siRNA	Small Interfering RNA
RV	Rhinovirus
SEM	Standard Error of the Mean
SIM	Structured Illumination Microscopy
SM	Single Mutant
SREBP	Sterol Regulatory Element Binding Protein
TfnR	Transferrin Receptor
TGN	Trans Golgi Network
TIRF	Total Internal Reflection Fluorescence
UTR	Untranslated Region
UV	Ultra Violet
VRO	Viral Replication Organelle
WHO	World Health Organization
WT	Wild Type
YFP	Yellow Fluorescent Protein

CHAPTER 1

BACKGROUND AND INTRODUCTION

Enterovirus Classification

Viruses are small obligate intracellular infectious agents. Viruses can infect cells of almost all life forms from humans and plants to bacteria. The most widely adopted animal virus classification system is based on the genome composition and structure, and taxonomic rank. According to the 8th report of the International Committee on Taxonomy of Virus (ICTV), there are seven groups of viruses: Double-stranded DNA viruses (dsDNA), Double-stranded RNA viruses (dsRNA), Positive sense single-stranded DNA (+ssDNA) viruses, Negative sense single-stranded DNA (-ssDNA) viruses, Positive sense single-stranded RNA (+ssRNA) viruses, Negative sense single-stranded RNA (-ssRNA) viruses, Reverse transcribing dsDNA viruses, and Reverse transcribing +ssRNA viruses.

The generally known enteroviruses are a group of +ssRNA viruses that belong to the Family *Picornaviridae.* Among viruses in this group, are the human infecting viruses such as *Poliovirus* (PV), *Coxsackievirus* (CV), *Echovirus* (ECV), *Enterovirus* (EV), *Hepatitis A virus* (HEPA), and *Rhinovirus* (RV). The Genus *Enterovirus* is divided into 5 species groups that infect humans: *Human enterovirus A* (with 11 CV-A and 2 ENV serotypes), *Human enterovirus B* (with 1 CV-A, 6 CV-B, 6 ENV, and 28 ECV serotypes)*, Human enterovirus C* (with 9 CV-A serotypes)*, Human enterovirus D* (with 2 ENV serotypes), and *Poliovirus* (with 3 serotypes) and all share the following characteristics. The infective virion

measures ~30nm in diameter and has an icosahedron shape. It is composed of a capsid (or protein coat) surrounding a core of +ssRNA. The capsid is made of identical units (protomers) composed of 1 internal and 3 surface proteins. The core houses a single molecule of +ssRNA, measuring 7-8.8 kb in size (Fauquet, et al. 2005; Holland, et al 1960).

Human Enterovirus and Disease

Enteroviruses are one of the most common human infecting viruses. This group of viruses has been estimated to infect 50 million people in the United States and more than a billion around the world (Palacios and Oberste, 2005). Enteroviruses can cause a wide range of diseases from mild skin rashes and the common cold to severe degenerative diseases of the central nervous system (CNS) and heart muscle to even death of the patient (Jubelt and Lipton 2014). These viruses are primarily transmitted via the fecal-oral, fomite, or respiratory tract routes and are associated with poor sanitary conditions and tropical environments (CDC 2015). These viruses can infect any member of the population but infants, children, and teenagers are more susceptible since they do not have immunity from prior illness (CDC, Overview, 2015).

The most well known virus in this group is Poliovirus responsible for causing Poliomyelitis (Polio). Poliomyelitis is a highly infectious degenerative disease of the CNS leading to paralysis or even death if breathing muscles are affected (WHO website). Since the establishment of the effort to eradicate Polio in 1988, more than 99% of cases were reduced, when over 350,000 cases were reported from more than 125 countries. By 2014 only 416 cases were reported

and only 3 countries remain polio endemic (Afghanistan, Nigeria, and Pakistan) (Wassilak et al., 2014; Palacios and Oberste 2005). In 2007, the Center for Disease Control (CDC) reported that Coxsackievirus B1, another member of these group of viruses, has been responsible for over 25% of the enteroviral infections reported that year in the United States; causing severe neonatal diseases such as encephalomyocarditis (inflammation of the heart muscle and brain) (CDC 2008 report; Tebruegge, et al. 2009). A very recent outbreak of Enterovirus D68 (EV-D68) started in August 2014, and until January 2015 a total of 1153 cases from 49 states have been reported to the CDC. The majority of reported cases were from respiratory illnesses in children and 14 fatalities (CDC, Enterovirus D68, 2015).

Enteroviral Life Cycle

The enteroviral life cycle starts with receptor mediated (depending on the type of virus, for example for CV is the coxsackie and adenovirus receptor) viral uptake into the host cell. The primary site of infection is the epithelial cells of the respiratory or gastrointestinal tract (Bopegamage et al. 2005; Iwasaki et al. 2002). Inside the host cell, the virion looses its coat and the viral +ssRNA is released into the cytoplasm, through an unidentified mechanism. The released +ssRNA attaches to the host ribosomes, with the aid of an internal ribosome recognition site (IRES) encoded into the 5' untranslated region (UTR) of the viral genome, to initiate translation of a single ~250 kDa polyprotein. The new viral polyprotein is autocatalytically processed in *cis* and *trans* during and after translation. The resulting proteins are responsible for making the host cell environment suitable

for viral RNA replication with minimal interference from host components. The viral nonstructural proteins assemble the viral replication complex where the +ssRNAs docks and serves as a template to make complementary -ssRNA. The -ssRNA strand now serves as the template to synthesize new +ssRNA that can be part of one of three processes either be part of the replication cycle, be translated into new viral proteins, or be packaged by the structural proteins into new infective virions to be released into the extracellular environment (Whitton, et al. 2005).

Coxsackievirus and Poliovirus Selected Model System

Apart from its importance as human pathogens of great medical and economic concern, the selection of CV and PV as my model system was mainly due to the wide range of tools available to facilitate experimentation such as antibodies and fluorescently tagged constructs. Additionally, these viruses have been characterized for causing acute viral infections, meaning that the entire life cycle is short, it takes place within 8-10 hours with a peak replication time of 4 hours post infection. Another important reason for selecting these viruses is that their genomes are well characterized providing a wealth of useful information. In this project, most of the experiments are performed using CV and PV but also EV and RV when necessary to provide experimental evidence for results that apply not only to CV and PV.

Viral Genome Structure

The genome structure of CV and PV is identical. The +ssRNA is made up of ~7440 nucleotides (nt) organized as follows: a long 5'UTR of ~742nt, a single open reading frame (ORF) of ~6628nt, and a 3' UTR of ~70nt (Mueller et al. 2005; Holland, et al. 1960) (Figure 1). The 5' end of the 5'UTR is covalently linked to a virus encoded protein, VPg (or 3B), responsible for the initiation of RNA synthesis (Lee et al, 1977; Paul et al, 1998; Kitamura, et al 1981). The 5' and 3' UTR regions contain secondary structures that are important for viral replication and translation. The cloverleaf secondary structure is located within the first 100nt of the 5'UTR. It binds the 3' UTR that contains 2 secondary stem loop structures followed by a poly(A) tail. The 3' and 5' secondary UTR structures associate with each other by forming a complex with viral and host proteins (Figure 1). This complex helps to circularize the viral RNA and initiate RNA synthesis (Herold and Andino 2001). Following the cloverleaf structure, there is another secondary structure, the internal ribosome entry site (IRES) (Figure 1). The IRES allows binding of the viral +ssRNA to the host ribosomes to begin a cap independent translation of viral proteins (Palletier, Kaplan, et al. 1988; Palletier, Sonenberg, et al. 1988).

The ORF encodes for one polyprotein that is auto processed into 11 viral proteins and its precursors. The ORF is organized into 3 regions in order from 5' to 3', P1, P2, and P3. The P1 region includes the capsid proteins VP4, VP2, VP3, and VP1. Both P2 and P3 regions contain the nonstructural proteins, which interact with viral RNA, among viral nonstructural proteins, and host cell proteins.

The P2 region includes 2A, 2B, and 2C. And the P3 region includes 3A, 3B, 3C, and 3D (Wimmer, et al. 1993; Mueller et al. 2005) (Figure 1).

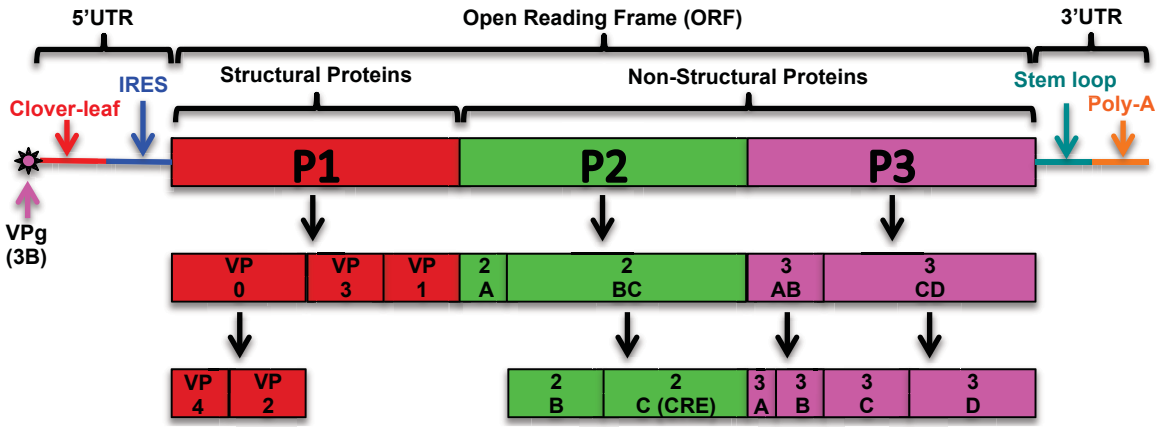

Figure 1. Coxsackie and Poliovirus Genome Organization

The terminal viral protein VPg is linked covalently to the 5' end. The 5' UTR consists of the 5' cloverleaf structure followed by the IRES element. The single open reading frame is translated into a polyprotein of ~247 kDa that is processed by the virally encoded proteinases, $2A^{pro}$ and $3C^{pro}/3CD^{pro}$, into the intermediate protein products (VP0, 2BC, 3AB, 3CD) and the final viral proteins (VP1, VP2, VP3, VP4, 2A, 2B, 2C, 3A, 3B, 3C, and 3D). The 3' UTR consists of 2 stem loop structures followed by a poly(A) tail.

Processing and Viral Protein Function

Upon viral exposure, host cells expressing the specific receptors take up the virions and release of the +ssRNA in to the host cell cytoplasm. The receptor that recognizes poliovirus is the human Poliovirus Receptor (PVR) or CD155 and for coxsackievirus is the Coxsackie and Adenovirus Receptor (CAR) (He, et al. 2003; Bergelson et al. 1997). The +ssRNA through the IRES encoded into its

genome attaches to the host ribosomes to initiate translation of the viral polyprotein (Palletier, Kaplan, et al. 1988; Palletier, Sonenberg, et al. 1988). The viral proteases $2A^{pro}$, $3C^{pro}$, and $3CD^{pro}$ start the auto cleavage process as the polyprotein is being translated and after translation has ended, producing the structural and nonstructural precursor and protein products. The cascade of highly specific *cis* and *trans* cleavage events follows a 3-step process. First, $2A^{pro}$ carries out the cleavage in *cis* of the Tyrosine-Glycine bond between P1 and P2, releasing the P1 precursor, while the polyprotein is still being translated. Second, $3CD^{pro}$ catalyzes the cleavage in *cis* of the Glutamine-Glycine bond between P2 and P3, releasing P3. In addition, the $3C^{pro}$ and $3CD^{pro}$ in a series of *cis* and *trans* cleavage events process the P2, P3, and P1 regions generating 2A, 2BC, 3AB, 2B, 2C, 3A, 3B (or VPg), $3C^{pro}$, $3D^{pol}$, VP0, VP1, and VP3. Finally the third step, or maturation cleavage, is the processing of VP0 into VP4 and VP2, and this step is required for the new virion to be infectious (Mueller et al. 2005; Malcolm 1995; Cameron, et al. 2010; Palmenberg 1987 & 1990). The protease responsible for the maturation cleavage has not yet been identified; but it has been proposed to be and autocatalytic process involving the newly encapsidated +ssRNA (Basavappa et al. 1994).

P1 proteins, VP1, VP2, VP3, and VP4, make up the virion capsid. Capsid is composed of 60 identical units, protomers, each made up of 3 surface proteins, VP1, VP2, VP3, and 1 internal protein VP4 (Fauquet et al. 2005). P2 proteins, aside from the viral processing activity of viral $2A^{pro}$, have the following functions. $2A^{pro}$ is also responsible for inhibiting cap dependent host mRNA translation by

interfering with the function of the eukaryotic initiation factor 4F (eIF4F) complex, which is responsible for the recruitment of the 40s ribosomal subunit to capped mRNAs. $2A^{pro}$ cleaves the N-terminal domain of the eIF4G disrupting the association with eIF4E (which bind mRNA) preventing the formation of the complex and inhibiting the eIF4F activity (Flint et al. 2009; Cameron et al. 2011; Krausslich et al. 1987). The 2B and 2BC are associated with host cytoplasmic membranes to generate viral replication organelles (VROs) (Cho et al. 1994; Suhy et al. 2000). The 2C or *cis*-acting replication element (*cre*) is responsible for the catalyzing the uridylylation of VPg and servers as the template for $3D^{pol}$ (Sean and Semler 2008). The P3 proteins are mainly involved with activities required for viral genome replication. Protein 3AB can remodel viral RNA and stimulate the activity of the RNA-dependent RNA polymerase (RdRp), or $3D^{pol}$. In addition to the processing activities previously mentioned, protein $3CD^{pro}$ is critical for the formation of the replication complex, priming viral RNA synthesis (Andino et al. 1990; Cornell and Semler 2002). The 3A protein interacts with cytoplasmic membranes and interferes with the host secretory pathway. The 3B or VPg is linked to the 5'end of the viral RNA + and – strand and is necessary for viral RNA replication (Cornell and Semler 2002).

Viral Replication Mechanism

Viral RNA replication begins with the translation of the viral proteins involved in this process (2A, 2BC, 2B, 2C, 3AB, 3A, 3B, 3CD, 3C, and 3D) (Sean and Semler 2008). This process requires host intracellular membranes from where viral proteins build platforms to assemble the replication machinery. These

platforms are called viral replication organelles (VROs) and viruses replicate the RNA in the cytosolic leaflet of the VRO membranes (Denison 2008; Miller and Krijnse-Locker 2008). VRO membranes can originate from different host intracellular compartments for example picornavirus, flavivirus, and coronavirus from endoplasmic reticulum (ER), Golgi apparatus, and trans-Golgi network (TGN) (Schlegel et al. 1996), while togavirus and nodavirus from endosomes, lysosomes, and mitochondria (Magliano et al. 1998). The VROs for CV and PV start appearing at 3hr post infection and by 7hr post infection the host cell cytoplasm is almost completely filled with VROs. VROs measure approximately 50-400 nm in diameter and have a compact or rosette-like shape (Schlegel et al. 1996; Cho et al. 1994).

Coxsackievirus and PV replication process can be divided into 2 basic steps: 1) the synthesis of the complementary negative RNA strands to be used as template for positive strand RNA synthesis, and 2) the synthesis of new genomic positive RNA strands to be used for translation into more viral proteins, serve as template for more negative strand RNA synthesis, or for encapsidation into new infective virions.

The negative strand RNA synthesis process begins with the formation of the ribonucleoprotein (replication) complex that is made of the host Poly (rC) binding protein 2 (PCBP2) and the viral 3CD protein bound to the 5’ cloverleaf structure. Since the RNA dependent RNA polymerase (RdRp) reaction takes place in a 5’ to 3’ direction, the positive strand RNA template circularizes and the 5’ replication complex is able to associate with the host Poly A binding protein 1

(PABP1) that is bound to the 3' polyA segment of the RNA template (Herold and Andino 2001; Parsley et al. 1997). This association allows the transfer of the 5' replication complex to the 3' end of the positive strand RNA template. At the 3' end of the template, the viral $3D^{pol}$ catalyzes the uridylylation of the viral VPg (3B) protein using as a template the viral 2C protein also know as the *cis*-replicating element (cre) (Paul et al. 2000). Uridylylation of VPg is the first step in synthesizing the new RNA strand because it serves as the primer for the RNA polymerization reaction. After uridylylation of VPg, the $3D^{pol}$ begin to synthesize and elongate the negative strand RNA until it reaches the 5' end of the template, producing a double stranded RNA intermediate called the replicative form (RF). The RF will be separated during positive strand RNA synthesis. The negative strand of the RF is left on the VRO membranes as template for positive RNA synthesis (Mueller et al 2005; Sean and Semler 2008).

The positive strand RNA synthesis is also initiated with uridylylation of the VPg with *cre* as the template in the same way as for the negative strand synthesis (Goodfellow et al 2003). As the RF RNA is separated into positive and negative RNA strands, the replication complex containing the uridylylated VPg is recruited to the 3' cloverleaf structure of the negative strand RNA template where the uridylylated VPg anneals to the adenines on the polyA tail. Then the $3D^{pol}$ starts the polymerization and elongation reaction until it reaches the 5' end of the negative strand RNA template (Sean and Semler 2008). During viral infection, the ratio of positive to negative RNA strand is 40:1 because multiple positive RNA strands are being synthesized from 1 negative RNA template, producing a

multi-partial double strand RNA form known as the replicative intermediate (RI) (Giachetti and Semler 1991; Novak and Kirkegaard 1991).

Host Cell Secretory Pathway

As stated earlier, one of the requirements of viral replication is the formation of the VROs from host intracellular membranes. In the case of CV and PV, the ER, Golgi, and TGN are the source of these viral structures; and these organelles are a very important component of the host cell secretory pathway, (Hsu et al. 2010). The main function of the secretory pathway is to transport and modify newly synthesized proteins that will be secreted out of the cell or that will be used inside the cell, (Alberts et al. 2002). In addition to this general function each of these specialized intracellular compartments has its specific function that assists in maintaining membrane composition and stability such as processing proteins that will be part of the different compartments in the cell, or maintaining lipid levels by synthesizing or storing them, (Alberts et al. 2002). The path includes transport from the ER to Golgi in COPII coated vesicles that leave the ER through the ER exit sites. Once in the Golgi, proteins, lipids, and other cargo are sorted and transported between Golgi compartments and secretory vesicles or the plasma membrane in COPI coated vesicles or to lysosomes in clathrin coated vesicles as part of the anterograde transport. Cargo in the Golgi that has escaped or that needs to be returned is packed and transported in COPI vesicles as part of the retrograde transport, (Alberts et al. 2002).

Regulation of membrane and protein trafficking through this path is carried out by a group of proteins called the secretory pathway proteins. Among them,

the most critical are the small GTPases and their effectors. ADP-ribosylation factor 1 (Arf1) is part of the family of small GTPases and is a master regulator of Golgi transport. Small GTPases are molecular switches that cycle between an active ATP bound (membrane anchored) state that bind to effectors for downstream signaling, and an inactive GDP bound (cytosolic) state. The switch between its inactive to active state is facilitated by a guanine nucleotide exchange factor (GEF) that helps dissociate GDP to bind GTP; and between its active to inactive state is facilitated by GTPase activating protein (GAP) that stimulates the hydrolysis of GTP to GDP (Cherfils and Zeghouf 2013). In its active state, which is catalyzed by Golgi-specific brefeldin-A-resistant factor 1 (GBF1) GEF, Arf1 localizes to ER, ER-Golgi intermediate compartment (ERGIC), and Golgi apparatus (Altan-Bonnet et al. 2004; Niu et al. 2005; Garcia-Mata and Sztul 2003; Kawamoto et al. 2002; Zhao et al. 2002). Arf1 recruits different effectors to the membranes. Among these effectors are the COPI coat complex responsible for coating the vesicles that will bud out of the Golgi, the clathrin coat complex responsible for coating the vesicles that will bud out of the TGN, and lipid modifying enzymes such as phosphatidylinositol 4 kinase type IIIβ (PI4KIIIβ) which catalyzes the production of phosphatidylinositol-4-phosphate (PI4P) lipids (Altan-Bonnet et al. 2004; Godi et al. 1999).

Host Endocytosis

Endocytosis is a process used by cells to internalize a diversity of molecules. The major endocytic pathways in mammalian cells can be grouped as the clathrin mediated endocytosis (CME) and the clathrin independent

endocytosis (CIE) pathways. The CIE pathways can be constitutive or triggered by specific signals and are different in their formation, associated machinery, and cargo destination (Mayor and Pagano 2007; Mayor, et al. 2014; Mousavi et al. 2004; Merrifield and Kaksonen, 2014).

Clathrin mediated endocytosis is characterized by the formation of clathrin-coated structures, pits and vesicles, responsible for selective uptake of cargo from the plasma membrane. Its main components are clathrin, adaptor protein 2 (AP2), and dynamin. The major component is the coat protein clathrin that is made of 3 heavy chains and 3 light chains forming a 3-legged structure called a triskelion, which is the basic unit of the clathrin coat. Triskelions assemble on the cytosolic surface of the plasma membrane into basketlike convex hexagonal and pentagonal structures termed clathrin-coated pits (CCPs). The most important clathrin adaptor, AP2, is a heterotetrameric adaptor protein complex composed of 4 subunits (α, β2, μ2, and δ2); and it is in charge of linking clathrin to the plasma membrane and binding to specific cargo in the CCPs. The accessory protein dynamin is high molecular weight GTPase that is recruited to the neck of deeply invaginated CCPs where it is responsible for pinching off the clathrin-coated vesicles (CCVs) by a cycle of oligomerization and GTP hydrolysis. CCVs are uncoated very soon after scission by the cytosolic chaperone heat-shock cognate protein 70 (Hsc70) (Merrifield and Kaksonen, 2014; Mousavi et al. 2004; Kirchhausen et al. 2014).

All the CIE components, its mechanism, and regulation have not been identified as well as the CME counterparts. This field is an emerging research

topic that has been rapidly growing with the development of new tools but there is still a lot to be elucidated. At present, the CIE pathways can be divided into two groups according to their requirement for dynamin and coat proteins. The first CIE group consists of the dynamin dependent (DD-CIE) pathways, (Mayor and Pagano 2007). One of these pathways is dependent on the coat forming protein caveolin and the GTPase protein dynamin. It is characterized for the formation of caveolae, plasma membrane invaginations, coated with a complex of caveolin-1, caveolin-2, and cavins. Dynamin is localized to the neck of caveolae. This pathway has been linked to the uptake of glycosylphophatidylinositol-anchored protein aminopeptidase-P (GPI-AP). An additional DD-CIE is the RhoA dependent pathway. This pathway is also dependent on dynamin and no coat protein has been identified. It has been linked to the uptake of many cytokine receptors such as interleukin 2 (IL-2) and IL-15 receptors, and the amyloid precursor protein (APP) (Mayor and Pagano 2007; Mayor, et al. 2014).

The second CIE group includes the dynamin and coat independent pathways. It is characterized for the absence of dynamin and both coat-forming proteins, clathrin and caveolins. One of these is the CLIC/GEEC pathway characterized by the internalization of proteins such as GPI-APs and CD44 into a specialized early endosomal compartment that contains a major fraction of the internalized fluid phase. These compartments are called GEEC for GPI-AP enriched early endosomal compartment, and since they result from the fusion of the primary clathrin independent (CI) tubulovesicular carriers named CLICs (for CI carriers), hence the name of CLIC/GEEC pathway or CG pathway. Another is

the Arf6 pathway it has been associated with the uptake of proteins involved in nutrient transport (Glut1, CD98, Lat1), matrix interaction (CD44, CD147), immune function (MHC1, CD1a), and GPI-APs (CD55, CD59). The Arf6 pathway is dependent on cholesterol. Soon after internalization, CIE endosomes fuse homotypically and heterotypically with CME endosomes into Rab5-positive early endosomes or Rab5, PI3P, and EEA1 sorting endosomes (Mayor and Pagano 2007; Mayor, et al. 2014).

Host Recycling

The endocytosis process leads to the converging of cargo in the early endosomes from where the cargo can be sorted and can follow one of 2 fates: 1) cargo can be recycled to the same plasma membrane domain, or to a different plasma membrane domain known as transcytosis such as is the case in polarized cells; or 2) can be transported to other compartments or degraded in lysosomes such as the epidermal growth factor (EGF) and its receptor. During the recycling process, the receptor alone or both the ligand and the receptor can be sent back to the plasma membrane. For example, the low density lipoprotein (LDL) receptor dissociates from its ligand and buds off the early endosome to merge with the recycling endosomes that will be responsible for recycling the receptor back to the plasma membrane, while its ligand LDL is sent to lysosomes. On the other hand, the transferrin receptor (TfnR) and ligand complex follow the same path as the LDL receptor but the receptor/ligand complex is recycled back to the plasma membrane after releasing the bound iron in the early endosomes (Alberts, et al. 2002).

Thesis Project Introduction

Many +ssRNA viruses, including enteroviruses, remodel host membranes to form platforms with unique protein and lipid components to assemble replication complexes and synthesize new viral RNA often on the cytosolic leaflet of these membranes (Miller and Krijnse-Locker 2008). Coxsackievirus and poliovirus highjack important components of the secretory pathway such as Arf-1 and GBF-1 (GEF for Arf-1) and are required for enteroviral RNA replication (Belov, et al. 2007; Lanke, et al. 2009).

Our lab previously demonstrated that Coxsackievirus B-3 (CVB-3) and PV selectively recruit Arf-1 and GBF-1 over other components of the COPI complex, such as clathrin, (Hsu, et al. 2010). In addition through immunofluorescence and co-immunoprecipitation studies, PI4KIIIβ was found not only present in the VROs but associated with proteins from the viral replication complex, 3A, 3AB, 3CD, and $3D^{pol}$, (Hsu, et al. 2010). Concomitant with this, the expression in Hela cells of viral 3A-myc alone enhanced the selective recruitment of PI4KIIIβ (over PI4KIIIα) and caused the disassembly of the Golgi apparatus in a similar manner as viral infected cells. The PI4KIIIβ activity was also found to be responsible specifically for viral RNA synthesis, (Hsu, et al. 2010). Since PI4P lipids result from the activity of PI4KIIIβ, we tested to see if this lipid was part of the VROs. We found that VRO membranes are enriched in PI4P lipids, (Hsu, et al. 2010). Furthermore, we confirmed by lipid binding assays the specific and preferential binding of PI4P lipids to the viral protein $3D^{pol}$, (Hsu, et al. 2010). Based on these findings, the model for the reorganization of the secretory pathway in enteroviral

infections is that membrane-bound enteroviral 3A proteins bind and modulate host proteins Arf-1 and GBF-1 to enhance the recruitment of PI4KIIIβ to membranes where it will catalyze the production of PI4P lipids, leading to the biogenesis of a PI4P lipid enriched microenvironment. This lipid microenvironment in turn promotes the recruitment and stabilization of the RdRp $3D^{pol}$ from the cytosolic pool to the membranes. Viral RNA synthesis initiates on the cytosolic leaflet of the VROs after integrating $3D^{pol}$ to the viral replication complex made of 3A and other viral proteins, (Hsu, et al. 2010).

The detection of PI4P lipids on the VROs motivated us to investigate further the lipid composition of these exclusive organelles. We hypothesize that enteroviruses highjack the cellular CME and endosomal recycling to uptake and redistribute cellular plasma membrane cholesterol to VROs where it is necessary for viral protein processing. Therefore, the aims of this project are: 1. To identify if other host cellular lipid(s) are critical for viral replication. 2. To identify the host components and mechanisms that the virus can manipulate to incorporate the lipid into the VROs to achieve successful replication. 3. Finally, using various high-resolution microscopy techniques we want to investigate the dynamics and the spatio-temporal distribution of these lipids and protein components, in enteroviral infected cells.

CHAPTER 2

Materials And Methods

Plasmids and Antibodies

We are greatly thankful to the following labs for providing the following reagents: Plasmids: Arf1-GFP (Jennifer Lippincott-Schwartz, National Institutes of Health [NIH]), Clathrin-mRFP, and Rab5-mRFP (Mark McNiven, Mayo Clinic) FAPP1-mRFP (Tamás Balla, NIH), Rab11A-wt-RFP (Wei Guo, University of Pennsylvania), Rab11B-wt-pEYFP (Mikhail Khvochtchev, UCSF), Rab7A-mcherry (Nan Gao, Rutgers University) 2BC-GFP (Lindsay Whitton; The Scripps Research Institute, CA), Rab11A-mRFP (Alexis Gautreau, CNRS, France) Farnesyl-RFP (Julie Donaldson, NIH), Transferrin receptor with super ecliptic pH luorin (TfnR-phl) (C. J. Merrifield, Laboratoire D'enzymologie Et Biochimie Structurales, France). All plasmids were transfected to one-day-old cells using FuGENE6 Transfection Reagent (Roche, IN) and incubated for 24hours at 37°C/5% Carbon Dioxide (CO_2).

Replicons: Coxsackievirus B3 replicon pRib-Rluc (Frank van Kuppeveld; Nijmegen Institute for Infection, inflammation and Immunity, Netherlands), Poliovirus replicon pXpa-RenR encoding for Renilla Luciferase gene was described previously (Belov, 2007), Luciferase T7 control DNA and Live cell Renilla substrate Endu-Ren (Promega Corp., WI).

Primary antibodies against host proteins: PI4KIIIβ (Millipore, MA), Rab11A (Invitrogen Corp. CA), Rab11B, Clathrin Heavy Chain (Cell Signaling, MA), Rab5, RhoA, Dynamin II, HIP1R, Cav1, Cav2 (BD Biosciences, CA), Rab8, β-actin, and

TGN46 (Sigma, MO), NPC1L1, ADRP, AP2M1, Rab11FIP5, clathrin light chain (Abcam, MA), PI4P mouse monoclonal IgM (Echelon Biosciences, UT), GAPDH (Santa Cruz Inc., CA), EPS15L1 (OriGene, MD), LDL Receptor (Novus Biologicals, CO), TfnR (Luise Green, NIH), HMG-CoA Reductase (Dr. Simoni, Stanford University).

Primary viral antibodies: J2-dsRNA monoclonal antibody (English and Scientific Consulting Bt., Hungary), CVB3-3A protein (J. Lindsay Whitton, Scripps Research Institute), Poliovirus 3AB and 3D (Greg Cameron, Pennsylvania State University), Poliovirus 3A and 2C (Dr. Ellie Ehrenfeld, NIH), HRV2-3C (Dr. Svetlana Amineva, University of Wisconsin, Madison, WI).

Secondary antibodies: Horseradish Peroxidase conjugated goat anti-mouse and anti-rabbit secondary antibodies (Thermo Scientific), donkey anti-goat (Santa Cruz Inc., CA). Fluorescently labeled secondary antibodies anti-mouse, rabbit, and chicken (Invitrogen Corp. CA; Jackson Immunoresearch Labs Inc., PA).

Chemicals and Reagents

Bovine serum albumin (BSA) and Paraformaldehyde (PFA) (Fisher Scientific, PA), Formaldehyde (FA) Methanol Free (Electron Microscopy Science) Nonessential Amino Acids, Penicillin/Streptomycin (P/S), Dulbecco's Modified Eagle's Medium (DMEM), and Eagle's Minimal Essential Medium (EMEM) (Mediatech, VA), Heat Inactivated Fetal Bovine Serum (HIFBS) (Atlas Biologicals, GA), Neomicyn/G418 (Sigma, MO), Lovastatin (Enzo Life Sciences Inc., NY), Ezetimibe (Santa Cruz Inc., CA), PIK93 (Symansis, Auckland New Zealand),

Filipin III (Cayman Chemical, Michigan; Sigma, MO), Filipin, Mevalonate, Methyl-β-cyclodextrin (MβCD), Dynasore, Chlorpromazine Hydrochloride, Nile Red, and Saponin (Sigma, MO), Amplex Red cholesterol kit and BODIPY Low Density Lipoprotein from Human Plasma FL complex (LDL) (Invitrogen Corp., CA), Top Fluor (BODIPY) cholesterol 23-dipyrromethene boron difluoride-24-norcholesterol (Avanti Polar Lipids Inc., AL), Fluoromount (Electron Microscopy Science), Prolong Gold mounting media (Invitrogen, Corp. CA), AM4-65 dye (Biotium Inc., CA), restriction enzymes (New England Biolabs, MA).

Cell Culture and Virus Propagation

Cell Lines: HeLa cells (ATCC, VA) were maintained in DMEM supplemented with 10% HIFBS, 2mM L-glutamine, 1% P/S at 37°C/5%CO_2. HeLa-Ohio (Sigma, MO) and Vero cells (ATCC) were maintained in EMEM supplemented with 10% HIFBS, 1X non-essential amino acid, and 100 µg/ml Penicillin/ Streptomycin. Human Fibroblasts (GM03652) from healthy donor, NPC1 (GM03123 and GM23162), and NPC2 (GM18455 and GM17910) mutant fibroblast cells were facilitated from Coriell Institute of Medical Research, NJ; fibroblasts were maintained in EMEM containing Earle's Salts and Nonessential Amino Acids supplemented with 15% FBS at 37°C/5%CO_2. Clathrin-RFP expressing Hela (CRSH) cells were established and maintained in DMEM supplemented with 10% HIFBS, 2mM L-glutamine, 1% P/S, and 0.5 mg/ml G418 at 37°C/5%CO_2.

Virus Strains: Human Rhinovirus- 2 (Cat#: VR-482) and Human Echovirus-11 Gregory strain (Cat#: VR-41) were purchased from ATCC. CVB-3

Nancy strain was a gift from Dr. Frank van Kuppeveld, Netherlands. Poliovirus-1 Mahoney strain was a kind gift of Dr. George Belov, University of Maryland. To generate viral stocks of HRV2, 95% confluent HeLa-Ohio cells were infected and incubated at 34°C/5%CO_2 for 3 days. To generate CVB3 and PV viral stocks, confluent HeLa cells were infected with the appropriate virus and incubated at 37°C/5%CO_2 for 24 hrs. To propagate echovirus, 90% confluent Vero cells were infected and incubated at 37°C/5%CO_2 for 7 days in CCM but supplemented with 2% FBS. All infected cells underwent freeze-and–thaw cycle 3 times, cell debris was removed by centrifugation at 2,000 rpm for 5 min at room temperature, supernatant was collected and stored at -80°C. Virus titter was determined by plaque assay, a typical MOI of ~10-30 viral particles per cell was obtained.

Cell Viability Quantification

Optimal plasmid expression times, siRNA concentrations, siRNA incubation times, drug concentrations and respective incubation times that maximize cell viability were assessed by quantifying cell number and by CellTiter-Glo cell viability assays (Promega Corp, WI). Plasmid concentration range tested was 0.1µg/µl-1µg/µl; and siRNA concentration range tested was 25nM-100nM.

Imaging and Analysis

Microscopes: Imaging was performed on a Zeiss LSM510 or LSM780 Confocal Laser Scanning microscopes (Carl Zeiss, USA); the microscopes were equipped with a heating stage and incubator with temperature, humidity, and

CO_2 control for live-cell imaging. Some samples that required UV excitation were imaged on a Nikon Eclipse TE200 Epifluorescence microscope (Nikon Inc.). Cells for live imaging were grown on coverslip-bottomed Lab-Tek chambers (Thermo Fisher, NY) and during the experiment, cells were maintained in imaging media (DMEM Phenol Red free supplemented with 10% HIFBS and 25-50mM HEPES pH 7.3), termed complete imaging culture media (CICM). Cells for fixed samples were grown on glass coverslips, processed according to experimental requirements, and mounted on glass slides. All obtained images were analyzed with Zeiss LSM/Zen or ImageJ software.

Immunofluorescence: Cells were plated on coverslips, fixed with 3.7% FA or PFA solution in 1xPBS for 10 minutes at RT (30 minutes for lipid fixation), and then washed 3 times with 1xPBS. Primary antibodies were diluted (1:25-200) in incubation buffer (0.2% Saponin; 1% BSA; in 1xPBS), for PI4KIIIβ (0.2% Saponin; 10% FBS; in 1xPBS), and incubated for 1 hour at RT; then rinsed 3 times 5 minutes each with 1xPBS. Fluorophore tagged secondary antibodies were diluted (1:500-1000), incubated for 1 hour at RT followed by rinsing the same way as with the primary antibodies.

Fluorescence Quantification and Statistical Analysis: To quantify the relative fluorescence of the target structures, Regions of Interest (ROI) were selected for the target areas (ROIt) and for background areas (ROIb) in target and control cells. The mean fluorescence intensity of the ROIs was obtained with ImageJ software. The percent mean fluorescence intensity was obtained with the following formula $[(ROIt)\text{-}(ROIb)_{targetcell}/(ROIt)\text{-}(ROIb)_{controlcell}] *100$, and calculated

for an average of 40 to 50 cells per condition. Plotted data were normalized to control values. Standard errors and p-values were calculated with KaleidaGraph software (Synergy Software; Reading, PA) using the Student t-test for unpaired data with equal variance function. We statistically assessed the degree of colocalization between two components using a classical Pearson's Correlation Coefficient for the image intensity in the red and green channels using the following formula ($r=n(\Sigma xy) – (\Sigma x)(\Sigma y) / \sqrt{[n\Sigma x^2 – (\Sigma x)^2] [n\Sigma y^2 – (\Sigma y)^2]}$), (Bolte and Cordelieres 2006).

Total Internal Reflection Fluorescence (TIRF) Imaging and Analysis: Cells were seeded in 35mm bottom glass dish (MatTek Corp. Ashland, MA) and incubated at 37°C/5%CO_2. After the required treatments, cells were imaged in an ELYRA PS.1 super resolution microscope (Carl Zeiss, USA) equipped with: 1) A 100x Plan Apochromat oil immersion lens with numerical aperture of 1.46 with TIRF capabilities. 2) A heated stage and incubator with temperature, humidity, and CO_2 control for live-cell imaging. Images were taken at continues scan mode for 30 seconds (~10 frames/sec) every 30 minutes for 4 hours; or one image every 5 minutes for 4 hours. Images were processed into movies and analyzed using Zen Black software (Carl Zeiss, USA). Individual images were analyzed for colocalization measurements, and quantification of independent endocytic and exocytic events by marking them starting from the appearance of a vesicle at the plasma membrane until it is internalized and disappears from the field of view (endocytosed); or from when the vesicle appears at the plasma membrane until the vesicle membrane fuses with the plasma membrane and the fluorescence

disperses in the immediate area adjacent to the vesicle fusion location (recycled).

Lipid Assays

Lipid Loading: Top Fluor (Bodipy) cholesterol powder was dissolved in chloroform; solvent was evaporated using argon or nitrogen gas to yield the lipid film. MβCD was dissolved in sodium phosphate (NaCl/Pi) buffer (8 mM Na_2HPO_4; 1.5 mM KH_2PO_4; 137 mM NaCl; 2.7 mM KCl, pH 7.2) and then added to the thin film of sterol at a molar ratio of Sterol:MβCD (1:10). Solution was incubated overnight in a rotator at RT, and then sonicated in ice for 20 minutes in a water bath sonicator, and centrifuged at 14,000 rpm for 5 minutes before aliquoting under oxygen-free conditions. The complex was added to cells at 10-20µg/ml concentration in serum free (SF) DMEM for 5 minutes at 37°C/5%CO_2; and further incubated in CCM for additional 20 minutes.

Lipid Staining: Nile Red fluorescent stain was used for the detection of intracellular lipid droplets. In live cells, Nile red was incubated at 0.5 µg/ml solution in SFM for 5 min at 37°C/5%CO_2. Cells were washed and imaged with CICM. For fixed samples, cells were incubated with 0.5 µg/ml Nile Red solution in 1xPBS for 10 min at room temperature (RT), rinsed once, and mounted. Filipin III fluorescent stain was used for the detection of intracellular cholesterol. Filipin III was diluted in DMSO under oxygen free conditions. Cells were fixed with 3.7% FA or PFA in PBS for 30 minutes at RT, washed 3 times in 1xPBS, and incubated with 50 µg/ml Filipin III (diluted in1xPBS supplemented with 10% HIFBS) for 30 minutes at 37°C, followed by three washes with 1xPBS. In fixed

samples, Filipin III and Nile Red staining was performed as the last step before mounting.

Bulk Cholesterol Quantification**:** Cholesterol levels were determined in HeLa cell extracts using Amplex Red Cholesterol assay (Invitrogen Corp.). Cells were harvested, resuspended in the 1x Amplex Red reaction buffer containing Halt Protease Inhibitor Cocktail (Thermo Scientific), and passed 20 times through a 25-gauge needle fitted to a syringe. The lysates were additionally sonicated twice for 10 seconds using a Qsonica XL-2000 misonix sonicator, and centrifuged for 5 minutes at 14,000 rpm. Protein concentration was measured and samples were diluted to equal amount of protein. Total cholesterol and cholesterol ester content was determined by incubating 50ml of cell extract containing 20mg of protein with 50ml Amplex Red assay reagent in the presence or absence cholesterol esterase for 30 minutes at 37°C in the dark. Fluorescence was detected with a HT Multi-Well Plate Reader (BioTek, VT) at 535 nm excitation and 595 nm emission wavelengths. Cholesterol content was calculated using a standard curve.

Cholesterol Biosynthesis: HeLa cells were seeded at 50,000 cells/well in a 6-well plate and 48h after transfected with siRNAs for 48 hours. After 48 hours of transfection the culture medium was changed to SFM medium supplemented with 2μCi/ml of Acetic Acid Sodium Salt [1,2-14C] ([14C]) (Perkin Elmer Health Sciences Inc., CT) and incubated for 3 hours at 37°C. For the cholesterol biosynthesis experiment in infected cells the cells were infected with CVB3 or mock virus in complete medium and 2μCi/ml of [14C] was added immediately.

The cells then remained with the isotope containing media for 2 hours, 4 hours or 6 hours. After incubation the cells were washed with ice-cold 1xPBS over ice, and lipids were extracted by adding Hexane:Isopropanol (3:2; v/v) to cell monolayers 2 times for 30 minutes each. The solvent in the organic phase was evaporated to dryness under a nitrogen stream at RT. The lipids were redissolved in hexane and sonicated in a water bath sonicator. To evaluate the incorporation of labeled acetate into cellular sterols, lipid extracts and known standards were spotted on Silica Gel G TLC plates and developed using a nonpolar solvent system (hexane/diethyl ether/acetic acid, 70:30:1; by volume) to separate the lipid classes. Then the plates were dried. For [14C]-labeled lipids, the TLC plate was exposed to a phosphorimager screen, and the percent of total lipid extract radioactivity present in each lipid class was analyzed using Storm 840 phosphorimager software.

Lipid extraction: In Triton X-100 extraction experiments, live cells were cooled over ice, washed in ice cold 1% Triton X-100 diluted in 1xPBS and incubated for 20 minutes, then washed in 2% FA diluted in 1xPBS; finally, fixed for 30 min in PFA and stained with Filipin III. Cholesterol depletion was carried out by incubating cells in the presence of 10mM MβCD, diluted in serum free DMEM, for 1 hour at 37 °C/5%CO_2. After incubation with MβCD, cells were washed with serum free DMEM once, and replicon assay was performed without serum in both control and MβCD treated cells.

LDL Uptake: BODIPY-LDL was added to control and infected cells (time zero of infection) at a concentration of 20µg/ml in complete culture media and

incubated at 37°C/5%CO2 for the required amount of time, 2 or 4 hours. After each time point, cells were quickly rinsed with media before confocal imaging and intracellular fluorescence quantification.

AM4-65 Uptake

Dye was dissolved to a 10mM stock solution with sterile ddH2O, and stored at -20°C. During experiments, HeLa cells were transfected with 2BCGFP plasmid using Fugene6 reagent, according to manufacture protocol, and incubated at 37°C/5%CO2 overnight. Transfected cells were then incubated over ice with 5μM AM4-65 dye, in SFM; cultures were then rinsed twice with SFM, and further incubated in SFM at 37°C/5%CO2 for 20 minutes. When needed, cultures were pre-treated with 80μM Dynasore, diluted in CCM, for 3 hours at 37°C/5%CO2; and maintained in Dynasore solution, diluted in SFM, after the dye. Cells were then fixed in 2% paraformaldehyde for 5 minutes at room temperature. Coverslips were mounted and imaged in a confocal microscope.

siRNA Transfection

On-Target plus siRNAs non-targeting, AP2A1, AP2A2, AP2B1, AP2M1, ARF6, clathrin B, CAV1, CAV2, DAB2, DNM2, EPS15L1, Rab11FIP5, HIP1, HIP1R, RAB5A, RAB11A, and Rab11B were purchased from Dharmacon, CO; PI4KIIIβ siRNA was purchased from Qiagen, CA. Cells were seeded 1-2 days before siRNA transfection as follows: in 96-well plates for the replicon assay; in 12-well plates for Western Blot analysis to verify gene knockdown efficiency; and on coverslips for immunofluorescence imaging. 50nM of each siRNA was

transfected to cells via Dharmafect 1 (Dharmacon, CO) following manufacturer's recommendations. Transfected cells were incubated for a period of 48 hours at 37°C/5%CO_2. PI4KIIIβ was depleted from cells by triple knockdown in HRV2 experiments. HeLa-Ohio (HeLa cell line that express the rhinovirus receptor) cells were infected with HRV2 and incubated for 1 hour at 34°C/5%CO_2. Virus was then washed off and cells were transfected with the first siRNA treatment. Transfected cells were incubated at 34°C/5%CO_2 for 12 hours. After that, siRNA media was replaced with fresh CCM and incubated for an additional 8 hours before the second siRNA treatment. The same procedure was followed for the second and third siRNA treatments.

Replicon Assays

Viral RNA replication was measured with pRib-Ruc (CVB3) or pXpA-RenR (PV) plasmids with Renilla Luciferase gene as reporters in place of structural genes. Plasmids were linearized with SalI or EcoR1 and transcribed using MEGAscript (Ambion, Life Technologies, NY). RNA transfection and Renilla Luciferase measurement was performed as described [Hsu, 2010]. The total cell count was normalized using CellTiterGlo (Promega Corp., WI) in a parallel plate to adjust for differences in growth among different conditions. All measurements are an average of 4-6 wells in 2-4 independent experiments. Capped *Firefly* Luciferase mRNA containing a poly-A tail was used for control of RNA transfection and translation efficiency. Luciferase T7 control DNA was ScaI linearized, transcribed using mScript mRNA production System (Epicentre Biotechnologies, WI), and lastly capped and transfected into cells via Mirrus

TransIT-mRNA transfection kit (Mirrus, WI) for 6-8 hours. The cells were washed with 1xPBS and lysed in lysis buffer (Corp., WI) and 2 freeze-and-thaw cycles. *Firefly* Luciferase activity was determined using Luciferase Assay System (Promega Corp., WI) according to the manufacturer's protocol. The light emitted was measured using a BioTek Synergy 2 Luminescence Plate Reader.

Drug Treatments and Analysis

Cells were incubated in the presence of Lovastatin in concentration of 5, 10 or 25mM and Mevalonate in concentration 250mM for 72 hours in cholesterol-depleting medium in the presence of 5% LPDS. Lovastatin was converted to its active form as described previously (Morimoto 2006). Sodium Mevalonate was prepared from the Mevalonic acid lactone as described (Jeong 2008). Control cells were processed in parallel in the absence of Lovastatin or Mevalonate. After 72 hours, cells were transfected with CVB3 or PV viral replicon RNA and measured for *Renilla* Luciferase. For HRV2 infection, cells were infected for 1 hour; the medium removed and exchanged with cholesterol-depleting medium, as above, in absence or presence of drugs. Cells were harvested for immunoblot analysis 72 hours after infection. For Ezetimibe experiments, cells were vehicle treated or treated with drug at a concentration range of 1-30mM in complete DMEM for 1 hour before or 1 hour after viral RNA transfection. Dynasore stock solutions were prepared with DMSO in an oxygen-free environment. Cells were pretreated with 80μM Dynasore or treated 1 or 2.5 hours after viral RNA transfection. Chlorpromazine was added to cells at the indicated concentrations at the time of replicon RNA transfection.

Western-Blot Analysis

Cells were harvested in lysis buffer (50 mM Tris-HCl, pH 7.4, 1% NP-40, 0.25% Na-deoxycholate, 150 mM NaCl, 1 mM EDTA) supplemented with a Halt Protease Inhibitor Cocktail and centrifuged for 10 min at 14,000 rpm at 4°C. Supernatant was mixed with Laemmli buffer including β-mercaptoethanol and heated at 98°C. A total of 10-30 µg of protein was loaded on a 10% SDS-polyacrylamide gel and separated on an electrophoresis system (Bio-Rad, CA). Proteins were transferred to Hybond Nitrocellulose membranes (Amersham Pharmacia, NJ). Membranes were blocked with 5% milk in 1xPBS-T (1xPBS; 0.05% Tween-20) for 1 hour and incubated overnight with selected primary antibodies and subsequently for 1 hour with horseradish peroxidase (HRP) secondary antibodies at dilution 1:10,000. Bound antibody complexes were detected with Super Signal West Pico Chemiluminescent Substrate (Thermo Scientific) visualized on Super RX X-ray film (FujiFilm) and quantified using GelPro32 software (NIH). Actin or GAPDH intensities were used to normalize protein expression levels.

Immunoprecipitation

Cells were scraped and suspended in ice-cold hypotonic lysis buffer (50mM KCl, 25mM HEPES, 1mM DTT, 1mM EDTA) or IP-lysis buffer (Thermo Scientific) supplemented with Halt Protease and PhosphataseArrrest (G-Biosciences, MO) inhibitor cocktails. Suspended cells were broken up using a cell homogenizer (Isobiotec, Germany) or by vortexing for 30 seconds every 5 minutes for 20 minutes over ice. Lysates were centrifuged at 14,000g for 10

minutes at 4°C. Target proteins were immunoprecipitated overnight at 4°C with 5μg of monoclonal or polyclonal antibodies. Lysates were then incubated with Protein-A or G magnetic beads (New England Biolabs, MA; Life Technologies) for 2 hours. Lysate was discarded, and beads bound to the proteins of interest were washed 3 times with lysis buffer with inhibitors. Precipitated proteins were suspended in loading buffer; and the pull down fractions were resolved by SDS-PAGE and transferred to nitrocellulose membrane. Immunoblotting was performed using monoclonal or polyclonal antibodies.

Rab11A Mutant Constructs

Single and double point mutations to Histidine 130 and Leucine 131 into Alanine were incorporated into the wild type Rab11A amino acid sequence along with HA tag sequence for selection of positive clones. Sequences were commercially synthesized and cloned (Genewiz; South Plainfield, NJ) into the mammalian expression vector pcDNA 3.1(+) (Life Technologies) via BmaHI restriction site. Upon selection and purification of clones, mutant plasmid DNA was extracted and transfected into experimental and control HeLa cells.

CHAPTER 3

Cholesterol Is Part Of The Viral Replication Organelles

Cholesterol is a critical component of cellular membranes. Approximately 80-90% of the total cellular cholesterol is associated with the plasma membrane, the rest in the recycling endosomes and TGN, and only ~1% in the ER (Lange 1991; Mukherjee et al. 1998). In addition, it regulates membrane permeability and fluidity; which is indispensable for proper assembly and function of membrane-based protein-lipid complexes. The biophysical properties of its structure, allows cholesterol to increase the packing of negatively charged adjacent lipids to form stable platforms to associate with the protein-lipid complexes (Alberts 2002; Ikonen 2008).

RESULTS:

Cholesterol Localizes to Viral Replication Organelles

In this chapter, we determined if cholesterol was part of the VROs. For this set of experiments, we seeded HeLa cells on coverglasses and infected them with 10MOI of each CVB-3, PV-1, Echovirus-11, or RV-2. Then cells were fixed at peak replication time and immunolabeled with antibodies against viral RNA, viral replication proteins (3A or 3AB), and/or endogenous PI4P lipids. We used filipin, a lipid stain that binds unesterified cholesterol and is fluorescent upon UV light exposure, to locate the unesterified cholesterol pool in uninfected and infected cells. Samples were imaged using a high-resolution confocal microscope.

We found that in the uninfected control cells, cholesterol was localized mainly to the plasma membrane and to the perinuclear (Golgi/TGN) region of the cells (Figure 2A). Furthermore, endogenous PI4P lipids colocalized with the cholesterol pool (Figure 2A). In the CVB-3 and PV-1 infected cells at peak replication times, all VROs were enriched in both cholesterol and PI4P lipids, and that these lipids were colocalized with viral replication proteins 3A and 3AB (Figure 2B & 2C). We also wanted to know if these results were present in other +ssRNA viruses, so in addition to CVB-3 and PV-1, we looked at Echovirus-11 and RV-2 that belong to the same genus. And we found that the distribution of cholesterol and PI4P lipids was the same as in CVB-3 and PV-1 infections, and that the lipids are in VROs, identified by viral RNA labeling (Figure 2D & 2E). The Pearson's Coefficient of Colocalization in the viral proteins confirmed these results: for CVB-3 is 0.70±0.03 in n=10, and for PV1 is 0.79±0.04 in n=10.

Viral Replication Organelles have Cholesterol Domains

We then wanted to have a better spatial resolution of the organization of cholesterol and PI4P in the VROs since the size of these structures are at the limit of resolution with conventional diffraction limited microscopy (Belov et al. 2013). Therefore, for the following experiment we used structured illumination microscopy (SIM) in live cells. SIM is achieved when the microscope takes an image at different angles (5 images on average at 60 degrees) around the structure creating a Moiré pattern or grid pattern, and through the Fourier Transform we can calculate the center (brightest spot) in the superimposed images, giving us the final processed image, which has a resolution of

approximately 140nm in the x and y axis, and 250nm in the z axis (Gustafsson et al. 2008).

Cells were seeded in LabTek bottom glass chambers and incubated overnight. Then, the cells were transfected with Four-phosphate-adaptor protein (FAPP) 1-mRFP construct and further incubated overnight. FAPP1 and 2 bind PI4P lipids and Arf, through its plekstrin homology (PH) domain (Godi et al. 2004). Therefore, we used FAPP-1 PH proteins, tagged with either GPF or RFP, as markers for the VROs since it has the same cellular distribution during infection as Arf1 and PIP4 lipids (Hsu, et al. 2010). For live cells it is not recommended to use filipin due to its cytotoxic effects; so to visualize the cellular cholesterol we used Bodipy-cholesterol. Bodipy-cholesterol has many advantages: 1) it is a fluorescent analog of cellular free cholesterol. 2) It can also be esterified as endogenous cholesterol. 3) It is suitable for live imaging. 4) It gets inserted into the plasma membrane and at steady state, it is trafficked among: plasma membrane, endosomal compartments, and Golgi/TGN (trans Golgi network) area, which are all the corresponding sites for endogenous cholesterol. 5) Finally, it is highly photostable (low photo bleaching with continues imaging) (Holtta-Vuori et al. 2008). We loaded cells with Bodipy-cholesterol according to the protocol in materials and methods, and infected the cells with CVB-3 for 4 hours. SIM images showed that the cholesterol in the replication organelles was not evenly distributed, but was organized in separate domains that vary in size from 100 to 400 nm (Figure 2F).

CONCLUSION:

Together the data from this chapter shows that cholesterol is present at viral replication organelles together with PI4P lipids proven previously to be critical for viral replication (Hsu et al. 2010). Additionally, we provided evidence that the cholesterol distribution to VROs is not limited to CVB and PV but within the picornavirus family of viruses, such as EV and RV. Finally, we show with super resolution microscopy techniques that the cholesterol distribution on the VROs is organized in discrete domains through out the entire surface of the organelles.

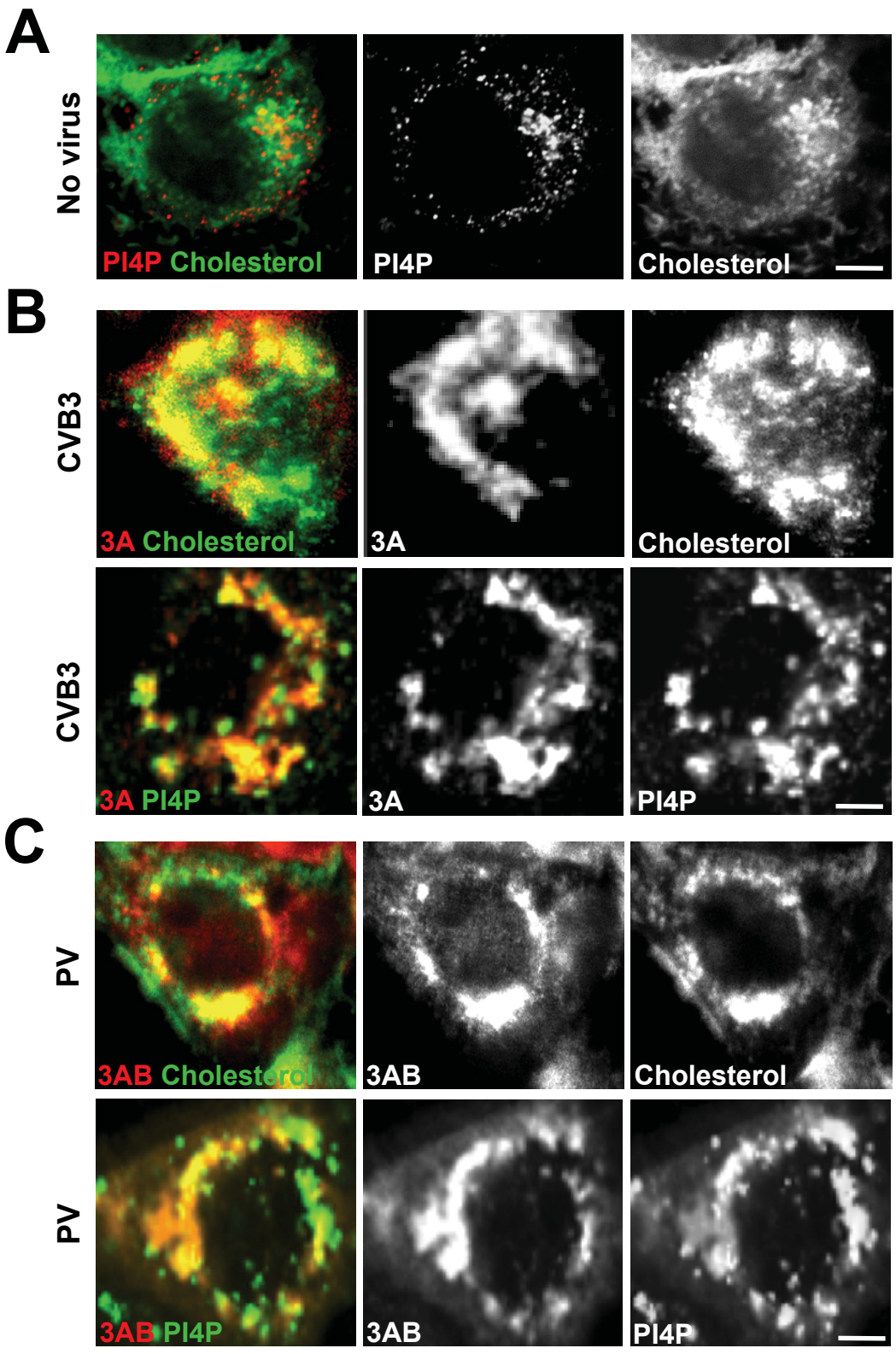
A
No virus
PI4P Cholesterol
PI4P
Cholesterol
B
CVB3
3A Cholesterol
3A
Cholesterol
CVB3
3A PI4P
3A
PI4P
C
PV
3AB Cholesterol
3AB
Cholesterol
PV
3AB PI4P
3AB
PI4P

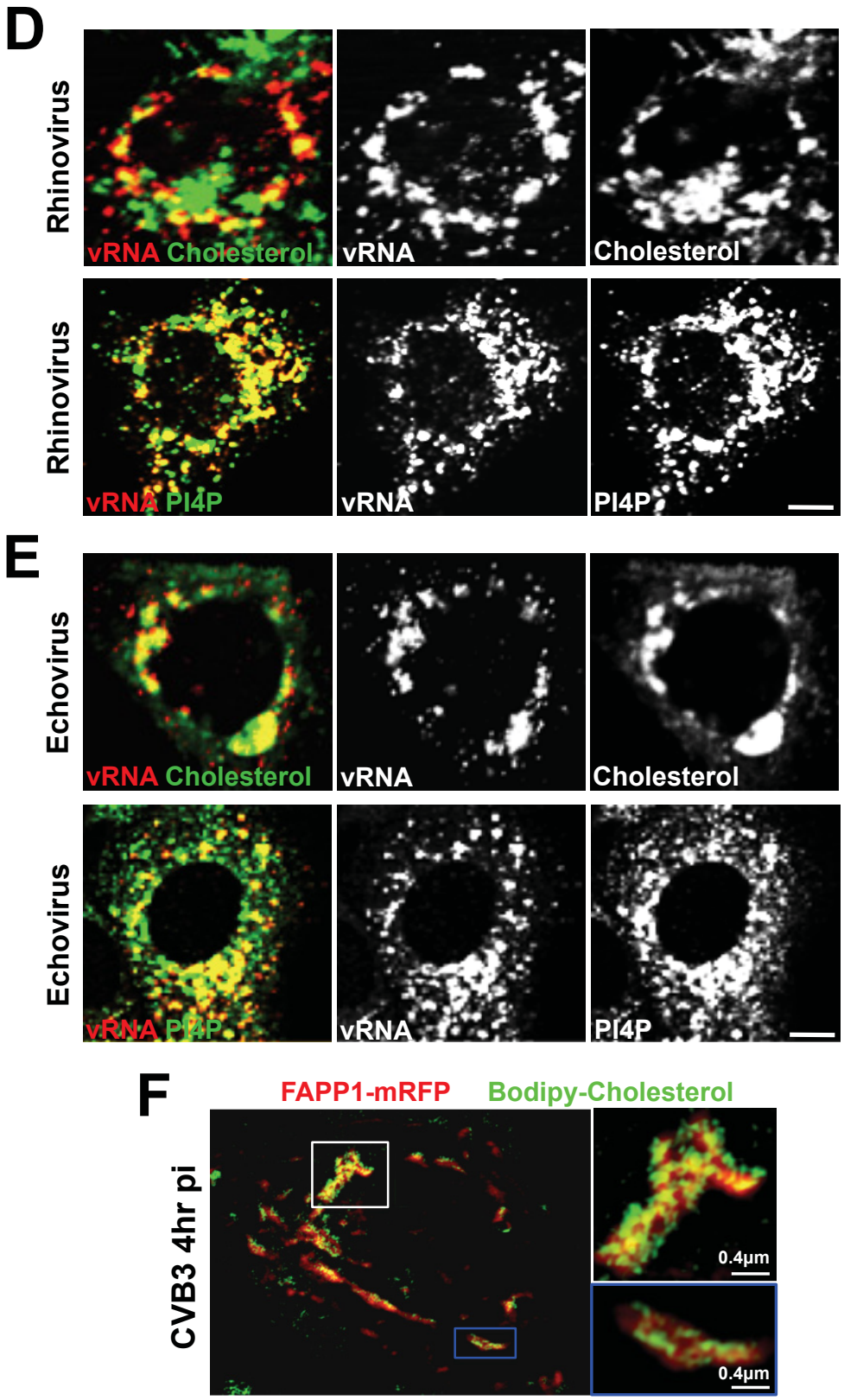
D
Rhinovirus
vRNA Cholesterol
vRNA
Cholesterol
Rhinovirus
vRNA PI4P
vRNA
PI4P
E
Echovirus
vRNA Cholesterol
vRNA
Cholesterol
Echovirus
vRNA PI4P
vRNA
PI4P
F
FAPP1-mRFP
Bodipy-Cholesterol
CVB3 4hr pi
0.4μm
0.4μm

Figure 2. Enteroviral Replication Organelles are Enriched in Cholesterol and PI4P Lipids

A. Free cholesterol (green) and PI4P lipid (red) distribution in control uninfected cells. Scale bar, 5μm.

B. CVB-3 infected cells at peak replication time. VROs (3A red) are enriched in cholesterol and PI4P lipids (green). Scale bar, 5μm.

C. PV-1 infected cells at peak replication time. VROs (3AB red) are enriched in cholesterol and PI4P lipids (green). Scale bar, 5μm.

D. Rhinovirus-2 infected cells show that cholesterol and PI4P lipids (green) are in VROs (red), identified by viral RNA labeling. Scale bar, 5μm.

E. Echovirus-11 infected cells show that cholesterol and PI4P lipids (green) are in VROs (red), identified by viral RNA labeling. Scale bar, 5μm.

F. SIM image of CVB3 infected cell showing the domain distribution of free cholesterol (green) on PI4P lipid (identified by FAPP1-mRFP) rich VROs. Scale bar, 0.4μm.

CHAPTER 4

Free Cholesterol Is Necessary For Viral Replication And Viral Protein Processing

Until now we established that cholesterol is present at VROs, but now we wanted to know if cholesterol was required during viral replication. Cholesterol's function during viral infection has been associated with its role in viral entry and antiviral immune response (Mackenzie et al. 2007; Mercer et al. 2010). In this chapter, we focus on investigating whether cholesterol has a role, other than virus entry, in viral infection by perturbing cholesterol levels in cells.

RESULTS:

Cholesterol Removal from Viral Replication Organelles Inhibits Replication

We wanted to know if the cholesterol in the VROs was necessary for viral replication. In the following experiments we aimed to lower the cellular cholesterol levels by different approaches to assess the influence on virus replication. To bypass the effects of cholesterol disruption on viral entry, the experiments were performed with viral replicons, with the exception of RV-2. The viral replicons for CVB and PV used in this project are viruses in which the gene coding sequence for the structural proteins (P1 region of the virus genome) has been replaced for the *Renilla* luciferase gene, and the replication is assessed by the levels of luciferase expression in the cells (Belov et al. 2007; Lanke et al. 2009).

First, we lowered the levels of the intracellular pool of cholesterol and incubated cells in serum free media or in LDL-deficient media for 48 hours before transfection with CVB or PV replicons, or 1 hour after replicon transfection. We found that in both conditions viral replication was inhibited by 40% as compared to untreated controls (Figure 3A). Then we considered the possibility of the cell sensing the depletion of intracellular cholesterol and triggering biosynthesis to compensate. To test this possibility, cells were treated LDL-deficient media supplemented with lovastatin at 5, 10, or 25μM for 72 hours. Lovastatin is a competitive inhibitor of HMG-CoA in the rate-limiting step of the mevalonate pathway, blocking the de *novo* production of cellular cholesterol (Alberts 1988; Goldstein and Brown 1990). After the 72hr treatment, cells were transfected with CVB or PV replicons. And for RV cells were infected before addition of the LDL-deficient/lovastatin media. After this treatment, we found that infection was inhibited up to 70% in a dose dependent manner compared to untreated controls (Figure 3B).

Secondly, we analyzed the effects of lowering the level of cholesterol from the plasma membrane pool that, as I noted previously, makes up to 90% of the cellular cholesterol. To test this, we acutely treated cells with MβCD, which is a drug used to remove cholesterol from cellular membranes (Christian, et al. 1997), at 10mM concentration for 1hr before transfecting them with an RNA reporter in control cells, and CVB or PV replicons. This mRNA reporter is capped and polyadenylated and encodes a fluorescent protein, and was included in these project as a control for RNA transfection and translation efficiency. The effects of

plasma membrane cholesterol depletion show inhibition of replication in both CVB and PV transfected cells. Furthermore, the inhibition was significantly rescued with the addition of exogenous cholesterol for 1 hour after the extraction assay was performed (Figure 3C & 3D). In addition, we found that viral replication organelle formation was inhibited (Figure 3E). For this experiment, we fixed samples under the same above conditions and immunolabeled with antibodies against either viral protein 3A or dsRNA, and stained the cholesterol pools with filipin.

High Levels of Cholesterol Stimulate Viral Replication

With the data from these experiments showing that cholesterol depletion inhibits viral replication, we wanted to find out what will be the effects of the opposite situation, where cellular cholesterol levels are high. For the following experiments, we selected as our model system Niemann-Pick type C (NPC) diseased cells. These cells come from patients suffering from Niemann-Pick disease and are characterized for the abnormal high levels of intracellular free cholesterol which is caused by the loss of function mutation in the NPC1 and/or NPC2 endosomal cholesterol transporter proteins that disrupts the export of cholesterol out of the endosomes while biosynthesis in the ER is unaffected (Rosenbaum and Maxfield 2011; Wang and Song 2012). Primary human wild type ($NPC1^{wt}$ and $NPC2^{wt}$) and mutant ($NPC1^{-/-}$ and $NPC2^{-/-}$) fibroblast cells' phenotype shows the increased levels of cholesterol in the diseased cells as compared to wild type control cells (Figure 4A) were transfected with PV replicon or control reporter and assessed for replication efficiency. We found that in the

mutant cells, there was an approximate 3-fold increase in replication compared to wild type cells (Figure 4B & 4C); and also a 3-fold increase in the amount of cholesterol at VROs (Figure 4D & 4E). Furthermore, acute MβCD treatment of mutant cells to lower the cholesterol pools inhibited replication by approximately 60% compared to mock treated wild type cells (Figure 4F). This showed that the cholesterol was stimulating viral replication in these mutant NPC cells.

Cholesterol is Critical in Viral Protein Processing

Finally, we sought to identify in which way was cholesterol involved during viral replication and looked at the levels of viral proteins when cholesterol is disrupted. Cells were pretreated with MβCD for 1 hour, or treated with filipin at 3hr post infection; and lysates were collected for western blot analysis. Filipin has been widely used to sequester cholesterol at the plasma membrane (Nichols et al. 2001). We found that the proteolytic processing of viral $3CD^{pro}$ in treated cells was stimulated by approximately 8-fold as compared to mock treated controls and was specific for $3CD^{pro}$, since no stimulation was evident in either 2BC or 3AB processing (Figure 5A & 5B). As previously stated, proteolytic processing has a very important role on viral replication, in particular, the processing of $3CD^{pro}$. Viral $3CD^{pro}$ is required for the formation of the replication complex, for priming viral RNA synthesis, and for processing capsids. Viral $3CD^{pro}$ is also cleaved in *cis* to generate the viral proteins $3C^{pro}$, responsible for the processing of other viral proteins, and $3D^{pol}$, the RNA-dependent RNA polymerase that replicates the genome (Andino et al. 1990; and Cornell and Semler 2002). Therefore, the decrease in $3CD^{pro}$ pools can inhibit both initiation of viral RNA

synthesis and viral encapsidation. Concomitant with these results, we looked at the mutant NPC cells and found that $3CD^{pro}$ processing in these cells was significantly attenuated as compared to the wild type control cells (Figure 5C).

CONCLUSION:

Together this data demonstrates that free cholesterol from both the internal pool or the plasma membrane has a facilitative role in enteroviral replication, and in addition, cholesterol is critical for viral replication organelle biogenesis. Since, removal of cellular cholesterol inhibits virus replication and the formation of VROs. Concomitant with the effects of lowering cellular cholesterol, the opposite happens in situations where cholesterol is in excess, in NPC mutant cells viral replication is stimulated. Moreover, we were able to confirm by analyzing the viral proteolytic processing kinetics that cholesterol is critical for regulating $3CD^{pro}$ processing and the levels of $3C^{pro}$ and $3D^{pol}$.

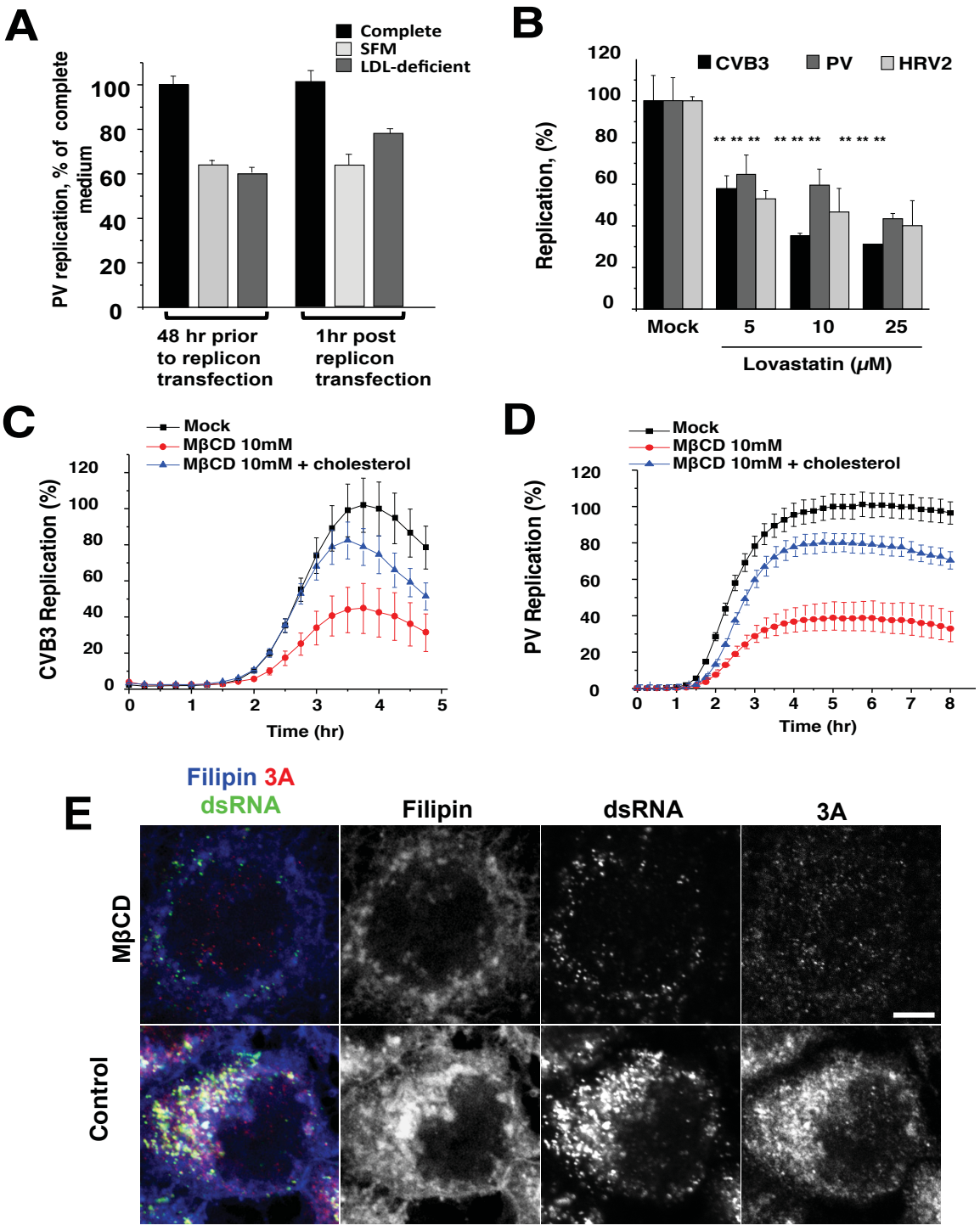
A
Complete
SFM
LDL-deficient
PV replication, % of complete medium
48 hr prior to replicon transfection
1hr post replicon transfection
B
CVB3
PV
HRV2
Replication, (%)
Mock
Lovastatin (μM)
C
Mock
MβCD 10mM
MβCD 10mM + cholesterol
CVB3 Replication (%)
Time (hr)
D
Mock
MβCD 10mM
MβCD 10mM + cholesterol
PV Replication (%)
Time (hr)
E
Filipin 3A
dsRNA
Filipin
dsRNA
3A
MβCD
Control

Figure 3. Cholesterol Removal from Viral Replication Organelles Inhibits Replication

A. Replication of PV replicon is inhibited when cells are in the presence of serum free or LDL-deficient media. Treatments were performed at 48 hours prior to or at 1-hour post replicon transfection. Values represent percent of replication in cells treated with complete media. Mean data from 3 independent experiments were normalized with respect to cell viability and plotted +/- SEM. Standard errors were calculated using the Student t-Test for unpaired data with unequal variance function.

B. Lovastatin treatment inhibits PV, CVB, and HRV replication in a dose dependent manner. Cells were grown in LDL-deficient media supplemented with Lovastatin and 250μM mevalonate for 72 hours before PV or CVB replicon transfection. For HRV, cells were infected prior to treatments. Mean data from 3 independent experiments were normalized with respect to cell viability and presented as percent of vehicle treated cells. Then plotted +/- SEM. **:$p<0.01$. Standard errors and p-values were calculated using the Student t-Test for unpaired data with unequal variance function.

C. Acute depletion of plasma membrane cholesterol with MβCD inhibits CVB replicon replication, but exogenous addition of cholesterol back to these membranes significantly rescues replication. Mean data +/- SEM from six replicates for each condition was normalized by luciferase mRNA expression. Standard errors were calculated using the Student t-Test for unpaired data with unequal variance function.

D. Acute depletion of plasma membrane cholesterol with MβCD inhibits PV replicon replication, but exogenous addition of cholesterol back to these membranes significantly rescues replication. Mean data +/- SEM from six replicates for each condition was normalized by luciferase mRNA expression. Standard errors were calculated using the Student t-Test for unpaired data with unequal variance function.

E. Acute depletion of plasma membrane cholesterol with MβCD inhibits viral replication organelle biogenesis. Cholesterol was stained with filipin (blue), viral replication organelles with antibodies against viral protein 3A (red) and viral dsRNA (green). Scale bar, 5μm.

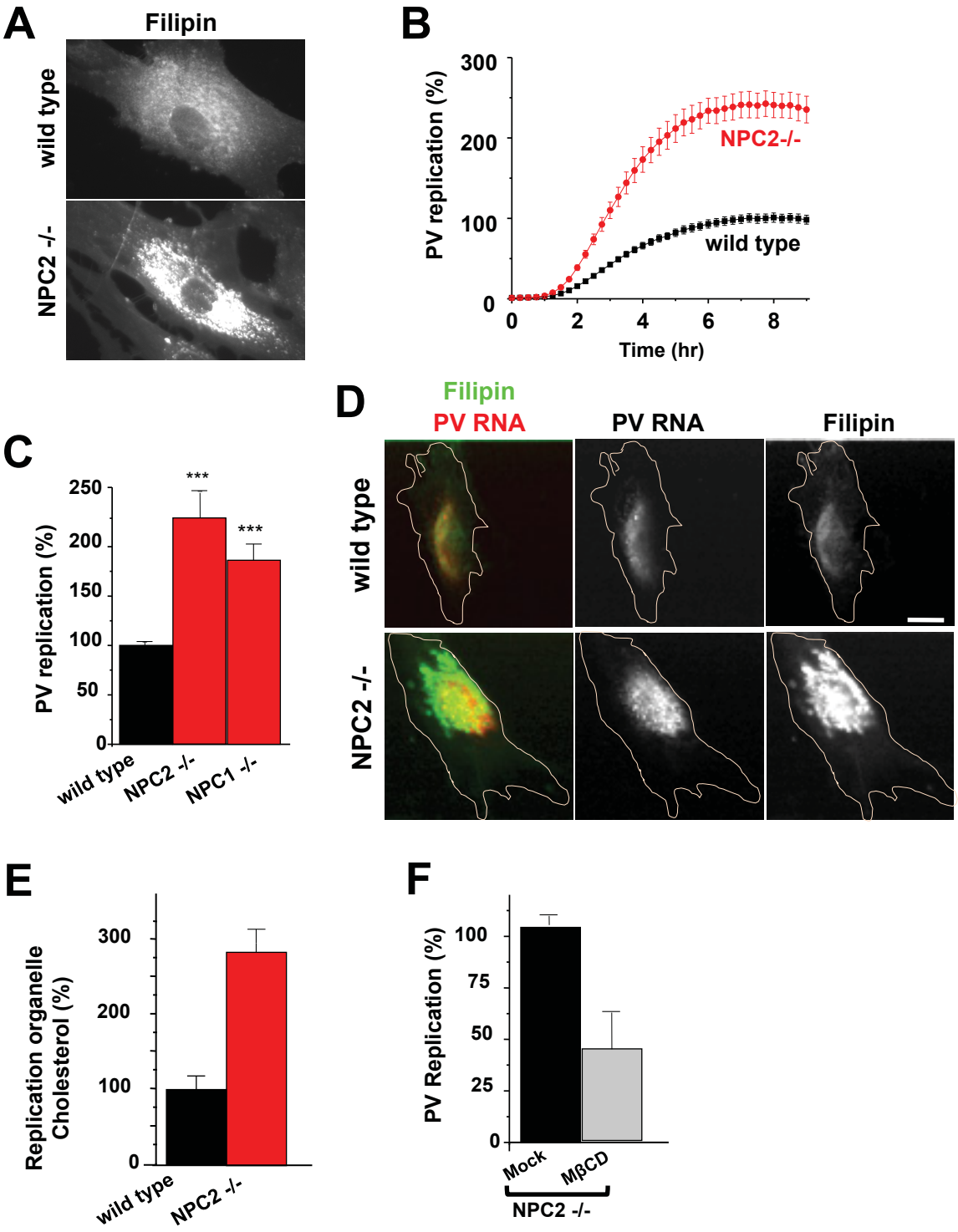
A
Filipin
wild type
NPC2 -/-
B
PV replication (%)
300
200
100
0
NPC2-/-
wild type
0
2
4
6
8
Time (hr)
C
PV replication (%)
250
200
150
100
50
0
***
***
wild type
NPC2 -/-
NPC1 -/-
D
Filipin
PV RNA
PV RNA
Filipin
wild type
NPC2 -/-
E
Replication organelle Cholesterol (%)
300
200
100
0
wild type
NPC2 -/-
F
PV Replication (%)
100
75
50
25
0
Mock
MβCD
NPC2 -/-

Figure 4. High Levels of Cholesterol Stimulate Viral Replication

A. Free cholesterol distribution in wild type and NPC2$^{-/-}$ mutant fibroblasts (high intracellular pools). Cholesterol was labeled with filipin.

B. PV replicon replication is stimulated in NPC2$^{-/-}$ fibroblasts. Mean data +/- SEM from 6 replicates was plotted. Standard errors were calculated using the Student t-Test for unpaired data with unequal variance function.

C. Peak PV replication levels are stimulated in both NPC1$^{-/-}$, and NPC2$^{-/-}$ mutant fibroblast cells. Mean data +/- SEM from 5 replicate experiments were normalized by expression of reporter luciferase RNA and plotted. ***$p<0.001$. Standard errors and p-values were calculated using the Student t-Test for unpaired data with unequal variance function.

D. Free cholesterol distribution at peak replication time in NPC2$^{-/-}$ fibroblast cells. Cholesterol was labeled with filipin (green) and VROs with an antibody against viral dsRNA (red). Scale bar, 10μm.

E. Free cholesterol levels at VROs in NPC2$^{-/-}$ mutant fibroblasts are ~3 fold greater than in wild type fibroblasts. Mean fluorescence data +/- SEM, from n=30 of each wild type and NPC2$^{-/-}$ fibroblasts are plotted. Standard errors were calculated using the Student t-Test for unpaired data with unequal variance function.

F. Acute depletion of cholesterol in NPC2$^{-/-}$ mutant fibroblasts with MβCD inhibits PV replicon replication by 60% as compared to mock treated wild type fibroblasts. Mean data +/- SEM from 2 independent experiments is plotted.

Standard errors were calculated using the Student t-Test for unpaired data with unequal variance function.

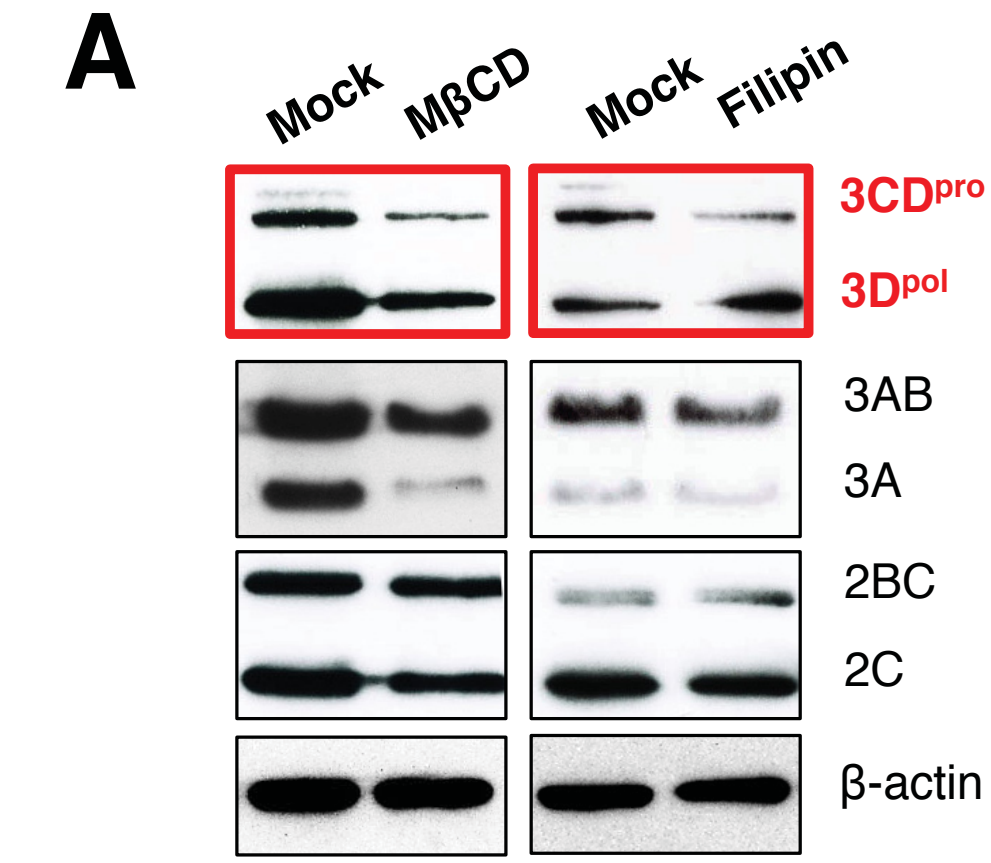
A
Mock
MβCD
Mock
Filipin
3CDpro
3Dpol
3AB
3A
2BC
2C
β-actin

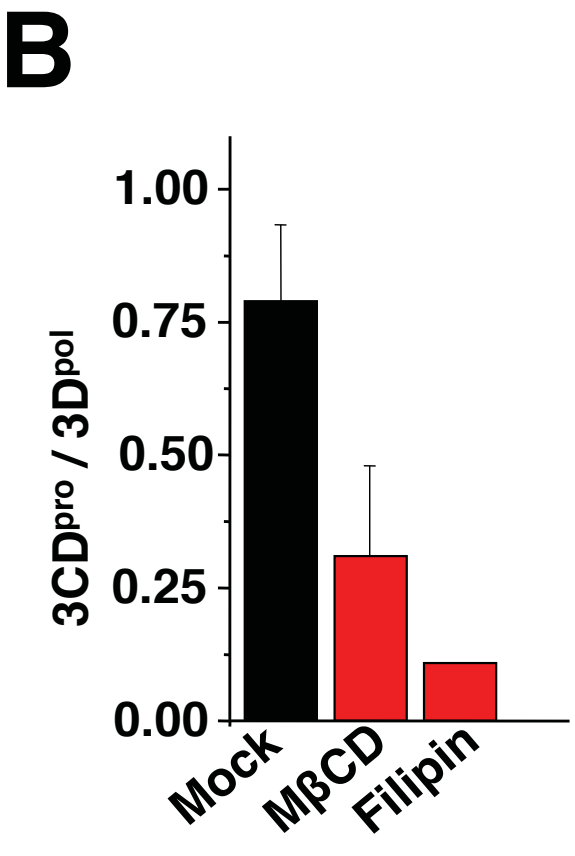
B
3CDpro / 3Dpol
1.00
0.75
0.50
0.25
0.00
Mock
MβCD
Filipin

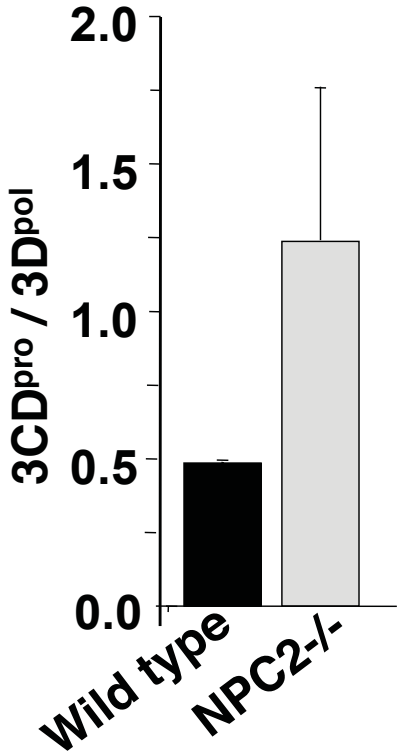
C
3CDpro / 3Dpol
2.0
1.5
1.0
0.5
0.0
Wild type
NPC2-/-

Figure 5. Cholesterol is Critical in Viral Protein Processing

A. Processing of viral $3CD^{pro}$ is stimulated when cholesterol is depleted with MβCD or its organization disrupted with Filipin before or during viral infection. The top 2 bands of the blot show the levels of $3CD^{pro}$ are lower than the $3D^{pol}$ in both treatment conditions. Immunoblot analysis of $3CD^{pro}$, 3AB, and 2BC processing into one of its viral protein products $3D^{pol}$, 3A, and 2C respectively after mock, MβCD (1 hour pretreatment), or filipin treatment (at 3 hour post infection). Viral proteins were harvested at 5-hour post infection.

B. $3CD^{pro}$ to $3D^{pol}$ protein ratio after cholesterol perturbation is lower as compared to mock treated cells meaning $3CD^{pro}$ processing is significantly stimulated. Mean data +/- SEM from 3 independent experiments are plotted. Standard errors were calculated using the Student t-Test for unpaired data with unequal variance function.

C. $3CD^{pro}$ to $3D^{pol}$ ration in $NPC2^{-/-}$ mutant fibroblasts is significantly higher as compared to wild type fibroblasts meaning $3CD^{pro}$ processing is attenuated. Mean data +/- SEM from 3 independent experiments are plotted. Standard errors were calculated using the Student t-Test for unpaired data with unequal variance function.

CHAPTER 5

Cellular Cholesterol Homeostasis And Dynamics Of Plasma Membrane Free Cholesterol Redistribution

Thus far, we have established that cholesterol is in the VROs and is necessary for VRO production, $3CD^{pro}$ processing, and viral replication. This chapter is focused on identifying the source of free cholesterol and the possible mechanism by which the cellular free cholesterol pool gets localized to the VROs during infection. Cholesterol in cells can be found in 2 forms: unesterified (free) intercalated in the cellular membranes, and available for cellular processes, or esterified into cholesteryl esters and stored in lipid droplets. And cells can obtain cholesterol from 2 sources: by receptor mediated uptake of low-density lipoproteins (LDLs) from dietary sources, or from de *novo* synthesis through the mevalonate pathway in the ER (Ikonen 2008).

RESULTS:

Free Cholesterol Levels Increase During Viral Infection

The initial step was to assess any changes in the levels of unesterified and esterified cholesterol. Hela cells were seeded and infected with CVB or PV. Infected samples were collected at 4hr post infection along with uninfected control samples and processed using the Amplex Red Cholesterol Assay kit following the procedure described in Chapter 2. We found that the bulk levels of unesterified cholesterol had a net increase of 40% and the levels of esterified

cholesterol had a net decrease of 50% in infected samples at 4hr post infection as compared to uninfected controls (Figure 6A).

To determine the potential mechanism responsible for these changes, we first measured the levels of LDL uptake. In this experiment, we loaded control and CVB infected Hela cells with LDL tagged with the fluorescent probe Bodipy Fluor at 20μg/ml in CCM, and incubated the cells for 2 or 4hr. At each time point CCM was replaced with CICM and cells were imaged immediately. We found that LDL uptake was stimulated by approximately 30% within 2hr post infection, but by 4hr post infection, LDL uptake was inhibited by more than 50% (Figure 6B). Then we evaluated biosynthesis by measuring the incorporation of radioactive isotope 14C into the newly made cholesterol at 2, 4, and 6 hours post infection. Hela cells were labeled following the protocol described in Chapter 2. We found that biosynthesis is not interrupted during infection, but the levels of synthesis decreased by 30% within 2 hours post infection, perhaps due to the increased uptake of LDL in the same time frame; and synthesis increased back to control levels by 4+ hours post infection, this could be due to the removal of cholesterol as VROs are being formed (Figure 6C). On the other hand, lipid esterification levels were inhibited throughout infection (Figure 6C). This and the LDL results support the net increase in the bulk free cholesterol.

Plasma Membrane Cholesterol is Redistributed During Infection by Viral Protein 2BC

We next wanted to investigate the fate of the existing free cholesterol pools. Thus, we first studied the dynamics of the plasma membrane free

cholesterol pool. HeLa cells seeded the day before were transfected with FAPP1-mRFP (biomarker for VROs) and incubated overnight. Then cells were loaded with Bodipy-cholesterol and further incubated for 1hr to let the labeled cholesterol reach steady state distribution. Next, cells were infected with CVB and imaged immediately. Confocal time-lapse images of control and infected cells were obtained for the duration of the infection. We observed that in the CVB infected cells there was a rapid internalization of the plasma membrane cholesterol. Within 2 hours post infection, more than 90% of the fluorescent cholesterol was depleted from the plasma membrane (Figure 7A & 7B). Soon after internalization, these cholesterol rich vesicles were seen fusing with and releasing the Bodipy-cholesterol to the VROs (Figure 7A), showing active transfer of cholesterol to VROs.

One potential viral protein responsible for the increase LDL levels and the uptake of plasma membrane cholesterol is 2BC. The viral proteins 2B and 2BC are associated with remodeling host cytoplasmic membranes to generate viral replication organelles (Cho et al. 1994; Suhy et al. 2000). And it has been reported that the ectopic expression of the viral protein 2BC upregulates endocytosis of major histocompatibility complex class 1 (MHC1) and of other molecules such as the AM4-65, a styryl dye, which is incorporated into the plasma membrane and follows the endocytic pathway (Cornell et al, 2007; Deligeorgiev et al. 2010). We transfected Hela cells to ectopically express the bicistronic 2BC construct and were able to reproduce the published AM4-65 dye data in our system (Figure 7C). Furthermore, we found that exogenous

expression of 2BC alone was able to increase the levels of intracellular free cholesterol (Figure 7D). This data demonstrated the potential involvement of 2BC in the uptake of free cholesterol. Even though, it is still to be determined the specific role of viral 2BC in cholesterol uptake.

CONCLUSION:

In this chapter we were able to establish that during infection, CVB modulates the cellular cholesterol pools to increase the levels of free cholesterol that it can use to build replication platforms. The virus achieves this by increasing the uptake of LDL and by internalizing the existing free plasma membrane pool, while decreasing (or maintaining) base levels of cholesterol biosynthesis and inhibiting esterification and storage of the free cholesterol pool. We also found that the viral protein 2BC alone is able to increase the internal free cholesterol pool, but it is important to mention that we still need to determine how is 2BC involved in this process.

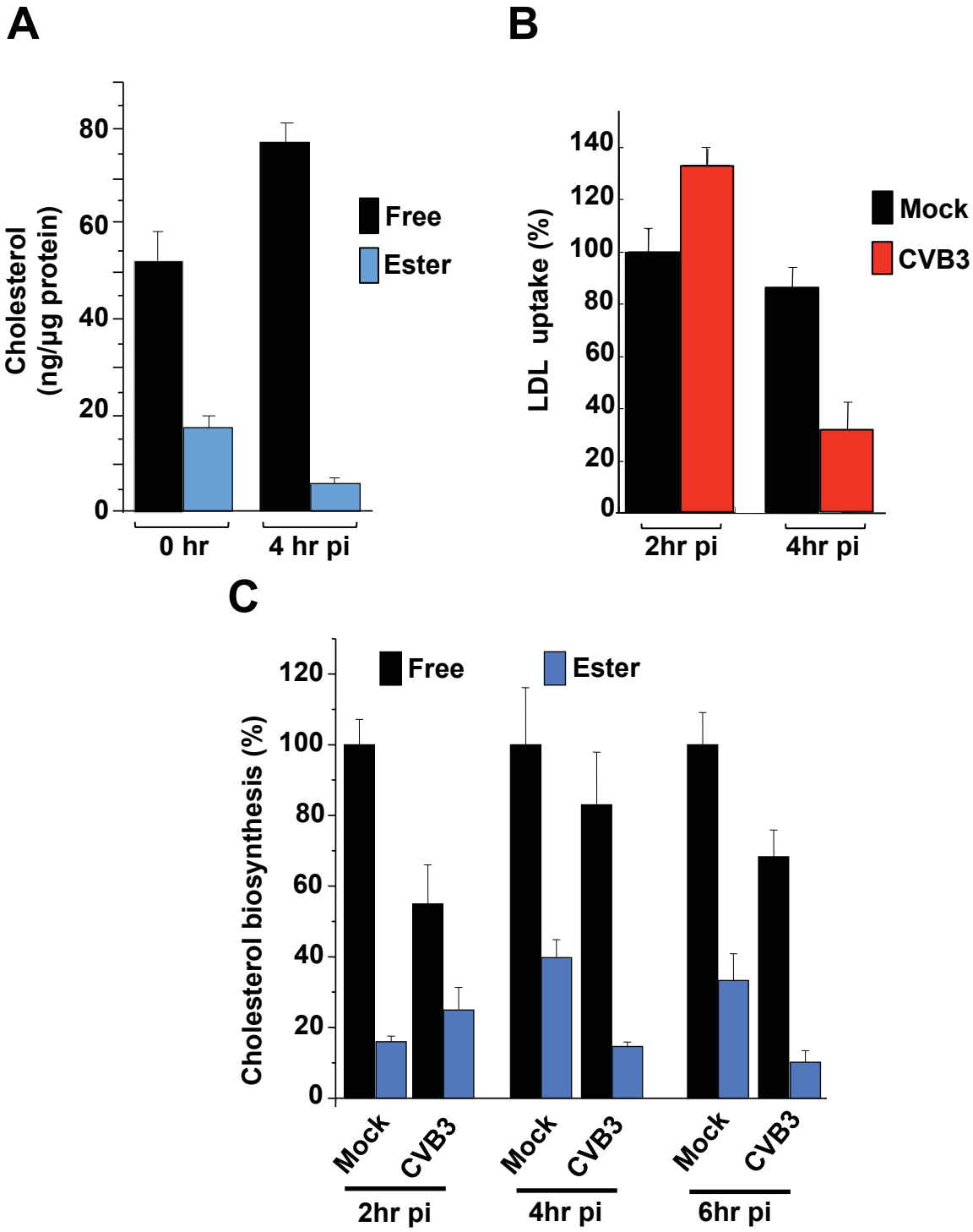
A
Cholesterol (ng/µg protein)
0
20
40
60
80
Free
Ester
0 hr
4 hr pi
B
LDL uptake (%)
0
20
40
60
80
100
120
140
Mock
CVB3
2hr pi
4hr pi
C
Cholesterol biosynthesis (%)
0
20
40
60
80
100
120
Free
Ester
Mock
CVB3
Mock
CVB3
Mock
CVB3
2hr pi
4hr pi
6hr pi

Figure 6. Free Cholesterol Levels Increase During Viral Infection

A. Free cholesterol pools (black bars) are increased while esterified cholesterol pools (blue bars) is decreased by peak CVB replication time as compared to mock infected control cells. Quantification of free and esterified cholesterol pools at 0 and 4 hours post CVB infection. Mean data +/- SEM from 3 independent experiments are plotted. Standard errors were calculated using the Student t-Test for unpaired data with unequal variance function.

B. LDL uptake is increased by 2 hours and it decreases by 4 hours post CVB infection. Mean Bodipy-LDL uptake data from CVB infected cells at 2 hours and 4 hours post infection and for mock infected at 4 hours post infection were plotted as percentage of uptake of mock infected cells at 2 hours post infection (n=30), +/- SEM. Standard errors were calculated using the Student t-Test for unpaired data with unequal variance function.

C. Free cholesterol biosynthesis decreases within 2 hours post infection and increases again by 4 and 6 hours post infection. Cholesterol esterification is maintained throughout infection. Free and esterified cholesterol biosynthesis at 2, 4, and 6 hours post CVB infection. Mean data +/- SEM from 1 experiment with 3 replicates are plotted. Standard errors were calculated using the Student t-Test for unpaired data with unequal variance function.

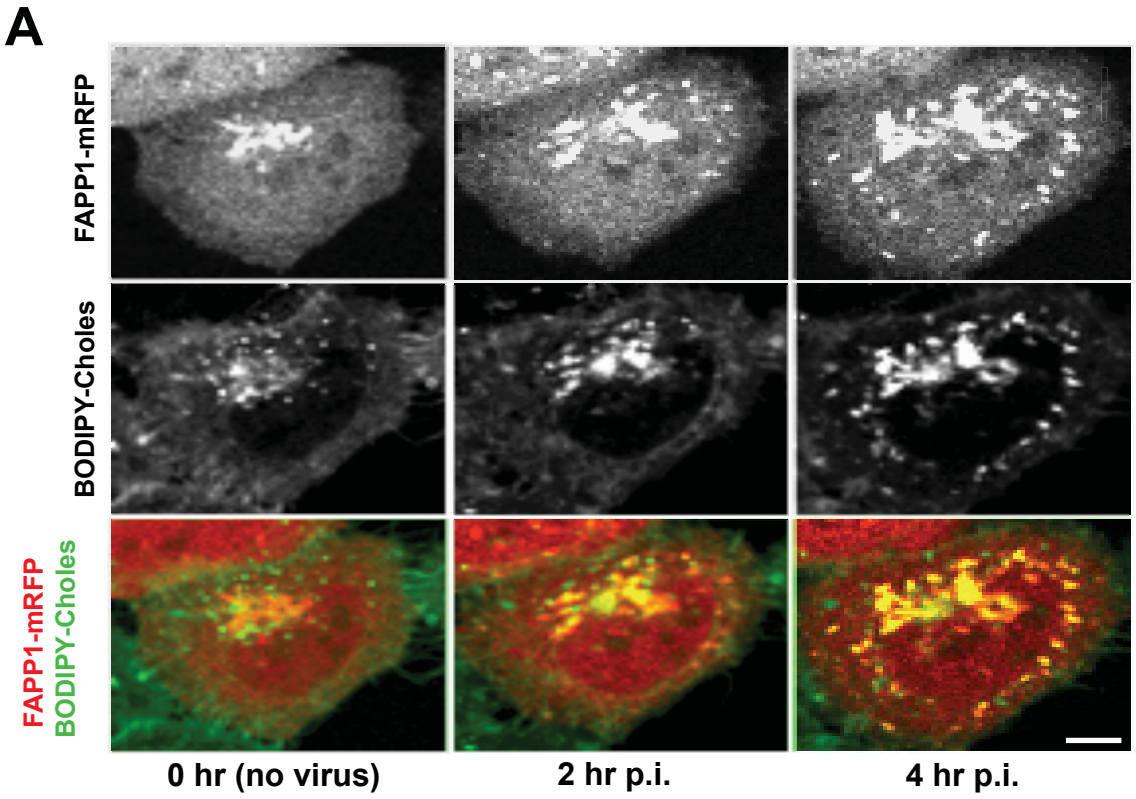
A
FAPP1-mRFP
BODIPY-Choles
FAPP1-mRFP
BODIPY-Choles
0 hr (no virus)
2 hr p.i.
4 hr p.i.

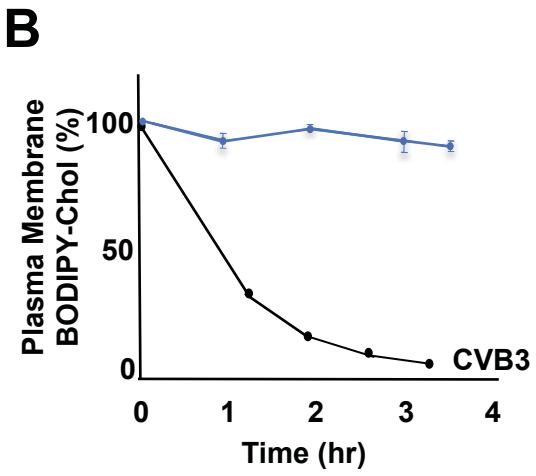
B
Plasma Membrane
BODIPY-Chol (%)
100
50
0
CVB3
0
1
2
3
4
Time (hr)

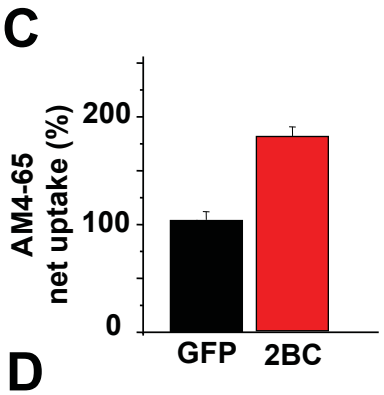
C
AM4-65
net uptake (%)
200
100
0
GFP
2BC

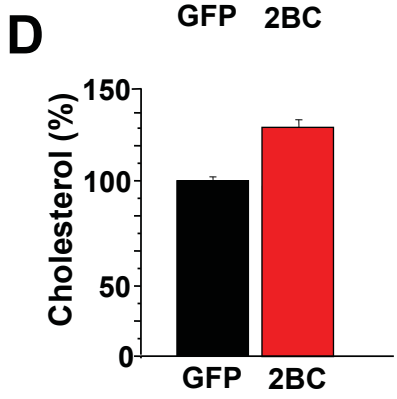
D
Cholesterol (%)
150
100
50
0
GFP
2BC

Figure 7. Plasma Membrane Cholesterol is Redistributed During Infection by Viral Protein 2BC

A. Free cholesterol (green) redistributes from plasma membrane to replication organelles (red) during CVB infection. FAPP1-mRFP (VRO marker) expressing cells were loaded with Bodipy-cholesterol then infected with CVB before time-lapse confocal imaging. Scale bar 5μm**.**

B. Plasma membrane Bodipy-cholesterol decreased by more than 60% within 2 hours post infection, and by peak replication time, over 90% of the plasma membrane cholesterol was depleted in CVB infected cells as compared to uninfected control samples. Mean fluorescence data +/- SEM from uninfected and CVB infected cells (n=10) are plotted. Standard errors were calculated using the Student t-Test for unpaired data with unequal variance function.

C. Quantification of perinuclear AM4-65 fluorescence in 2BC-GFP expressing cells show a 2 fold increase in internalized AM4-65 as compared to mock GFP transfected cells. Cells were pulsed with AM4-65 for 10 minutes, and chased for 30 minutes in media lacking AM4-65. Mean data from 2BC expressing cells is plotted as percentage of mock cells +/- SEM (from n=50 cells for each condition)**.** Standard errors were calculated using the Student t-Test for unpaired data with unequal variance function.

D. Quantification of intracellular free cholesterol pools in 2BC-GFP expressing cells show ~30% increase as compared to mock GFP transfected cells. Cells were labeled with filipin prior to imaging. Mean data from 2BC expressing cells is plotted as percentage of mock cells +/- SEM (from n=50 cells for each

condition). Standard errors were calculated using the Student t-Test for unpaired data with unequal variance function.

CHAPTER 6

The Endocytic Machinery Is Required For Cellular Cholesterol Homeostasis And Viral Replication

The increase in uptake of LDL, the redistribution of the plasma membrane cholesterol, and the 2BC upregulation of endocytosis provided us with an initial evidence of the involvement of the clathrin mediated endocytosis pathway. Consequently, in this chapter we will focus on understanding the role of the main components of the endocytic machinery in enteroviral infection, independent of viral entry.

RESULTS:

Endocytic Machinery Regulates Viral Replication

To identify the impact on viral replication, we performed a siRNA screen on a subset of genes involved in CME and endosomal compartmentalization. siRNA constructs were designed to specifically target the following human genes: clathrin, AP2, dynamin 2, Rab5, Rab11, Huntingtin interacting protein 1 (HIP1), Disabled 2 (DAB2), and Epsin15L. In this set of experiments, we transfected into cells either CVB or PV replicons to bypass the impact on replication from viral entry, disassembly, and/or export. HeLa cells were treated with a non-target (control) siRNA or with siRNA targeted to specific genes before transfecting the cells with CVB or PV replicons. We were able to achieve more than 75% depletion of the target proteins in our siRNA treated cells (Figure 8A). We found that in the target siRNA treated cells; there was a significant inhibition of CVB

and PV replication (Figure 8B & 8C). Furthermore, in samples fixed and immunolabeled against the target proteins and viral 3A, we found that replication organelle biogenesis was disrupted (Figure 9A, 9B, & 9C).

In addition to the above target genes, we also studied the effects of Cav1 and Cav2 siRNA depletion, which are part of the CIE. We found that when Cav1 or Cav2 was depleted, viral replication in these cells was stimulated by 3-fold compared to non-target treated control cells (Figure 10A, 10B, & Table 1). We analyzed the transfection levels and found that Cav2 depletion did not affect Cav1 levels, but Cav1 depletion decreased Cav2 levels (Figure 10B); suggesting that Cav2 mediates the increase of cholesterol in internal pools consequently stimulating viral replication. Measurements were normalized for cell viability that was largely unaffected by siRNA treatment; and there was no correlative impact on transfection/translation efficiency of the control reporter mRNA (Table 1).

Depletion of CME, Endosomal Machinery, and CIE Proteins Modify Host Cellular Free Cholesterol Pools

Maintaining cellular cholesterol homeostasis is a tightly controlled process. Homeostasis is regulated mainly by the sterol regulatory element binding protein (SREBP) pathway that activates the transcription of genes involved in either synthesis or storage of cholesterol (Rawson 2003). When there is a need for cholesterol, cells either upregulate the receptor-mediated uptake of LDL molecules from the extracellular matrix or synthesize new cholesterol in the ER (mevalonate pathway). And when there is an excess of cholesterol, the cells esterify and store it in lipid droplets through an esterification process in the ER

catalyzed by acyl CoA cholesterol acyltransferase (ACAT) (Hsieh, et al. 2012; Ikonen 2008). Therefore, we moved our attention to assaying the fate of the cellular cholesterol in uninfected cells. We wanted to see if any changes in the cellular cholesterol homeostasis would potentially result in the effects on viral replication observed in the experiments from the siRNA screen.

Cells were depleted of target proteins by siRNA treatment followed by pulse chase experiments with Bodipy-cholesterol; images were acquired within 30 minutes of Bodipy-cholesterol loading. We found that in cells depleted of either CME or endosomal target proteins (clathrin, AP2, dynamin, Rab5, Rab11, HIP1, DAB2, and Epsin15L), Bodipy-cholesterol was trafficked to abundant, spherical cytoplasmic structures that we identified to be lipid droplets since these stained with Nile Red (Figure 11A). Nile Red binds to neutral lipids and has been used to successfully label intracellular lipid droplets (Greenspan and Fowler 1985; Greenspan et al. 1985). In addition, we fixed siRNA treated samples and immunolabeled for the target proteins and for the adipose differentiation-related protein (ADRP), this protein is universally expressed in storage lipid droplets, (Faleck et al. 2010); and we were able to confirm that the observed structures were storage lipid droplets (Figure 11B).

Moreover, at steady state in these target siRNA treated cells, there was up to 6-fold more lipid droplets per cell as compared to the non-target treated control cells (Figure 11C). Concomitant with the increase in lipid droplet number, these cells' bulk cholesterol measurement revealed an approximately 3-fold increase in the esterified pool (Figure 11D), while the free unesterified pool had a small

decrease of less than 20% (Figure 11E). To further clarify if the increase in the esterified cholesterol pool was due to an increase in LDL uptake or not, we grew Hela cells in media supplemented with LDL-deficient serum, before siRNA transfection, and found that cholesterol storage was still enhanced (Figure 11F). In addition, we transfected Hela cells grown in LDL deficient media with the PV replicon, and found that viral replication was inhibited by approximately 50% similar to control cells grown in CCM (Figure 11G); suggesting that the intracellular free cholesterol pools, mainly from the plasma membrane, were being trafficked to the ER for storage in lipid droplets.

On the other hand, when we depleted cells of Cav1 or Cav2, the Bodipy-cholesterol distribution at steady state was the same compared to the non-target control cells; but after bulk measurements of the cholesterol pools, there was up to 50% increase in free cholesterol (Figure 12A). And was confirmed in fix samples labeled with filipin, that the cholesterol was more abundant at plasma membrane and intracellular membranes (Figure 12B). We measured the level of SREBP-2 in Cav1/Cav2 siRNA treated cells, and we found that the level did not increase providing evidence that the increase of free cholesterol in these cells was not due to cholesterol biosynthesis (Figure 12C). In contrast, when cells were treated with media supplemented with LDL-deficient serum, the free cholesterol level did not increase (Figure 12D); moreover, we found that in cells grown in LDL deficient media and transfected with the PV replicon, viral replication was inhibited as compared with control cells grown in CCM (Figure 12E); showing that the free cholesterol in these cells was derived from the uptake

of LDL. These results give an insight that caveolin 1 and 2 may be modulating the transfer of cholesterol, derived from LDL uptake, to the ER.

CONCLUSION:

In this chapter, we show that essential components of the CIE, CME, and endosomal trafficking pathways regulate enteroviral replication downstream of viral entry. Depletion of CME and endosomal trafficking proteins by siRNA inhibits replication; while, depletion of Caveolins stimulates replication. We also found that these proteins are essential for maintaining cellular cholesterol homeostasis. Depletion of CME and endosomal trafficking proteins gave a strong phenotype, where the free cellular cholesterol pool was being esterified and stored in lipid droplets, which could be the reason for the inhibition or viral replication; since free cholesterol is unavailable for the virus to form stable viral replication platforms. Parallel to these results, we found that depletion of Caveolins gave the opposite phenotype; these cells had an increased free cellular cholesterol pool derived from the uptake of LDL. Consequently, viral replication is stimulated during infection, since host cells have more free cholesterol available for the virus to use.

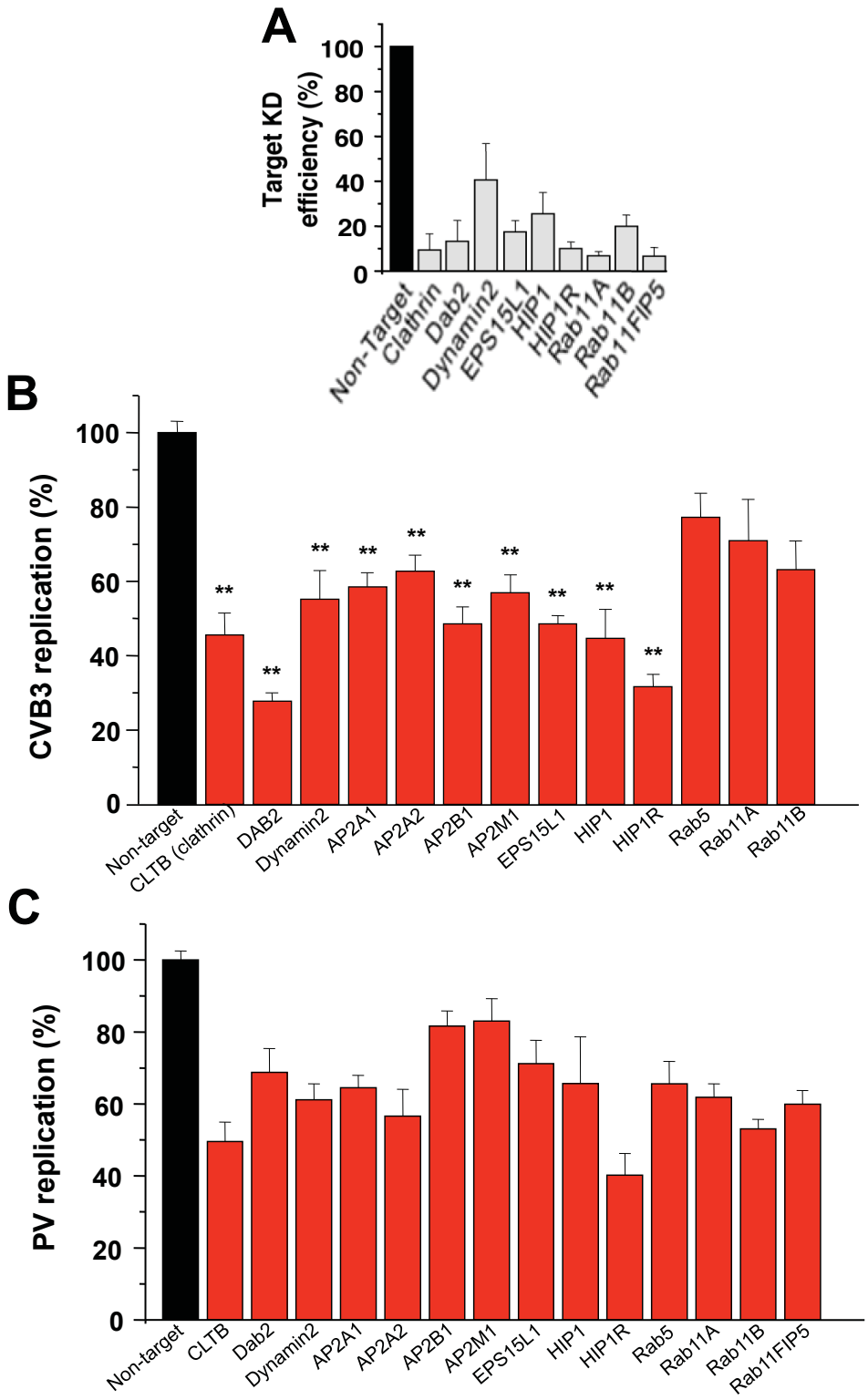
A
Target KD efficiency (%)
100
80
60
40
20
0
Non-Target
Clathrin
Dab2
Dynamin2
EPS15L1
HIP1
HIP1R
Rab11A
Rab11B
Rab11FIP5
B
CVB3 replication (%)
100
80
60
40
20
0
**
Non-target
CLTB (clathrin)
DAB2
Dynamin2
AP2A1
AP2A2
AP2B1
AP2M1
EPS15L1
HIP1
HIP1R
Rab5
Rab11A
Rab11B
C
PV replication (%)
100
80
60
40
20
0
Non-target
CLTB
Dab2
Dynamin2
AP2A1
AP2A2
AP2B1
AP2M1
EPS15L1
HIP1
HIP1R
Rab5
Rab11A
Rab11B
Rab11FIP5

Figure 8. Endocytic Machinery Regulates Viral Replication

A. Knockdown efficiency of selected endocytic machinery genes was performed in HeLa cells. Up to 75% depletion of the target proteins was achieved with our siRNA treatment. Knockdown of AP2 subunits (A1, A2, B1, and M1) deplete AP2M1 (Motley2003, Gu 2013). Bar graphs represent quantification of knockdown efficiency in immunoblot analysis. Data are expressed as percent of the mean values ± SEM from 3 independent experiments for each knockdown normalized to Non target siRNA.

B. CVB replicon replication is inhibited by up to 50% as compared to non-target siRNA treated control cells when components of the endocytic machinery are depleted by siRNA treatment. Mean peak replication data +/- SEM, from 2 independent experiments with six replicates each, were normalized with respect to cell viability and plotted as percentage of non-target siRNA treated cells. **$p<0.01$.

C. PV peak replicon replication was inhibited by up to 50% as compared to non-target siRNA treated control cells when components of the endocytic machinery are depleted by siRNA treatment. Data was normalized by cell viability and represented as percentage of the non-target siRNA sample. Data from 2 to 4 independent experiments with 4 to 6 replicates each +/-SEM was plotted.

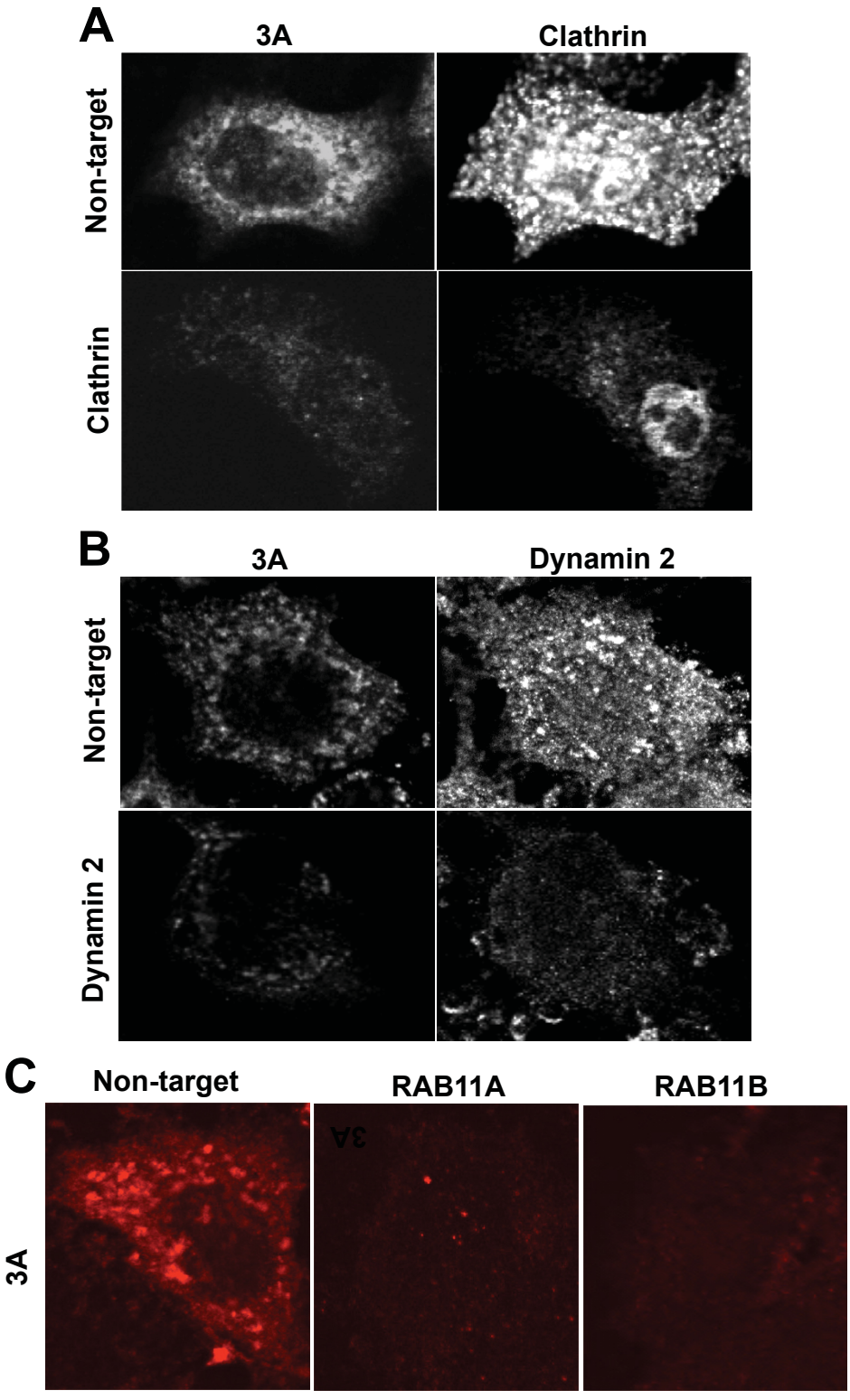
A
3A
Clathrin
Non-target
Clathrin
B
3A
Dynamin 2
Non-target
Dynamin 2
C
Non-target
RAB11A
RAB11B
3A

Figure 9. Endocytic Machinery Regulates Viral Replication Organelle Biogenesis

Replication organelle biogenesis is severely inhibited in cells depleted of endocytic components. Clathrin light chain (A), Dynamin (B), Rab11 A or Rab11B (C) was depleted by siRNA treatment for 48 hours prior to CVB3 infection. Cells were subsequently immunolabeled with antibodies against target proteins; and antibodies targeting enteroviral 3A protein were used to detected replication organelles.

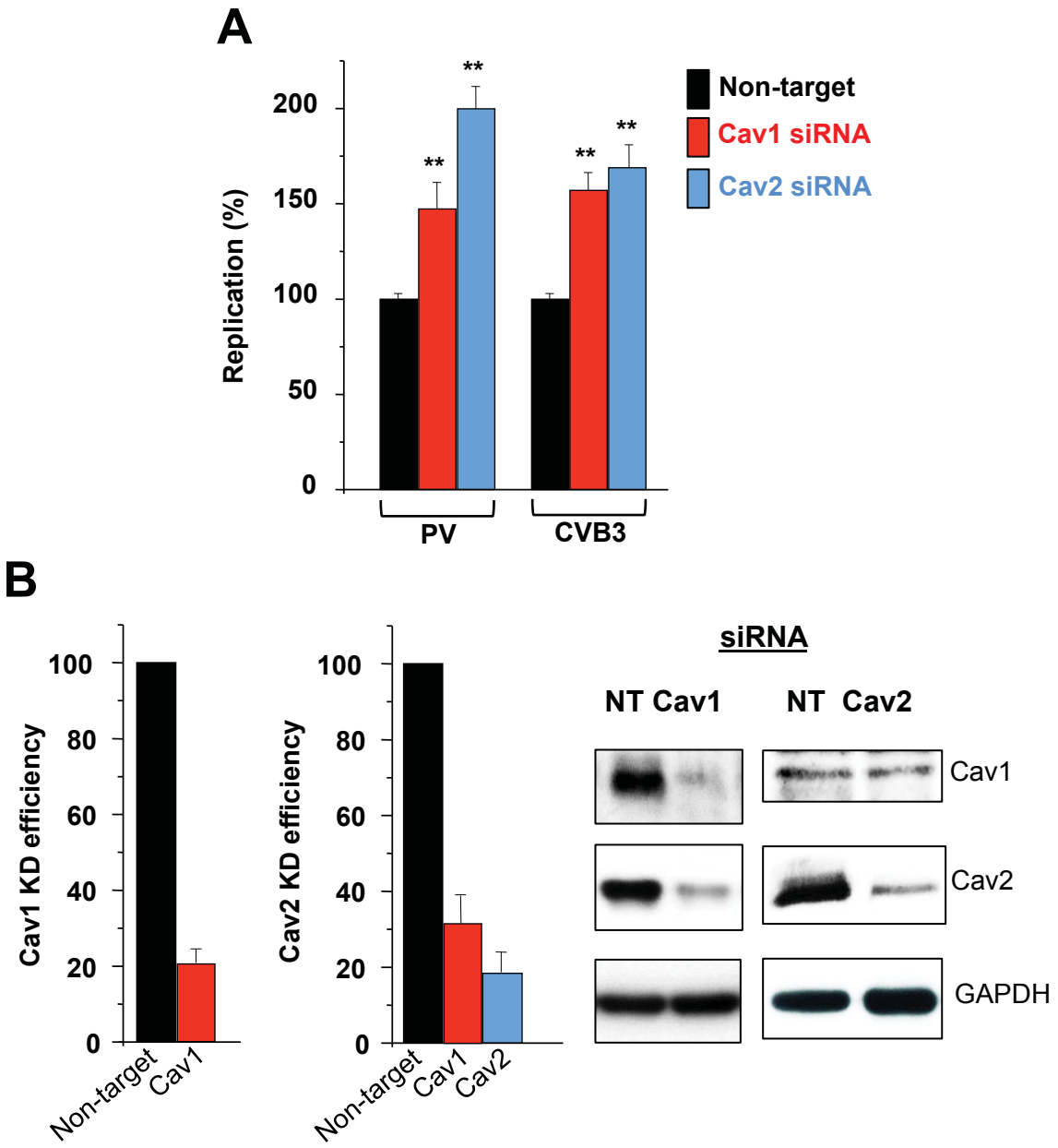
A
Replication (%)
200
150
100
50
0
**
**
**
**
Non-target
Cav1 siRNA
Cav2 siRNA
PV
CVB3
B
Cav1 KD efficiency
100
80
60
40
20
0
Non-target
Cav1
Cav2 KD efficiency
100
80
60
40
20
0
Non-target
Cav1
Cav2
siRNA
NT Cav1
NT Cav2
Cav1
Cav2
GAPDH

Figure 10. Caveolin Depletion Stimulates Viral Replication

A. PV and CVB replication is highly stimulated when either Caveolin 1 or Caveolin 2 was depleted from HeLa cells by siRNA treatment as compared to non-target treated control cells. Mean peak replication data +/- SEM, from 2 independent experiments with six replicates each, were normalized with respect to cell viability and plotted as percentage of non-target siRNA treated cells. **$p<0.01$.

B. Caveolin 1 and Caveolin 2 were efficiently knocked down by siRNA treatment. Bar graphs shows up to 80% of endogenous protein depletion from cells in our experiments. Note in our western blot analysis, Caveolin 1 depletion also reduces Caveolin 2 expression levels but Caveolin 2 depletion does not affect Caveolin 1 protein levels.

	cell viability		PV replication		CVB3 replication		Luciferase mRNA	
	(normalized with respect to cell viability)							
	%	SEM	%	SEM	%	SEM	%	SEM
Non-target	100.0	1.9	100.0	2.5	100.0	3.1	100.0	3.2
CLTB	78.5	2.5	49.5	5.4	45.6	5.8	85.3	8.4
Dab2	85.2	3.7	68.8	6.6	27.8	2.3	113.2	12.5
DNM2	81.2	2.6	61.1	4.4	55.1	7.8	129.4	21.9
AP2A1	77.7	5.1	64.5	3.5	58.5	3.9	98.3	10.2
AP2A2	83.0	5.7	56.6	7.5	62.7	4.4	87.0	5.0
AP2B1	85.8	5.8	81.6	4.2	48.6	4.5	112.2	5.5
AP2M1	87.5	4.2	83.0	6.2	57.0	4.8	104.5	3.0
EPS15L1	89.5	5.2	71.2	6.5	48.5	2.2	131.4	12.9
HIP1	93.2	5.6	65.6	13.0	44.7	7.8	97.2	17.5
HIP1R	92.2	6.0	40.2	6.1	31.6	3.4	184.4	12.5
Rab5	89.4	5.0	65.6	6.3	77.2	6.5	143.8	19.7
Rab11A	84.2	4.6	61.9	3.8	70.9	11.2	83.3	12.7
Rab11B	90.2	5.0	53.1	2.7	63.1	7.8	129.0	7.4
Rab11FIP5	92.5	3.3	59.9	3.8	58.0	10.4	95.5	15.7
Cav1	101.2	5.3	147.3	14.0	157.1	9.4	116.0	7.9
Cav2	80.1	2.9	199.9	11.8	168.9	12.1	112.0	9.5

Table 1. Cell Viability Assays for siRNA Treatment Experiments

Table presents cell viability assays 48 hour after on-target and non-target siRNA transfection and peak PV and CVB3 replication values for each siRNA condition. Mean CVB3 and PV peak replication data were normalized for cell viability and presented as percent of non-target siRNA treated cells. Data from 2 independent experiments for CVB3 and from 2-4 independent experiments for PV with 4-6 replicates in each experiment are presented. Mean Luciferase mRNA expression data, as a transfection/translation control for cells depleted of endocytic proteins, are also presented.

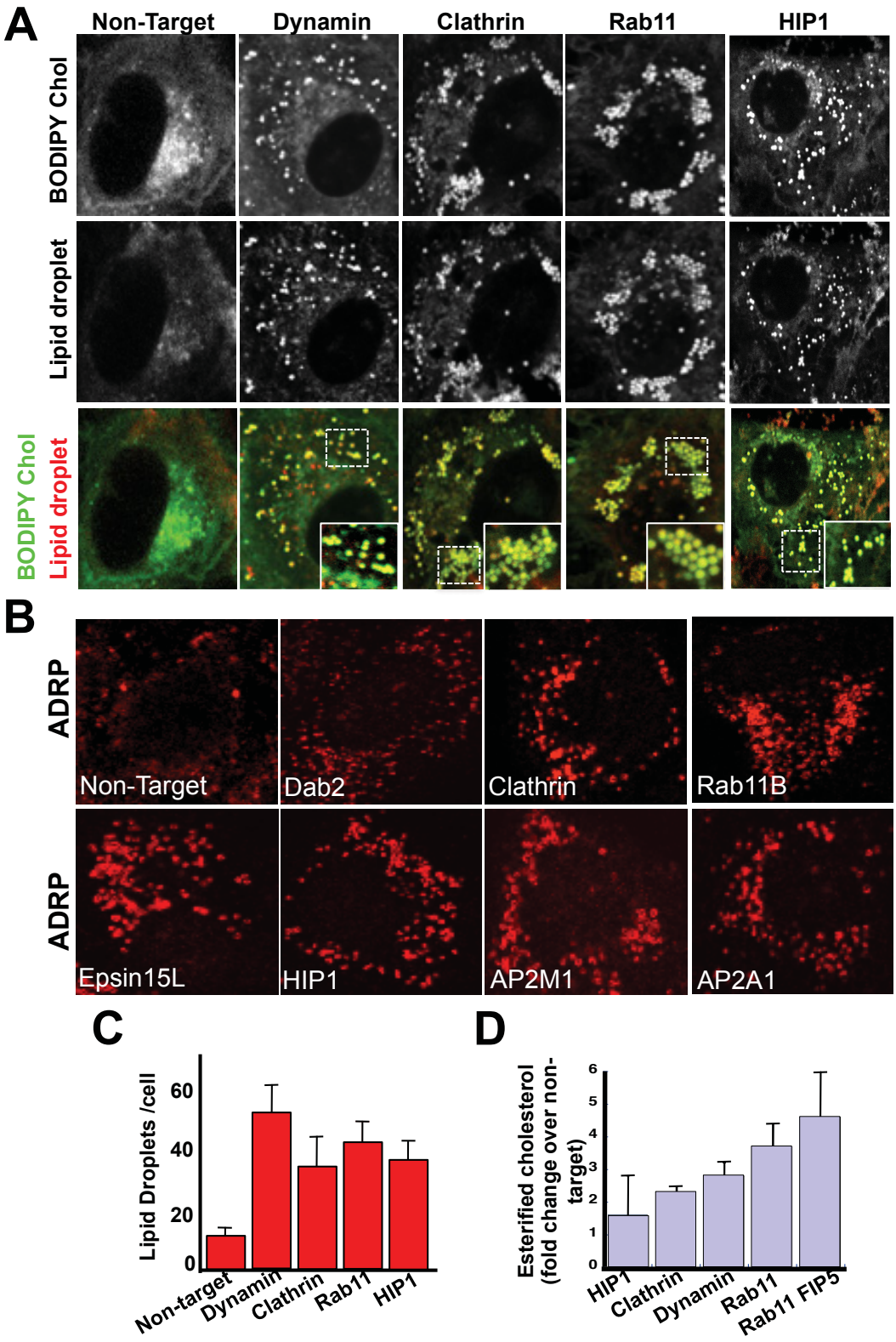
A
Non-Target
Dynamin
Clathrin
Rab11
HIP1
BODIPY Chol
Lipid droplet
BODIPY Chol
Lipid droplet
B
ADRP
Non-Target
Dab2
Clathrin
Rab11B
ADRP
Epsin15L
HIP1
AP2M1
AP2A1
C
Lipid Droplets /cell
60
40
20
0
Non-target
Dynamin
Clathrin
Rab11
HIP1
D
Esterified cholesterol (fold change over non-target)
6
5
4
3
2
1
0
HIP1
Clathrin
Dynamin
Rab11
Rab11 FIP5

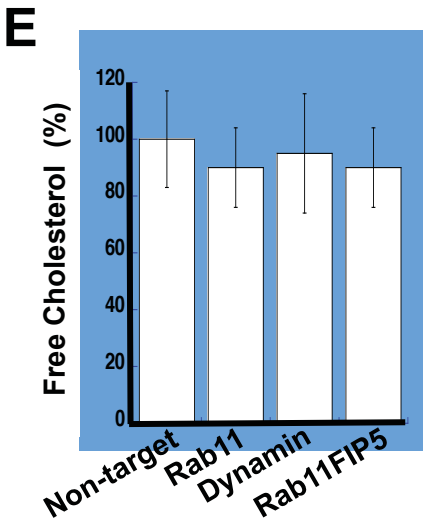
E
Free Cholesterol (%)
120
100
80
60
40
20
0
Non-target
Rab11
Dynamin
Rab11FIP5

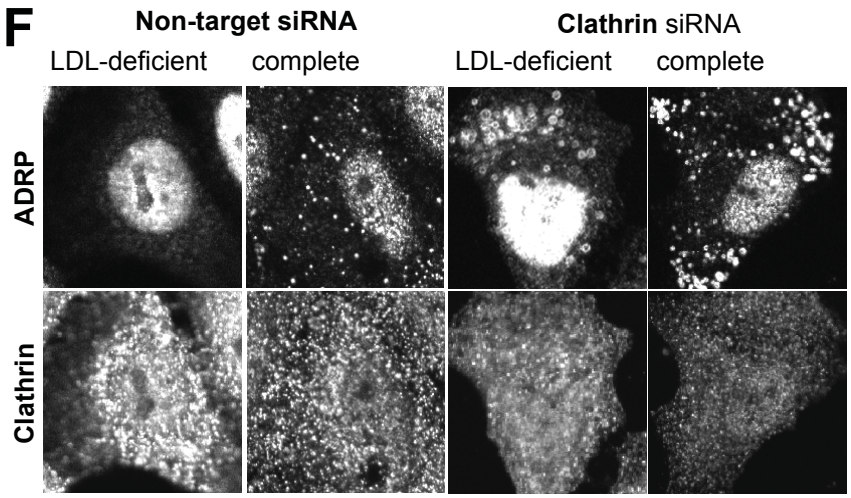
F
Non-target siRNA
Clathrin siRNA
LDL-deficient
complete
LDL-deficient
complete
ADRP
Clathrin

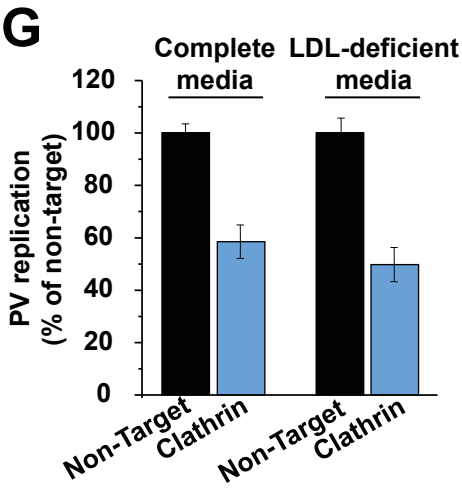
G
Complete media
LDL-deficient media
PV replication (% of non-target)
120
100
80
60
40
20
0
Non-Target
Clathrin
Non-Target
Clathrin

Figure 11. Depletion of CME, Endosomal Machinery, and CIE Proteins Modify Host Cellular Free Cholesterol Pools Toward Esterification

A. Plasma membrane cholesterol is stored in lipid droplets after siRNA depletion of CME components. Numerous Bodipy-cholesterol vesicle-like structures in CME siRNA treated HeLa cells colocalized with Nile Red lipid droplet stain as compared to non-target siRNA treated control cells. Scale bar 5μm.

B. Lipid droplet distribution in siRNA treated HeLa cells as confirmed by immunolabeling of the lipid droplet resident protein ADRP.

C. Lipid droplet number was increased by up to 6 fold in cells depleted of CME or Endosomal recycling proteins, as compared to non-target siRNA control cells. Mean data +/- SEM from n=50 cells for each siRNA treatment was plotted.

D. Steady state esterified cholesterol levels are higher when CME or Endosomal machinery components are depleted from HeLa cells, as compared to non-target siRNA treated control cells. Mean data +/- SEM of 3 independent experiments for each siRNA.

E. Steady state free cholesterol levels decreased by only up to 20% when CME or Endosomal machinery components are depleted from HeLa cells, as compared to non-target siRNA treated control cells. Mean data +/- SEM of 3 independent experiments for each siRNA.

F. Lipid droplet formation was still enhanced in clathrin siRNA depleted cells maintained in complete medium and LDL-deficient medium at 48 hours after treatment, as compared to control non-target siRNA treated cells. Lipid

droplets and clathrin were visualized by immunolabeling with anti-ADRP and anti-Clathrin light chain antibodies, respectively.

G. Poliovirus replicon replication was inhibited in clathrin siRNA depleted cells maintained in complete and LDL-deficient medium. Values represent percent of corresponding control non-target siRNA treated cells for each condition. Data were normalized with respect to cell viability. Mean Data from 3 independent experiments with 4 replicates each are plotted +/- SEM.

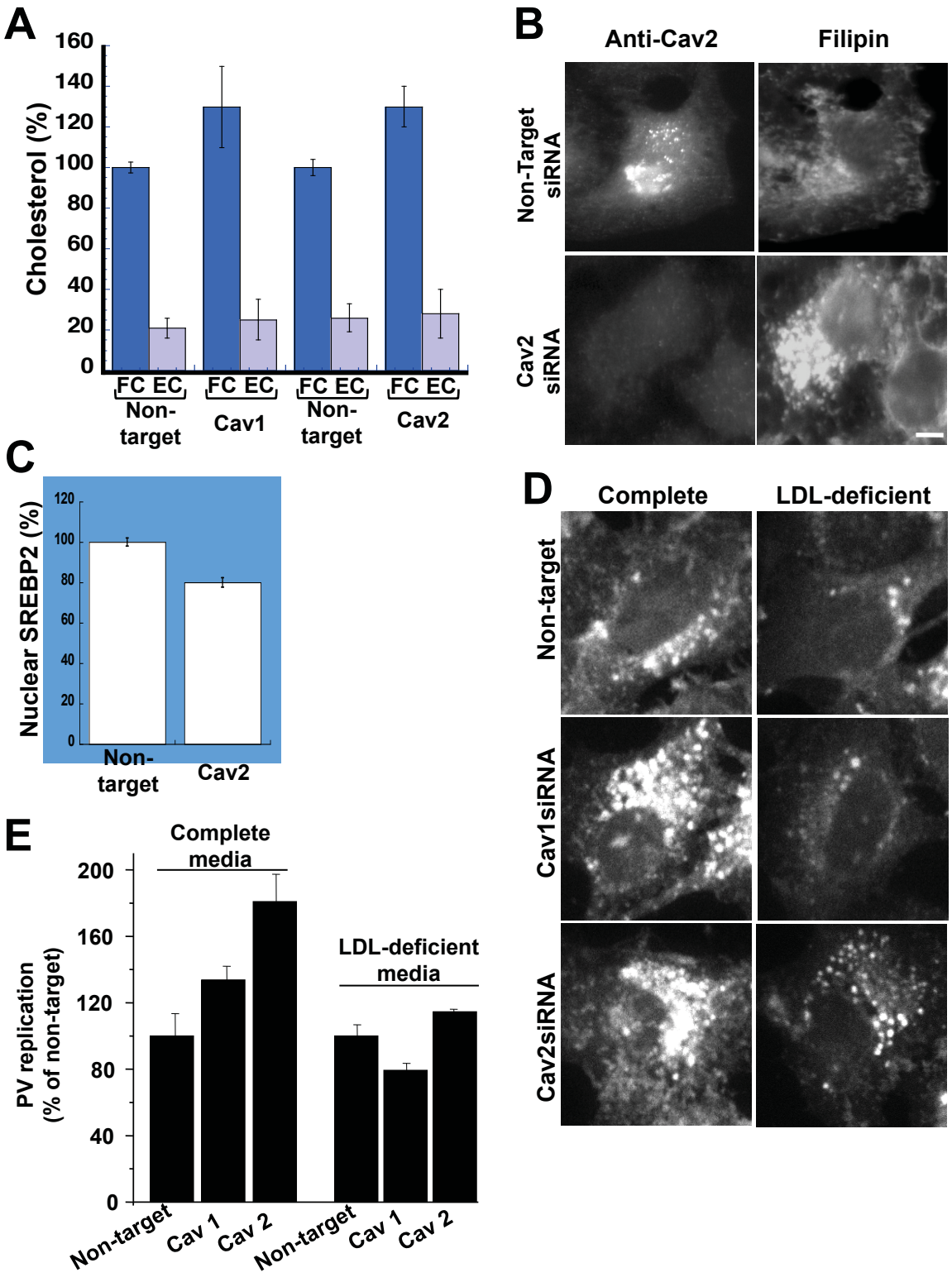
A
Cholesterol (%)
160
140
120
100
80
60
40
20
0
FC EC
Non-target
Cav1
Non-target
Cav2
B
Anti-Cav2
Filipin
Non-Target siRNA
Cav2 siRNA
C
Nuclear SREBP2 (%)
120
100
80
60
40
20
0
Non-target
Cav2
D
Complete
LDL-deficient
Non-target
Cav1siRNA
Cav2siRNA
E
Complete media
LDL-deficient media
PV replication (% of non-target)
200
160
120
80
40
0
Non-target
Cav 1
Cav 2
Non-target
Cav 1
Cav 2

Figure 12. Depletion of Caveolin Proteins Modify Host Cellular Free Cholesterol Toward Enrichment of Internal Pools

A. Levels of steady state free cholesterol (blue bars) are elevated in cells depleted of caveolin 1 or caveolin 2, while esterified cholesterol (grey bars) levels are unchanged. Mean data +/- SEM of 3 independent experiments for each siRNA.

B. Internal pools of free cholesterol are enriched in cells depleted of caveolin by siRNA treatment. Cells were immunolabeled with anti caveolin antibody and cholesterol was stained with filipin. Scale bar 5μm**.**

C. Nuclear SREBP2 levels were slightly lower in caveolin 2 siRNA treated cells as compared to control non-target siRNA treated cells. HeLa cells were immunolabeled with SREBP2 antibody. Cells were subsequently imaged by confocal microscopy and nuclear fluorescence was measured.

D. Free cholesterol pools decreased in caveolin 1 or caveolin 2 depleted cells maintained in LDL-deficient media, as compared to control cells maintained in complete media. Free cholesterol was detected by filipin staining. Representative images are shown.

E. Poliovirus replicon replication in caveolin 1 and caveolin 2 depleted cells in complete and LDL-deficient medium show that in complete media replication was enhanced while in LDL deficient media replication was inhibited. Values represent percent of corresponding control non-target siRNA treated cells for each condition. Data were normalized with respect to cell viability. Data from 3 independent experiments with 4 replicates each are plotted +/- SEM.

CHAPTER 7

CME Uptake And Endosomal Recycling Pathway Dynamics Are Essential For Cholesterol Redistribution To VROs And Viral Replication

The viral replication inhibition by the siRNA screen of CME and endosomal recycling proteins, the increase in LDL uptake, and the increase in free cholesterol uptake and its redistribution from the plasma membrane to internal membrane pools, all these data show the importance of the CME and endosomal-recycling pathways during viral infection. Furthermore, the caveolin siRNA data showing stimulation of viral replication in these cells provides evidence that the caveolin dependent CIE is unlikely involved. In the previous chapters, we show that during infection there is a total net increase in LDL uptake (Figure 6B) and a total net decrease in the free plasma membrane cholesterol (Figure 7B) to enrich internal free cholesterol pools; to achieve these results at steady state, we hypothesize that the dynamics of cellular uptake and recycling are modulated by the enteroviruses. With this in mind, we wanted to study the CME and the endosomal-recycling pathway in more detail. Therefore, in this chapter we focus on the redistribution mechanism and dynamics of free cholesterol by studying protein components of the CME and the endosomal recycling pathway using techniques such as confocal and TIRF microscopy.

RESULTS:

Clathrin Mediated Endocytosis is Associated with Free Cholesterol Uptake and Redistribution to Viral Replication Organelles

We first wanted to further verify the involvement of CME during enteroviral infection. In the following experiment, we performed a Bodipy-cholesterol pulse chase experiment on Hela cells transiently expressing clathrin-mRFP during CVB infection. We found that within 2hr post infection, Bodipy-cholesterol was frequently localized to clathrin positive structures (Figure 13A, 13B & 13C). We then disrupted CME with chlorpromazine, a drug used in research to inhibit CME uptake, (Mercer et al. 2010). Hela cells were treated with 1, 5, or 10μg/ml of chlorpromazine at the same time as the control reporter or the PV replicon was transfected; then we measured the replication kinetics. We found that replication was inhibited up to 60% in a dose dependent manner as compared to mock treated control cells (Figure 13D).

Additionally, we used Dynasore, a noncompetitive dynamin GTPase inhibitor that is used to disrupt CME, to prevent CME uptake (Dutta and Donaldson 2012; Kirchhausen et al. 2008; Macia et al. 2006). Hela cells transiently expressing FAPP1-mRFP were treated acutely with 80μM of Dynasore at 3hr post infection, then pulsed with Bodipy-cholesterol for 5 minutes, and finally chased for 1hr before confocal imaging. We found that Dynasore treatment blocked trafficking of cholesterol to viral replication organelles (Figure 13E). We also measured viral replication in cells treated with either DMSO or Dynasore then transfected with the control reporter or CVB replicon, respectively, and found that in Dynasore treated cells the replication was inhibited by approximately 80% as compared to control cells (Figure 13F). Next, we measured the levels of the endogenous free cholesterol pool at the replication

organelles in Hela cells acutely treated with 80μM of Dynasore for 1hr at 3hr post infection, then fixed and immunolabeled with an antibody against viral 3A and stained with filipin. We found that cholesterol content at VROs was significantly decreased compared to mock treated control cells, supporting our previous observations in the live Bodipy-cholesterol experiment (Figure 13E & 13G). Collectively, these data show that CME is involved in trafficking of free cholesterol and that inhibition of CME can negatively affect viral replication.

Uptake Kinetics of Clathrin Mediated Endocytosis is Unaffected During Viral Replication

With the results from the CME disruption experiments strongly suggesting the CME involvement in viral replication, we decided to study the dynamics of CME to identify any changes in the uptake kinetics during infection. For the following experiments, we made a HeLa cell line stably expressing Clathrin tagged with red fluorescent protein, that we will refer to as CRSH (clathrin-RFP stable HeLa) cells and maintained in CCM supplemented with 0.5mg/ml of G418 to select for cells expressing the construct. The use of CRSH cells gave the advantage of minimizing variability in the expression levels of clathrin-RFP, and can lower the cytotoxic effects caused by simultaneous use of multiple techniques. First using confocal microscopy, we performed pulse chase experiments in live cells. We seeded CRSH cells in bottom glass multi-well chambers and incubated them for 1 to 2 days before pulsing Bodipy-cholesterol for 5 minutes, then rinsed and further incubated for an additional 30 min to allow the Bodipy-cholesterol to achieve steady state. Cells were then infected with

CVB and time lapsed images of the area closest to the coverglass were taken at 5 minutes intervals for the duration of the infection. We found that during infection clathrin positive structures where observed to colocalize with cholesterol rich structures at the plasma membrane and later disappeared as these were trafficked into the host cell cytoplasm (Figure 14A).

Since many of the changes were happening 1 - 4 hours post infection, such as uptake of LDL (Figure 6B) and depletion of free cholesterol from the plasma membrane (Figure 7B). We wanted to study the kinetics of clathrin uptake at or in close proximity to the plasma membrane and within the first 1 to 3 hours of infection, but with confocal microscopy we were limited by the background fluorescence emitted by internal pool of proteins. Therefore, we used TIRF microscopy time lapsed imaging to analyze the kinetics of either clathrin or the transferrin receptor. TIRF microscopy is achieved when the excitation light hits the coverslip/sample at an angle creating an evanescence wave of light ~100nm from the coverslip that will only excite fluorophores within this area, providing higher resolution with low background fluorescence (Axelrod, 2001).

We seeded CRSH cells in 35mm bottom glass dishes and incubated them for 1 to 2 days. Control and CVB infected samples were then imaged using a single laser channel at a 61.5 TIRF angle every 5 minutes for 3 hours. We found that the number of clathrin structures during initial infection was similar to the number in control cells, (Figure 14B). These data provides evidence that CME is involved in the uptake of cholesterol from the plasma membrane and that the rate of CME uptake is not changing, suggesting that the total net increase in LDL

uptake (Figure 6B) and a total net decrease in the free plasma membrane cholesterol (Figure 7B) is not due to and increase rate of CME uptake.

Endosomal Recycling is Inhibited During Viral Infection

Most of the endosomal recycling studies have been performed using techniques that require cell starvation periods and/or acid treatment of cells for the removal of plasma membrane bound ligands or antibodies to measure the levels of the target molecules recycled back to the plasma membrane from the internalized pool (Shen et al. 2014; Weigert and Donaldson 2005). But these harsh conditions may affect the viral life cycle; therefore to avoid any unnecessary cellular artifacts, we studied recycling of the human transferrin receptor tagged with a pH sensitive probe. The transferrin receptor is constitutively internalized via the CME pathway and recycled back to the plasma membrane through endosomal compartmentalization, (Hsu, V., et al. 2012). The pH sensitive tag, super-ecliptic phluorin, is a modified version of GFP (Merrifield et al. 2005; Miesenbock et al. 1998); and it is attached to the extracellular leaflet of the human transferrin receptor (hTfnR-phl) (Merrifield et al. 2005). The plasmid is highly fluorescent at neutral pH (~pH7.1) such as the extracellular matrix, but the fluorescence is quenched at acidic pH (~pH5.5) such as inside endosomal compartments (Merrifield et al. 2005; Miesenbock et al. 1998).

Therefore with this construct and using time-lapse TIRF microscopy, we were able to track vesicles containing the receptor as these are exocytosed and fusing with the plasma membrane (Figure 15A). We seeded cells in bottom glass dishes and transfected them with hTfnR-phl. Then we imaged both uninfected

and CVB or PV infected cells in TIRF mode at a 61.5 angle; in continuous image acquisition mode (that captures ~20 images per second) for 30 seconds every half hour for 3.5hr, randomly selecting 5 cells at each time point for each condition. We counted the number of events and found that in CVB and PV infected cells the number of exocytic events was decreased by approximately 80% at 3.5 hours post infection, as compared to uninfected control cells (Figure 15B). This data shows that the recycling kinetics of hTfnR is inhibited during infection, therefore trapping the receptor inside endosomal compartments.

We followed the fate of the transferrin receptor inside the cells by transiently expressing TnfR-GFP in HeLa cells. Cells were then infected and confocal time-lapse imaging was performed throughout infection. We found that the plasma membrane pool of transferrin receptor was depleted and that intracellular compartments were enriched in transferrin receptor (Figure 15C). Then to identify the endosomal compartments where the receptor might be trapped, we looked at the transferrin receptor along with markers for early, late, or recycling endosomes. We seeded cells in coverslips and transfected with hTfnR-phl; then we infected them with CVB and fixed the samples at 3.5 post infection; followed by immunolabeling with antibodies against GFP and either Rab5 (early endosome), Rab7 (late endosome), or Rab11a (recycling endosome) (Wandinger-Ness and Zerial 2014). We found that in infected cells the transferrin receptor was present in higher levels only at Rab11a positive compartments as compared to uninfected cells (Figure 15D); showing that the recycling

endosomes were potentially modulated to reroute or store its contents to inhibit recycling to the plasma membrane.

Viral Protein 3A Recruits and Targets Free Cholesterol-Rich Rab11 Recycling Endosomes to Viral Replication Organelles

Although, due to the temporal correlation between the appearance of VROs from the ER exit sites (Hsu et al. 2010) and the continuation of cholesterol biosynthesis at ~4hr post infection (Figure 6C) suggesting that some cholesterol is being transferred from the ER to the VROs. Now with evidence that the endosomal-recycling pathway is inhibited during infection (Figure 15B) and that Rab11 endosomes are the potential stop or rerouting point for internalized transferrin receptor. We wanted to investigate if the redistribution and transfer of free cholesterol to VROs was through the Rab11 endocytic compartments.

We followed, by live pulse chase experiments, the localization of Bodipy-cholesterol during CVB infection in relation to Rab11 (recycling endosome marker). We found that by 2hr post infection plasma membrane free cholesterol was also redistributed to Rab11 recycling endosomes (Figure 16A); we were able to confirm this data by SIM imaging of Rab11-YFP expressing cells loaded with Bodipy-cholesterol. In these cells, Bodipy-cholesterol also localized to Rab11 compartments (Figure 16B). Lastly, we inhibited cholesterol trafficking through the endocytic pathway by acutely treating cells transfected with either a control transporter or PV replicon with Ezetimibe. Ezetimibe is a highly specific inhibitor of the cholesterol receptor NPC1-L1 (Chang, T. and Chang, C. 2008) which traffics cholesterol via clathrin/AP2 mediated endocytosis to Rab11 recycling

endosomes (Wang and Song 2012). We found that inhibiting NPC1L1 blocks PV replication by up to 50% as compared to mock treated controls (Figure 16C). This inhibition in replication further supports the involvement of the CME and endosomal-recycling pathway in the uptake and redistribution of free cholesterol from the plasma membrane.

With free cholesterol present at Rab11 positive endosomes, we further studied the fate of these recycling endosomes to find out if there is any relationship with the transport of free cholesterol to VROs. For this experiment we performed time-lapse imaging of Hela cells coexpressing Rab11-YFP and FAPP1-mRPF (VRO marker) during CVB infection. Images showed that many Rab11 recycling endosomes were actively trafficking and merging with FAPP1 positive replication organelles (Figure 17A, 17B, & 17C). In addition, we studied early and late endosomes to see if these were trafficked to VROs. Thus, Coxsackievirus infected Hela cells coexpressing Rab11-YFP and either Rab5A-mRFP (early endosome) or Rab7A-mCherry (late endosome) were imaged at 4hr post infection. We found that in infected cells, neither early nor late endosomes were present at the VROs (Figure 17D); therefore, endosome trafficking and merging to VROs was specific to Rab11 recycling endosomes.

Likewise, we performed coimmunoprecipitation assays between Rab11 and PI4KIIIβ and found that the physical interaction between Rab11 and PI4KIIIβ increased 4 fold by peak replication time, while the levels of both proteins did not change (Figure 17E). We also ectopically expressed in Hela cells the enteroviral protein 3A, which selectively enhances recruitment of PI4KIIIβ to membranes

(Greninger et al. 2012; Hsu et al. 2010) and found that viral protein 3A enhance the recruitment of Rab11 compartments to 3A positive membranes (Figure 17F); suggesting that 3A is the viral protein that might be modulating the transfer of Rab11 compartments to the VROs.

CONCLUSION:

In this chapter, we provide evidence that clathrin mediated endocytosis is involved in free cholesterol uptake from the plasma membrane and transport to VROs indicated by the presence of free cholesterol in clathrin coated structures during infection (Figure 13A, 13B, & 13C) and the decrease of free cholesterol levels in the VROs upon CME disruption with Dynasore (Figure 13E & 13G), or Ezetimibe (Figure 16C). Moreover, CME has a crucial role in enteroviral replication since the disruption of CME by siRNA depletion (Figure 8B) and chlorpromazine (Figure 13D) or Dynasore (Figure 13F) treatments all inhibit viral replication. We also identified that the potential mechanism by which at steady state, the net increased in LDL uptake (Figure 6B) and the net decrease of plasma membrane free cholesterol pools (Figure 7B) to enrich the internal membrane pools is in part due to the inhibition of the cellular endosomal recycling kinetics during infection. In addition, our data show that during infection there is a significant increase in the association between Rab11 and PI4KIIIβ. Concomitant with this, viral protein 3A alone is able to enhance not only PI4KIIIβ (Greninger et al. 2012; Hsu et al. 2010), but also Rab11 to 3A positive membranes (Figure 17F). Therefore, 3A, by harnessing Rab11, can prevent

recycling of free cholesterol to the plasma membrane, and instead targeting the internalized pool to the VROs.

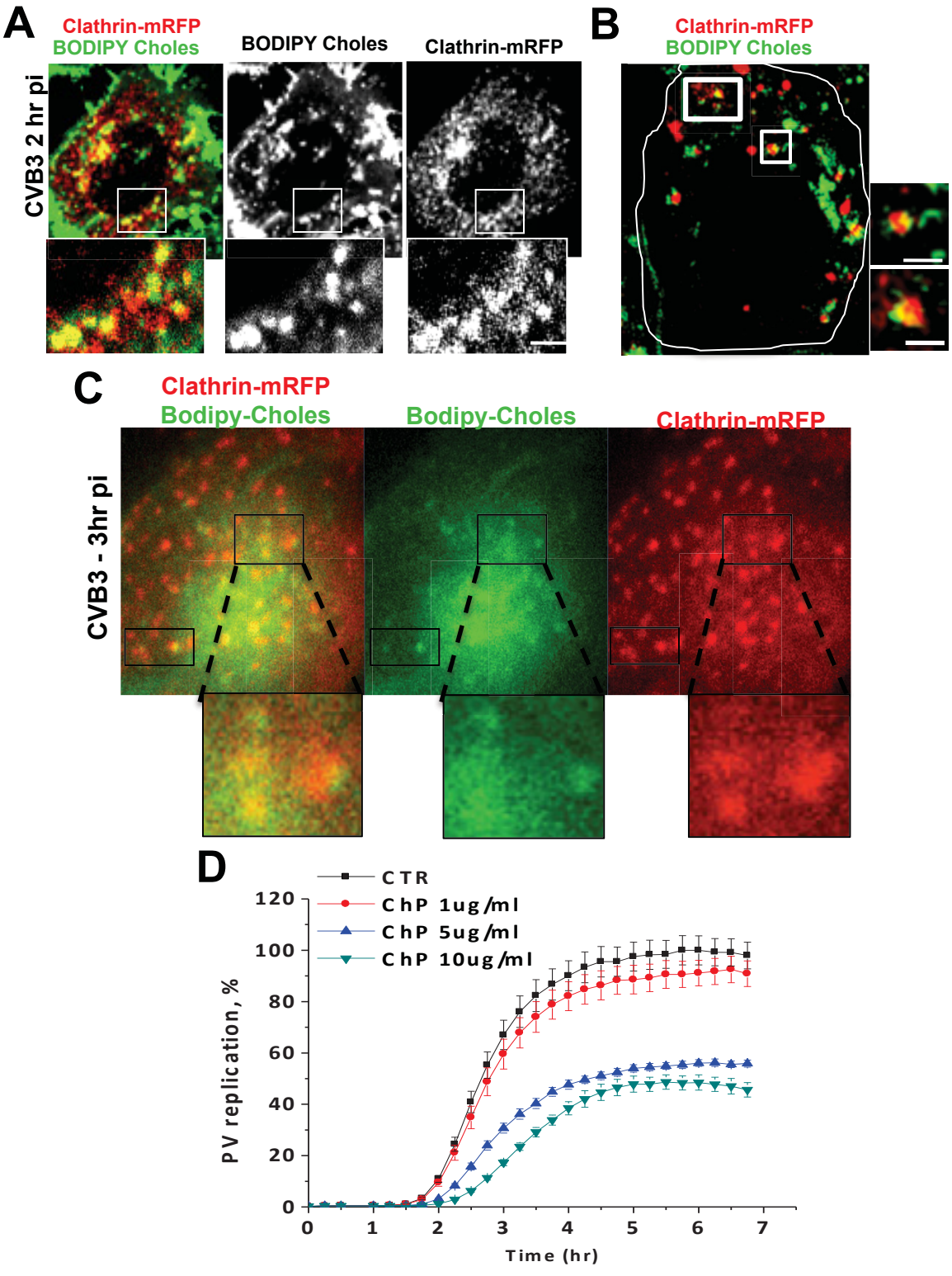
A
Clathrin-mRFP
BODIPY Choles
BODIPY Choles
Clathrin-mRFP
CVB3 2 hr pi
B
Clathrin-mRFP
BODIPY Choles
C
Clathrin-mRFP
Bodipy-Choles
Bodipy-Choles
Clathrin-mRFP
CVB3 - 3hr pi
D
CTR
ChP 1ug/ml
ChP 5ug/ml
ChP 10ug/ml
PV replication, %
Time (hr)
0
20
40
60
80
100
120
0
1
2
3
4
5
6
7

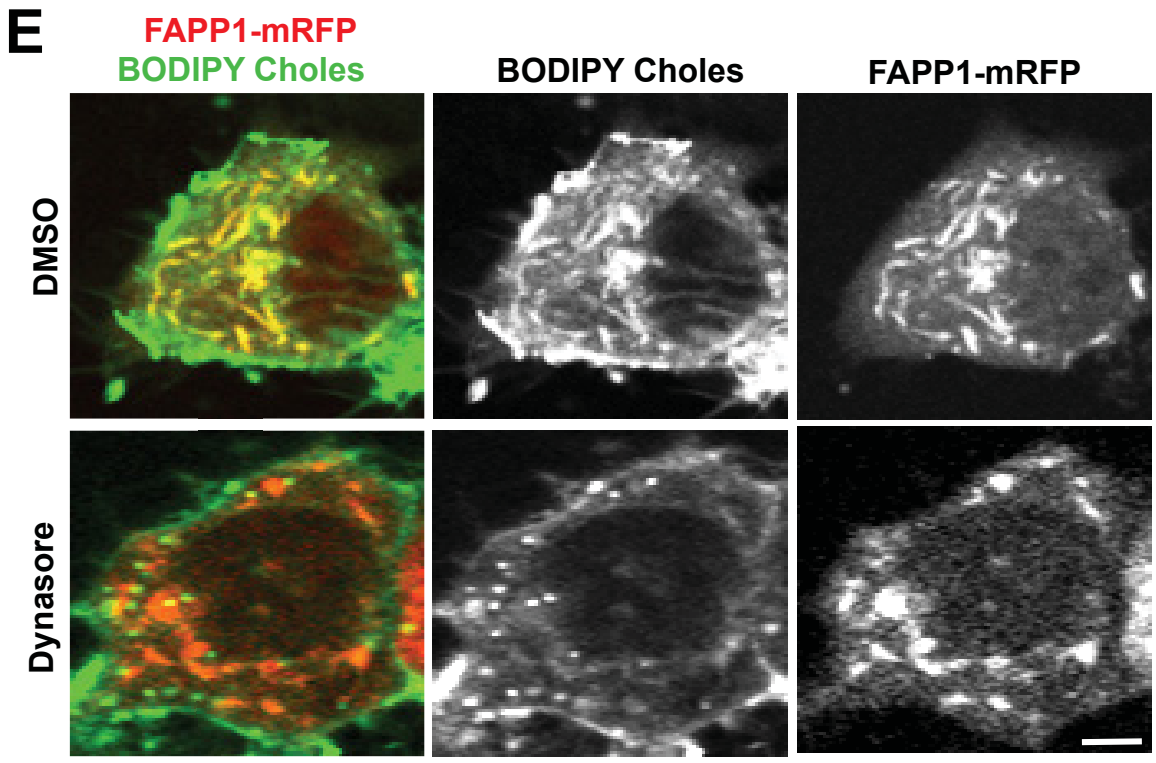
E
FAPP1-mRFP
BODIPY Choles
BODIPY Choles
FAPP1-mRFP
DMSO
Dynasore

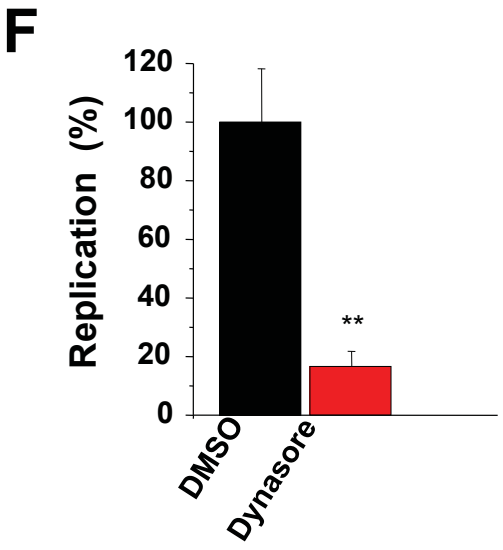
F
Replication (%)
120
100
80
60
40
20
0
**
DMSO
Dynasore

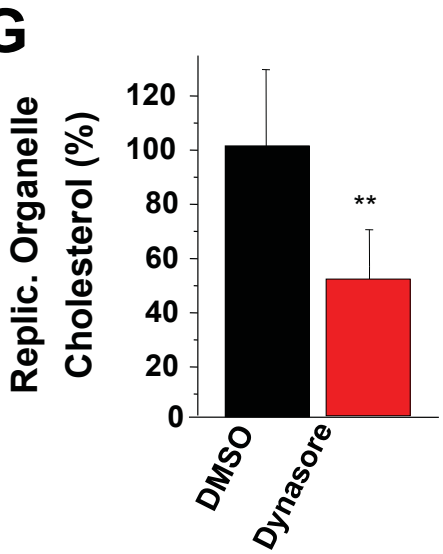
G
Replic. Organelle Cholesterol (%)
120
100
80
60
40
20
0
**
DMSO
Dynasore

Figure 13. Clathrin Mediated Endocytosis is Associated with Free Cholesterol Uptake and Redistribution to Viral Replication Organelles

A. BODIPY-cholesterol is internalized in clathrin-coated endosomes during infection. HeLa cells expressing clathrin-mRFP were infected with CVB3 and pulse labeled with Bodipy-cholesterol prior to confocal imaging. Scale bar is 2μm.

B. SIM image showing the localization of free cholesterol in clathrin coated structures. HeLa cells expressing clathrin-mRFP were infected with CVB3 and pulse labeled with Bodipy-cholesterol. Scale bar is 0.5μm.

C. TIRF image of clathrin coated structures combined with Epifluorescence of Bodipy-Cholesterol showing the localization of free cholesterol in close proximity to the plasma membrane. Inside the image: Top small square show deeper clathrin/cholesterol rich vesicles; lower small square show a vesicle/pit closer to/at the plasma membrane.

D. Chlorpromazine treatment inhibits PV replicon replication as compared to mock treated control cells. Chlorpromazine was added at the indicated concentrations at the start of replication.

E. Dynasore treatment blocks Bodipy-cholesterol trafficking from plasma membrane to replication organelles as compared to mock treated control cells. HeLa cells expressing FAPP1-mRFP were infected with CVB3 for 3 hours, then pulsed with Bodipy-cholesterol, and subsequently chased with either DMSO or Dynasore (80mM) for 1 hour prior to confocal imaging. Scale bar is 5μm.

F. Dynasore treatment blocks CVB replication as compared to mock treated control cells. Cells were treated with DMSO or Dynasore (80mM), then transfected with CVB3 replicons. Mean data ± SEM of peak replication levels in three independent experiments for each condition are plotted.

G. Dynasore treatment blocks endogenous free cholesterol pools from trafficking to replication organelles as compared to mock treated control cells. Experimental design for this experiment was similar to that in (E) but cells were fixed, labeled with anti viral protein 3A antibodies, and stained with filipin. Mean data ± SEM from n = 30 cells for each condition are plotted.

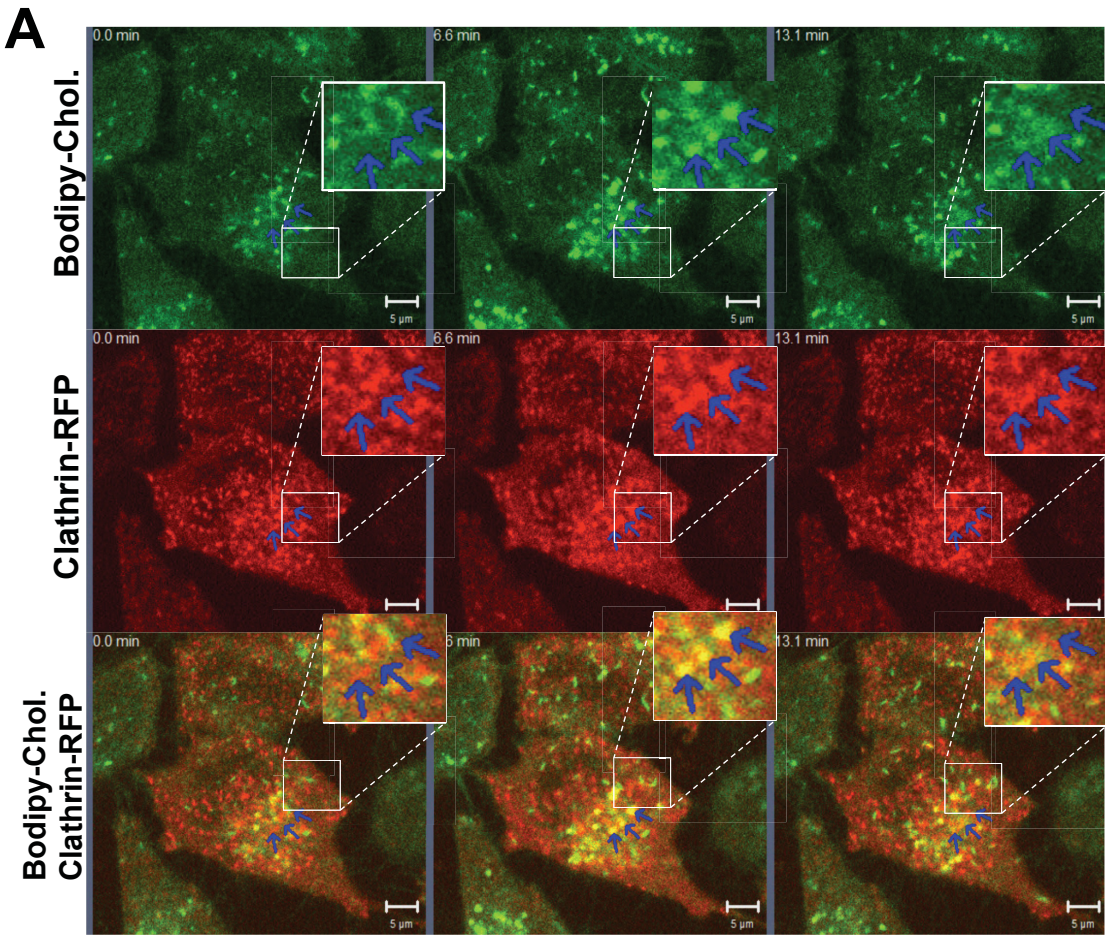
A
Bodipy-Chol.
Clathrin-RFP
Bodipy-Chol.
Clathrin-RFP
0.0 min
6.6 min
13.1 min
5 µm

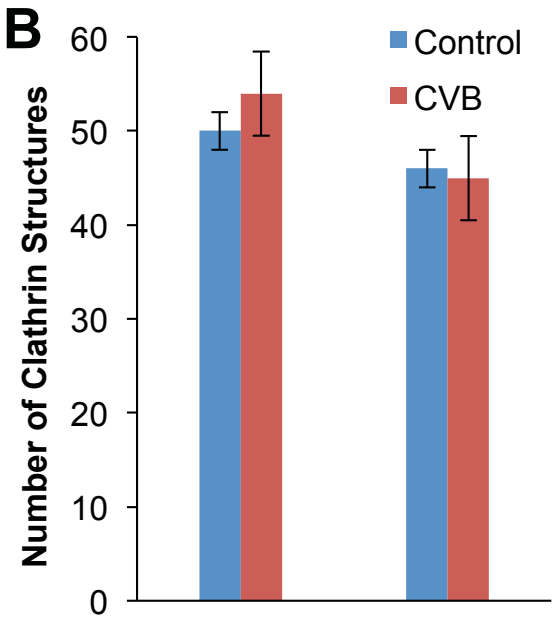
B
Number of Clathrin Structures
60
50
40
30
20
10
0
Control
CVB

Figure 14. Uptake Kinetics of Clathrin Mediated Endocytosis is Unaffected During Viral replication

A. Clathrin coated structures colocalize with free cholesterol at the plasma membrane and are later internalized into the cell. Figure shows representative time sequence image gallery of cholesterol rich clathrin structures (blue arrows) when they are internalized over time at peak replication. Time-lapse confocal images of clathrin-mRFP stable HeLa (CRSH) cells loaded with Bodipy-cholesterol and infected with CVB were take every 5 minutes for the duration of the infection. Scale bar is 5μm.

B. Clathrin coated structure abundances in CVB infected cells at 1 and 2 hours post infection were similar to uninfected control cells. TIRF images of clathrin-mRFP stable HeLa (CRSH) cells infected with CVB were taken at 0, 1, and 2 hours post infection; and control cells were imaged at 0, 1, and 2 hours after setting the sample on the stage. Clathrin structures were counted from a $10\mu m^2$ area per cell in both infected and control cells. Mean data ± SEM from n = 5 cells for each condition are plotted.

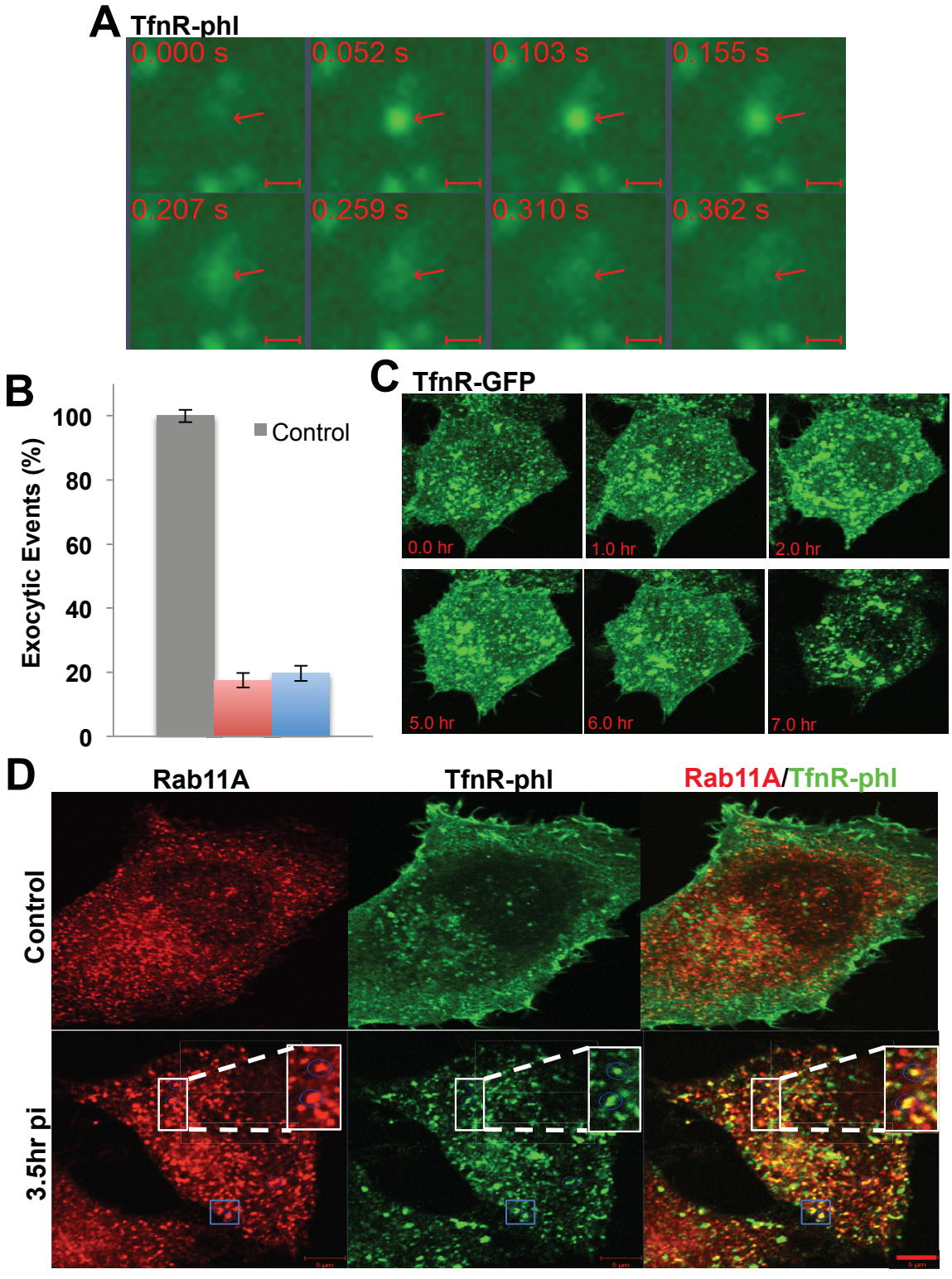
A
TfnR-phl
0.000 s
0.052 s
0.103 s
0.155 s
0.207 s
0.259 s
0.310 s
0.362 s
B
Exocytic Events (%)
100
80
60
40
20
0
Control
C
TfnR-GFP
0.0 hr
1.0 hr
2.0 hr
5.0 hr
6.0 hr
7.0 hr
D
Rab11A
TfnR-phl
Rab11A/TfnR-phl
Control
3.5hr pi

Figure 15. Endosomal Recycling is Inhibited During Viral Infection

A. TIRF microscopy time sequence image gallery of TfnR-phl shows the exocytosis of a vesicle containing the receptor. The images show the vesicle visible at and later fusing with the plasma membrane. Note the spread of the receptor in the immediate area of the vesicle fusion event. HeLa cells were transfected with TfnR-phl and imaged in TIRF mode at a 61.5 angle in continues imaging mode and capturing ~20 images/second. Scale bar is 0.5μm.

B. Cellular recycling is inhibited by more than 80% during enteroviral infection, as compared to uninfected control cells. Graph shows the number of exocytic events in a 30 second time frame taken at 3.5 hours, in cells with and without virus infection. HeLa cells transiently expressing the receptor were infected with CVB or PV, and images were collected every 30 minutes for 3.5 hours as described above. Mean data ± SEM from n = 5 cells for each condition are plotted. Standard errors were calculated using the Student t-Test for unpaired data with unequal variance function.

C. Confocal microscopy time sequence image gallery of TfnR-GFP during CVB infection shows transferrin being endocytosed and trapped in endosomes, not able to replenish the plasma membrane pool. HeLa cells were transfected with TfnR-GFP and infected with CVB. Images were taken every 5 minutes for the duration of the infection.

D. Transferrin receptor localizes to Rab11 recycling endosomes during CVB infection as compared to uninfected control cells. HeLa cells transfected with

TfnR-phl were infected with CVB, fixed at 3.5 hours post infection and immunolabeled with antibodies against GFP for the transferrin receptor (green) and Rab11A for recycling endosomes (red). Scale bar is 5μm.

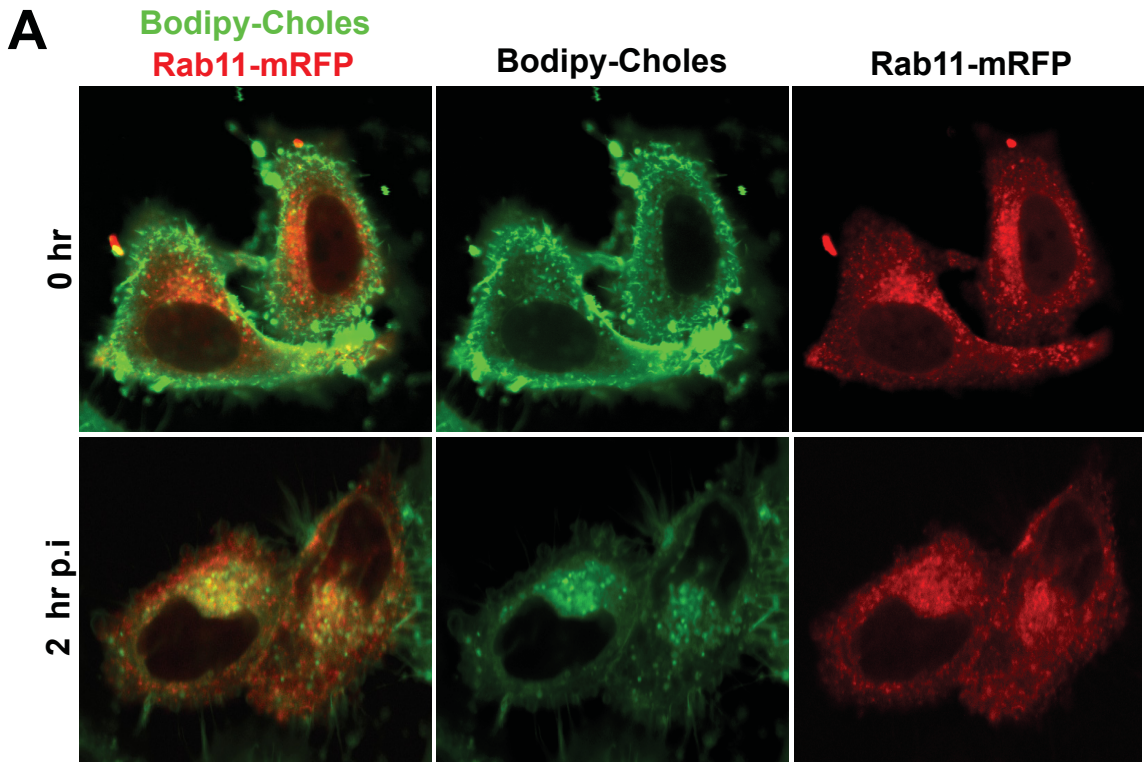
A
Bodipy-Choles
Rab11-mRFP
Bodipy-Choles
Rab11-mRFP
0 hr
2 hr p.i

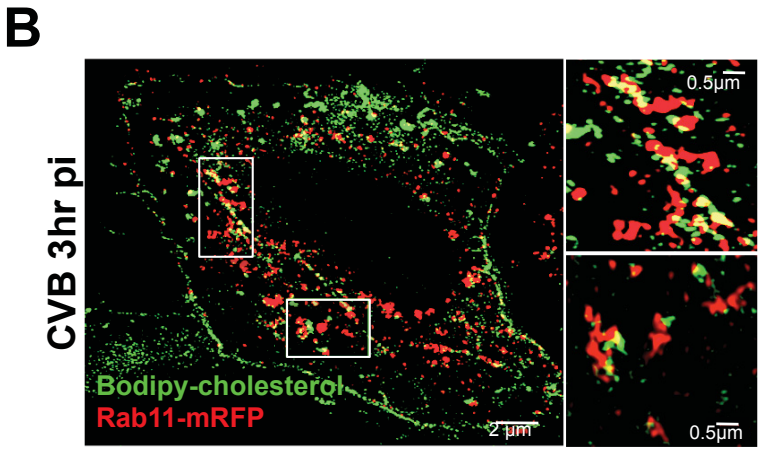
B
CVB 3hr pi
Bodipy-cholesterol
Rab11-mRFP
2 μm
0.5μm
0.5μm

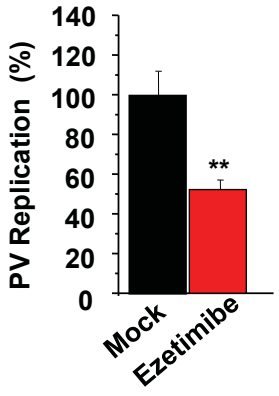
C
PV Replication (%)
140
120
100
80
60
40
20
0
**
Mock
Ezetimibe

Figure 16. Free Cholesterol Colocalizes with Rab11 Recycling Endosomes During Viral Infection

A. Bodipy-cholesterol is distributed to recycling endosomes in CVB3 infected cells post infection. Cells expressing Rab11-mRFP were loaded with Bodipy-cholesterol, infected with CVB, and monitored over time by live-cell confocal microscopy. Representative images for 0 and 2 hours post infection are presented. Scale bar is 10μm.

B. SIM images of Bodipy-cholesterol localizing to Rab11 positive endosomes. HeLa cells expressing Rab11-YFP were infected with CVB; images were taken at 3 hours post infection. Note the localization of Bodipy-cholesterol to Rab11 positive endosomes (inset).

C. Ezetimibe treatment inhibits PV replicon replication as compared to mock treated control cells. Mean peak replication data ± SEM of replicon transfected cells from three independent experiments with six replicates each are plotted. ***$p < 0.001$. Standard errors and p-values were calculated using the Student t-Test for unpaired data with unequal variance function.

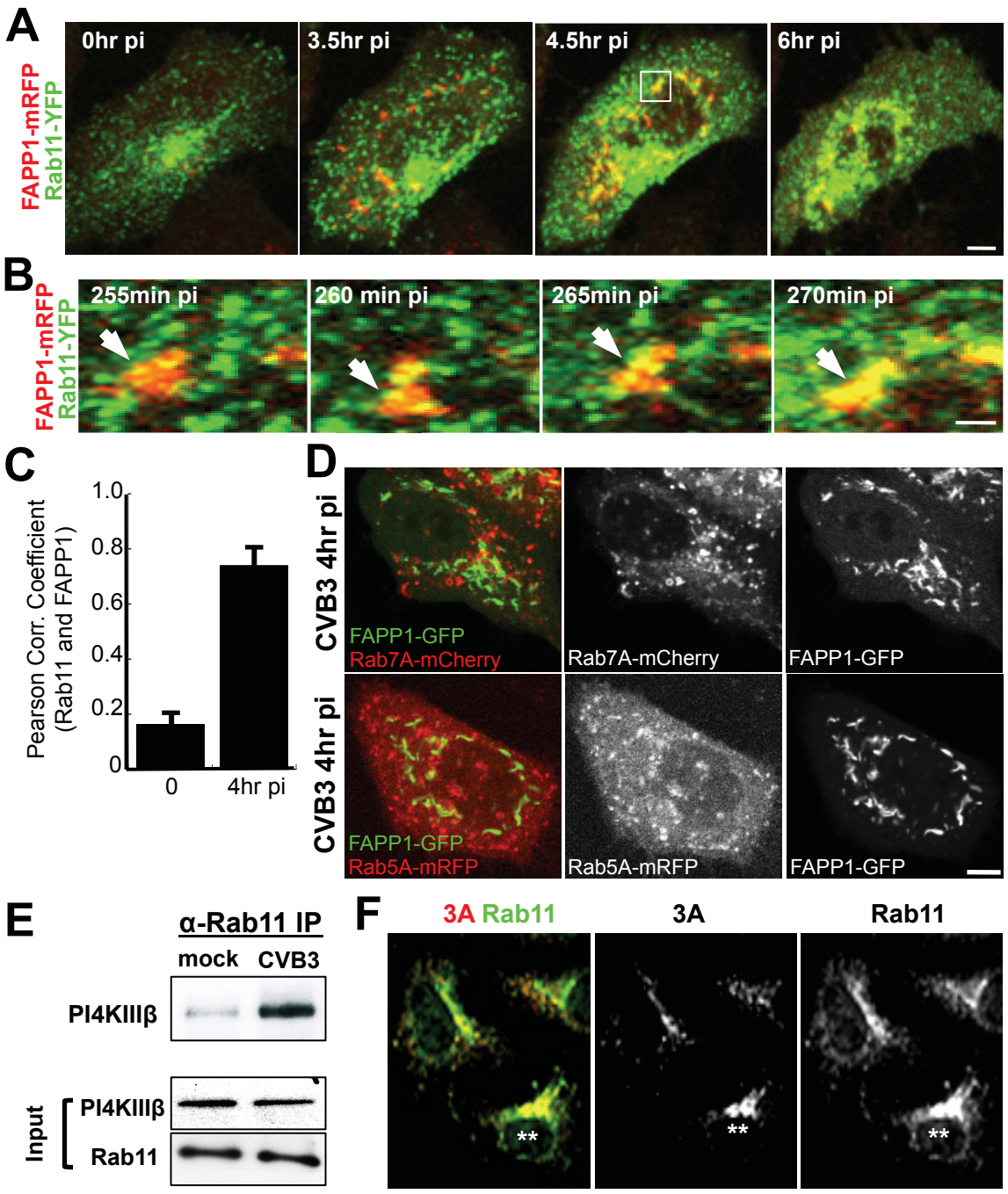
A
FAPP1-mRFP
Rab11-YFP
0hr pi
3.5hr pi
4.5hr pi
6hr pi
B
FAPP1-mRFP
Rab11-YFP
255min pi
260 min pi
265min pi
270min pi
C
Pearson Corr. Coefficient
(Rab11 and FAPP1)
1.0
0.8
0.6
0.4
0.2
0
0
4hr pi
D
CVB3 4hr pi
FAPP1-GFP
Rab7A-mCherry
Rab7A-mCherry
FAPP1-GFP
CVB3 4hr pi
FAPP1-GFP
Rab5A-mRFP
Rab5A-mRFP
FAPP1-GFP
E
α-Rab11 IP
mock
CVB3
PI4KIIIβ
Input
PI4KIIIβ
Rab11
F
3A Rab11
3A
Rab11
**
**
**

Figure 17. Viral Protein 3A Recruits and Targets Free Cholesterol-Rich Rab11 Recycling Endosomes to Viral Replication Organelles

A. Viral replication organelles were found to be actively recruiting Rab11 endosomes. Confocal time-lapse images of HeLa cells cotransfected with Rab11-YFP and FAPP1-mRFP (VRO marker), then infected with CVB. Scale bar is 5 mm.

B. Image gallery of fusion events between Rab11-YFP recycling endosomes with replication organelles, boxed region in A, at 3.5hr pi. Scale bar, 1 mm. Time lapsed 15 minutes.

C. Quantification of Rab11 colocalization with FAPP1-labeled replication organelles shows a significant increase at peak replication. Mean Pearson correlation coefficients ± SEM are plotted (n = 5 cells for each time point).

D. Rab5 (early endosomes) and Rab7 (late endosomes) are not colocalization with replication organelles at peak CVB replication. Scale bar is 10μm.

E. Association between PI4KIIIβ with Rab11 in CVB infected cells at peak replication is enhanced. Protein levels were measured from lysates by immunoprecipitation of Rab11 in CVB infected cells followed by western blot analysis of PI4KIIIβ.

F. Ectopic expression of viral protein 3A (red) recruits Rab11 (green) to 3A-containing membranes. Hela cells were transfected with enteroviral protein 3A, fixed, and immunolabeled with antibodies against viral 3A and Rab11. Scale bar, 5μm.

CHAPTER 8

Discussion And Future Aims

DISCUSSION:

The work presented in this thesis shows that CME is exploited by enteroviruses to enrich intracellular free cholesterol pools and subsequently traffic cholesterol to replication organelles where cholesterol modulates proteolytic processing of viral protein $3CD^{pro}$ and facilitates viral RNA synthesis. Furthermore, we found that enteroviral replication can be stimulated in cells with high free cholesterol pools and functional CME pathway. On the other hand, replication is inhibited when CME is disrupted. Upon disruption, the CME machinery is not only unavailable to traffic cholesterol to replication organelles, but plasma membrane free cholesterol pools are instead trafficked to lipid droplets for storage. Finally, enteroviruses further enhance internal free cholesterol pools by inhibiting endosomal recycling to facilitate the cholesterol enrichment of recycling endosomes to be recruited and trafficked to replication organelles.

Based on these findings, we propose the following model for the role of CME and endosomal recycling in regulating enteroviral replication. Early in infection, there is a net increase in cholesterol internalization through clathrin-mediated endocytosis (that is, LDL-cholesterol, NPC1L1-cholesterol, plasma membrane free cholesterol). This net increase is potentially modulated through the expression of newly synthesized viral 2BC proteins. A large fraction is then

transported to recycling endosomes, while the remainder to the ER through alternative pathways, leading to a decrease in cholesterol biosynthesis. Furthermore, this decrease in biosynthesis may be intensified by the gradual absorption of cholesterol-rich Golgi membranes into the ER, as a result of enteroviral 3A protein interference with coatomer recruitment (Hsu et al. 2010; Wessels et al. 2006).

By peak replication times (Figure 18A), replication organelles have emerged from ER exit sites. This event removes cholesterol from the ER, triggering once again cholesterol biosynthesis. Notably, cholesterol storage, through a yet unknown mechanism, is virally inhibited throughout infection, enhancing cellular free cholesterol pools even more. Meanwhile, inhibition of cellular recycling promotes cholesterol enrichment of Rab11 recycling endosomes (Figure 18D) that are recruited by viral 3A proteins to viral replication organelles; Rab11 recycling endosomes along with PI4KIIIβ enrich these organelles with both free cholesterol and PI4P lipids, facilitating viral polyprotein processing and RNA synthesis. Inhibiting cellular recycling and targeting recycling endosomes to viral replication organelles also prevents endocytosed cholesterol and plasma membrane proteins such as LDL receptor and MHC, from going back to the cell surface. Preventing LDL receptor recycling may explain the decrease in uptake at peak replication, while trapping MHC may contribute to evasion of the immune system (Deitz et al. 2000; Cornell et al. 2006).

When cellular free cholesterol is in excess, cells maintain homeostasis by esterifying and storing some of the plasma membrane free cholesterol in lipid droplets (Lange et al. 1993; Ikonen 2008). We found that free cholesterol esterification and storage was enhanced when CME and endosomal recycling was disrupted (Figure 18B). While the mechanism was not identified, CME and endosomal recycling perturbation may trigger trafficking of free cholesterol to the ER by clathrin independent vesicular or non-vesicular pathways such as direct exchange through ER-PM contact sites or ORP carriers (English and Voeltz 2013; Jansen et al. 2011). The increase in esterification activity and the physical proximity between the ER with the PM and endosomes suggest that free cholesterol is transferred first to the ER prior to storage, although some fraction of sterol may also be transferred directly to the lipid droplets.

We found that disrupting CME and endosomal recycling machinery had a negative impact on enteroviral replication. This disruption not only resulted in PM free cholesterol pools being stored but also prevented enteroviruses from harnessing the CME and endosomal recycling machinery to traffic these pools to replication organelles. On the other hand, in caveolin-depleted cells, as well as in NPC diseased cells, the presence of functional CME machinery and ample free cholesterol pools generated an ideal environment for enteroviral replication (Figure 18C). Although, in NPC cells intracellular cholesterol trafficking from the late endosomal stores to the PM occurs at a normal rate (Lange et al. 2002), the reduction in cholesterol movement to the ER, a primary defect in NPC, may make more PM sterol available for the viral replication machinery.

For the majority of the siRNAs tested, their impact on CVB3 and PV1 replication was of similar magnitude, and small differences observed were potentially a consequence of differences in replication kinetics, which may provide opportunity for cells to mount antiviral responses, which, combined with CME loss, can result in stronger inhibition of the slower replication virus. However, the impact of depletion DAB2, an adaptor for LDL-receptor, was significantly greater on CVB3 than on PV1, suggesting a larger dependence of CVB3 on LDL to enhance cellular free cholesterol pools.

Our data also revealed that by trafficking cholesterol to PI4P-rich replication organelle membranes, enteroviruses might be able to regulate the levels of $3CD^{pro}$ proteins. Cholesterol domains help partition and organize lipids and transmembrane proteins within membrane bilayers (Simons and Sampaio 2011; Lippincott-Schwartz and Phair 2010; Bretscher and Munro 1993). Replication complex components ($3CD^{pro}$, $3C^{pro}$, and $3D^{pol}$) all localize to PI4P lipid-specific binding domains (Hsu et al. 2010). PI4P-enriched membranes can be highly fluid (Zhendre et al. 2011), which may prevent viral proteins from assembling on them. Cholesterol can counter this fluidity, by stabilizing the replication membranes, and thereby may facilitate both replication complex assembly and positioning of $3CD^{pro}$ in a specific conformation such that autocatalytic processing will be attenuated.

Our findings here may also have implications for understanding the pathogenesis of enteroviral infections. The cells of the human gastrointestinal tract serve as initial replication sites for many enteroviruses before dissemination

to the rest of the body (Bopegamage et al. 2005; Iwasaki et al. 2002). These polarized cells are specialized for maximum absorption of dietary cholesterol and express high levels of NPC1L1 at the PM (Jia et al. 2011). Gastrointestinal cells would be ideal for enteroviral replication because due to their high cholesterol absorption quality along with a functional CME and cellular recycling machinery, including Rab11 recycling endosomes, these can traffic both apical and basolateral plasma membrane cholesterol pools (Maxfield and Wüstner 2002). Furthermore, mice made hypercholesterolemic by diet develop infections with high enteroviral loads, but whether this is due to compromised antiviral responses or enhanced replication remains to be investigated (Campbell et al. 1982).

Finally, cholesterol is a highly abundant critical component of the central and peripheral nervous systems (Chang et al. 2010; Karasinska and Hayden 2011). In Alzheimer's disease (AD) and Huntington disease (HD), disruptions of CME, endocytic recycling, and cholesterol homeostasis have been frequently reported, including a significant increase in the number of neuronal lipid droplets containing esterified cholesterol (Area-Gomez et al. 2012; Li and DiFiglia 2012; Martinez-Vicente et al. 2010; Chang et al. 2010; Cataldo et al. 2000). Huntingtin protein, the primary causative agent for HD, interacts with HIP1 and clathrin (Velier et al. 1998), and mutant huntingtin expression alone can disrupt cholesterol homeostasis (Trushina et al. 2006). The loss of Rab11 function and localization has also been linked to AD and HD, where disruption of the transport of recycling endosome to the plasma membrane contributes to neural

degeneration (Li et al. 2009). Similarly, in AD, amyloid β were shown to cause CME defects (Treusch et al. 2011), and cholesterol esterification, the latter a hallmark of familial AD (Area-Gomez et al. 2012; Chang et al. 2010). Indeed, blocking cholesterol esterification alleviates AD symptoms and reduces amyloid plaque formation (Bryleva et al. 2012). Our findings here coupling the disruption of CME and endocytic recycling with accumulation of esterified cholesterol may provide insight and therapeutic strategies for these neurological conditions. At any rate, whenever CME or endocytic recycling components are perturbed, the impact on cholesterol homeostasis should be given consideration when interpreting experimental results.

In summary, our results identify a wider role of host endocytic proteins in shaping the cellular cholesterol landscape and impacting the viral life cycle beyond attachment, entry and export. These findings may provide new panviral therapeutic strategies for treating enteroviral infections including blocking cholesterol uptake or biosynthesis, stimulating cholesterol storage, and preventing cholesterol from being trafficked to replication organelles by disrupting the viral recruitment of Rab11 proteins.

FUTURE AIMS:

This research project has various questions that have grabbed my interest and that I want to continue investigating. Associations between proteins can facilitate the transfer of factors necessary to build a stable structure or function. In this case, free cholesterol is needed in the VROs for viral protein processing. As previously mentioned, during viral infection there is an increase in the

association between Rab11 and PI4KIIβ; therefore, first I want to Identify if the association between Rab11A and PI4KIIIβ is involved in the targeting of the cholesterol to the viral replication organelles. A recent publication describes the crystal structure of the association interface between Rab11A and PI4KIIβ. The crystal structure details the target amino acids involved in this interaction (Burke, et al. 2014).

In our preliminary data, we used the information provided by the crystal structure to make site directed mutagenesis to make single and double point mutations to specific amino acids in the Rab11A sequence; we did not use the sequence from PI4KIIIβ for any mutations because the product of its activity, PI4P lipid, is necessary for viral replication (Hsu et al. 2010). The mutations were targeted to inhibit the binding between Rab11A and PI4KIIIβ, without modifying their function. We selected from the Rab11A WT sequence Histidine 130 and Leucine 131 and mutated either one or both of the amino acids into Alanine (SM130, SM131, and DM130/131).

Upon immunoprecipitation analysis of PI4KIIIβ, the association between Rab11 and PI4KIIIβ was lost in the single and double mutants (Figure 19A). We further checked the levels of endogenous association between Rab11A and PI4KIIIβ in the presence of the mutant constructs, and found that native association was highly inhibited in the double mutant (Figure 19A), while PI4KIIIβ was present in the sample. Although the Rab11 double mutant (Rab11A-DM) was not binding to and had a dominant negative effect on the endogenous association with PI4KIIIβ, during CVB infection the Rab11 double mutant was

unstable and degraded overtime (Figure 19C). The reason for the instability and degradation of the double mutant might be because during CVB infection the host protein transcription machinery is shutdown after 2hr post infection (Flint et al. 2009; Cameron et al. 2011; Krausslich et al. 1987) leading to the degradation of the existing pool of Rab11A-DM while the levels in the control culture are maintained because new protein is being made replacing the degraded pool; therefore the protein is maintained at a steady level. The instability of the double mutant renders this protein not useful in our studies. Finally, to overcome this obstacle, we can create new mutations at different sites to see if this stabilizes the protein while maintaining its inability to bind PI4KIIIβ during viral infection. If a successful mutant protein is produced, I expect to see a decrease in the levels of free cholesterol at the VROs; further more, the decrease in cholesterol levels at VROs should increase the processing of $3CD^{pro}$ resulting in a the inhibition of viral replication.

We also want to investigate how, during enteroviral infection, free cholesterol is transferred to the viral replication organelles. One group of host proteins potentially involved in this process is the lipid transfer proteins such as the oxysterol-binding protein (OSBP) and OSBP-related proteins (ORPs). A recent study linked OSBP as being a potential target for transferring cholesterol to the VROs; by treating cells with Itraconazole (an antifungal drug with potential antienteroviral activity) they were able to inhibit enteroviral replication and identified OSBP as the target for this drug (Strating et al, 2015).

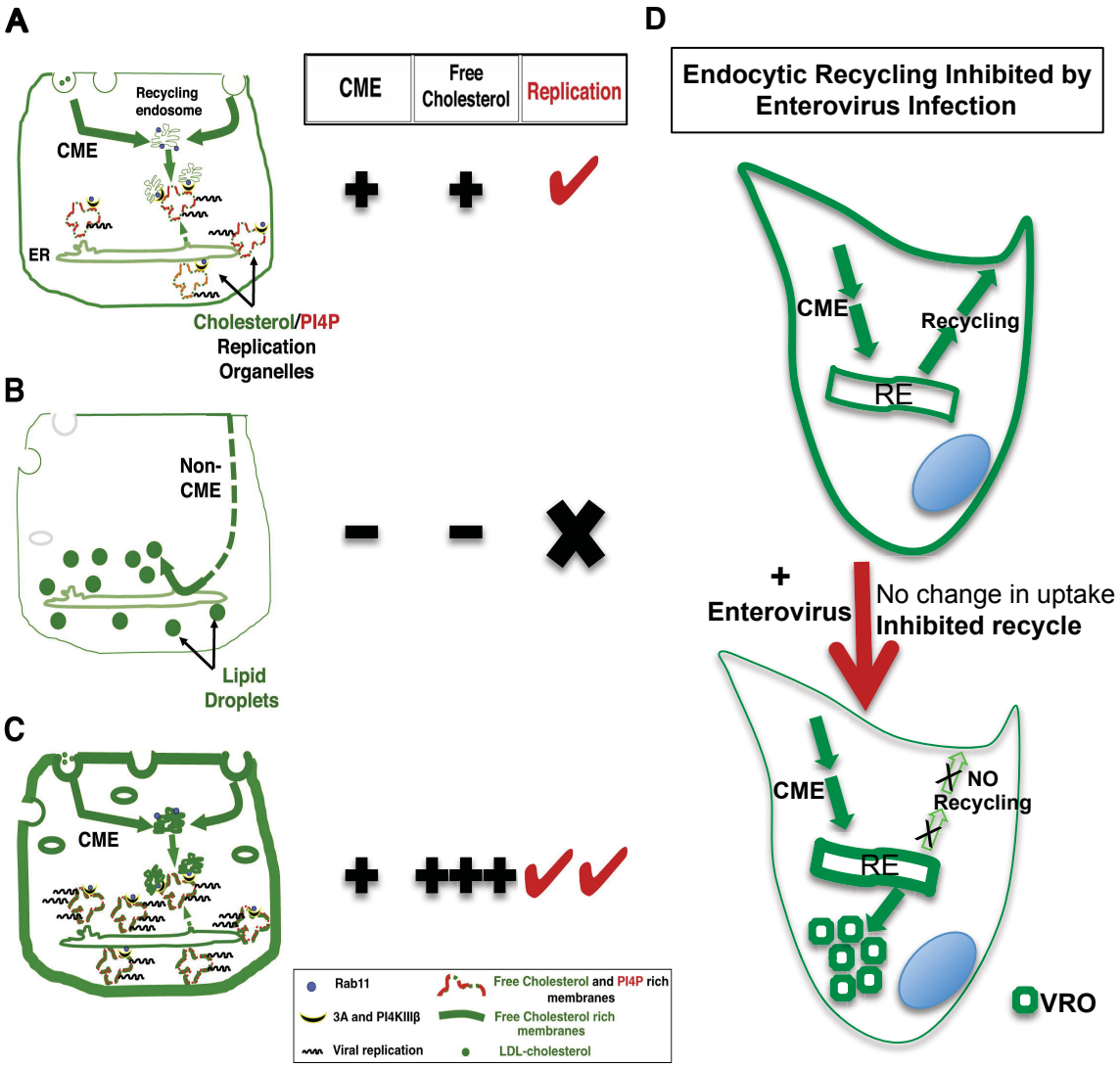
A
Recycling endosome
CME
ER
Cholesterol/PI4P
Replication
Organelles
CME
Free Cholesterol
Replication
+
+
✔
B
Non-CME
Lipid Droplets
-
-
✘
C
CME
+
+++
✔✔
Rab11
3A and PI4KIIIβ
Viral replication
Free Cholesterol and PI4P rich membranes
Free Cholesterol rich membranes
LDL-cholesterol
D
Endocytic Recycling Inhibited by Enterovirus Infection
CME
Recycling
RE
+
Enterovirus
No change in uptake
Inhibited recycle
CME
NO Recycling
RE
VRO

Figure 18. Model for Cholesterol Redistribution and Dynamics During Enteroviral Infection

A. Upon infection, viral proteins (e.g., 2BC) modulate CME to enhance the net uptake of PM and extracellular cholesterol pools. Internalized cholesterol is pooled in Rab11 recycling endosomes and targeted to PI4P-enriched replication organelles via protein-protein interactions among viral 3A, Rab11, and PI4KIIIβ proteins. Additionally, some endocytosed cholesterol is transferred to the replication organelles indirectly, through the ER, as the organelles emerge from ER exit sites.

B. Enteroviral replication is inhibited when CME is disrupted and cholesterol cannot be internalized/transported to replication organelles. PM free cholesterol pools are instead trafficked by alternate pathways to lipid droplets for storage.

C. Enteroviral replication is stimulated in cells with functional CME/Endosomal Recycling; and with high free cholesterol pools at the PM and endosomal compartments (e.g., NPC diseased cells and Cav1 or Cav2 depleted HeLa cells).

D. Enteroviral infection triggers the shut down of host cellular recycling within the first 4 hours of infection therefore inhibiting the recycle of cholesterol back to the plasma membrane and facilitating the enrichment of free plasma membrane cholesterol in recycling endosomes to be later recruited to viral replication organelles by viral protein 3A.

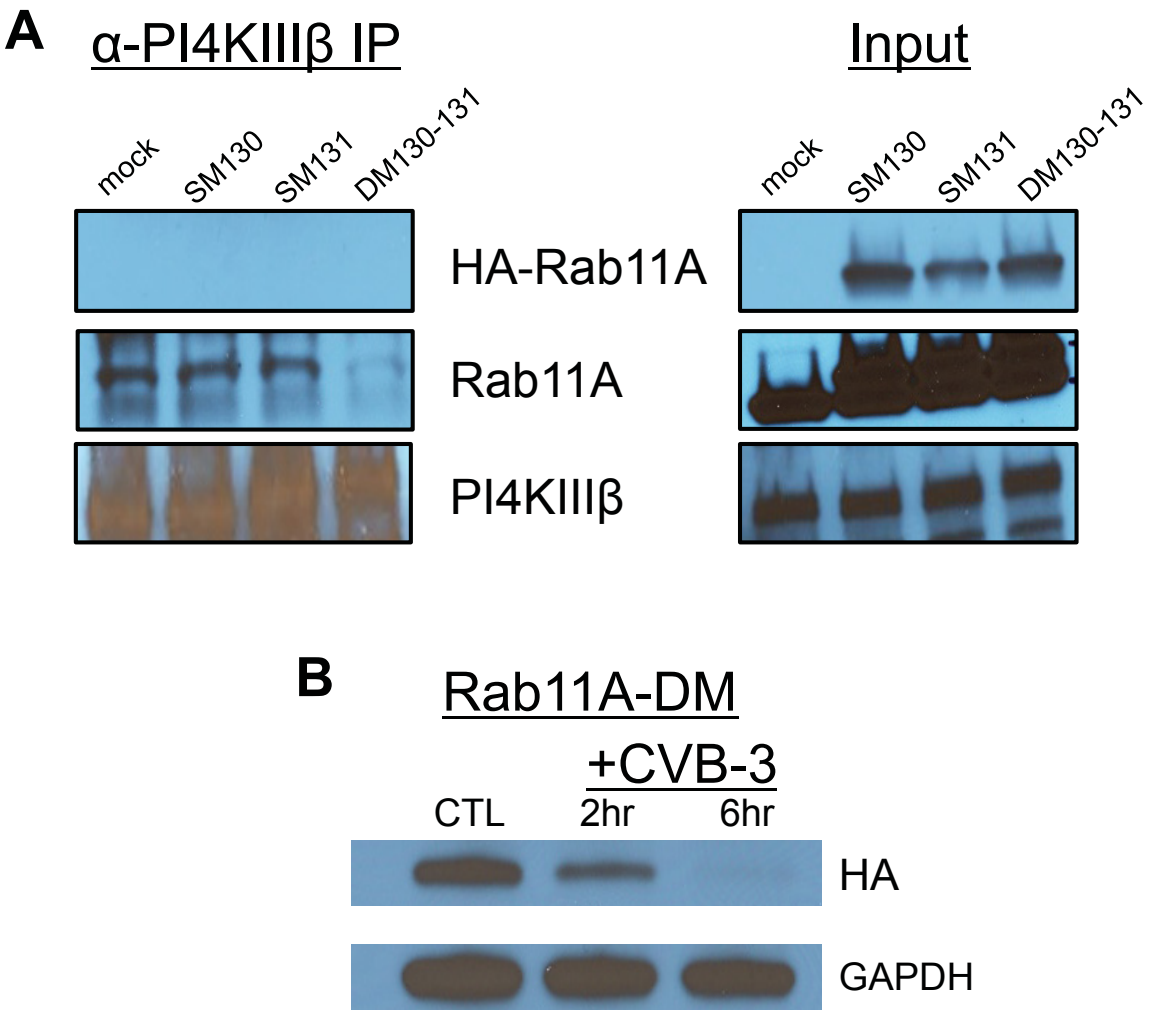
A
α-PI4KIIIβ IP
Input
mock
SM130
SM131
DM130-131
HA-Rab11A
Rab11A
PI4KIIIβ
B
Rab11A-DM
+CVB-3
CTL
2hr
6hr
HA
GAPDH

Figure 19. Mutant Rab11 Constructs

A. Mutant constructs analysis: Top left band shows that the association between the mutant constructs and PI4KIIIβ was lost. Middle left band shows endogenous Rab11A level was lowered in the presence of the DM130-131 mutant construct showing that PI4KIIIβ was not associating with Rab11A therefore having a dominant negative effect with the endogenous association. Lower left band shows PI4KIIIβ was successfully precipitated in the sample. Right bands shows that all 3 proteins (HA-Rab11A mutants, Rab11A, and PI4KIIIβ) were present in the lysate.

B. Infected samples: Top band shows Rab11A-DM (DM130-131) is being degraded overtime during infection, while the total protein levels are not affected, lower band.

BIBLIOGRAPHY

Alberts, A. W. (1988). Discovery, biochemistry and biology of lovastatin. *Am J Cardiol, 62*(15), 10J-15J.

Alberts, B., Johnson, A., Lewis, J., Raff, M., Roberts, K., & Walter, P. (2002). *Molecular Biology of the Cell* (4th ed.). New York: Garland Science.

Altan-Bonnet, N., Sougrat, R., & Lippincott-Schwartz, J. (2004). Molecular basis for Golgi maintenance and biogenesis. *Curr Opin Cell Biol, 16*(4), 364-372. doi: 10.1016/j.ceb.2004.06.011

Andino, R., Rieckhof, G. E., & Baltimore, D. (1990). A functional ribonucleoprotein complex forms around the 5' end of poliovirus RNA. *Cell, 63*(2), 369-380.

Area-Gomez, E., Del Carmen Lara Castillo, M., Tambini, M. D., Guardia-Laguarta, C., de Groof, A. J., Madra, M., . . . Schon, E. A. (2012). Upregulated function of mitochondria-associated ER membranes in Alzheimer disease. *EMBO J, 31*(21), 4106-4123. doi: 10.1038/emboj.2012.202

Basavappa, R., Syed, R., Flore, O., Icenogle, J. P., Filman, D. J., & Hogle, J. M. (1994). Role and mechanism of the maturation cleavage of VP0 in poliovirus assembly: structure of the empty capsid assembly intermediate at 2.9 A resolution. *Protein Sci, 3*(10), 1651-1669. doi: 10.1002/pro.5560031005

Belov, G. A., Altan-Bonnet, N., Kovtunovych, G., Jackson, C. L., Lippincott-Schwartz, J., & Ehrenfeld, E. (2007). Hijacking components of the cellular secretory pathway for replication of poliovirus RNA. *J Virol, 81*(2), 558-567. doi: 10.1128/JVI.01820-06

Belov, G. A., Nair, V., Hansen, B. T., Hoyt, F. H., Fischer, E. R., & Ehrenfeld, E. (2012). Complex dynamic development of poliovirus membranous replication complexes. *J Virol, 86*(1), 302-312. doi: 10.1128/JVI.05937-11

Bergelson, J. M., Cunningham, J. A., Droguett, G., Kurt-Jones, E. A., Krithivas, A., Hong, J. S., . . . Finberg, R. W. (1997). Isolation of a common receptor for Coxsackie B viruses and adenoviruses 2 and 5. *Science, 275*(5304), 1320-1323.

Bolte, S., & Cordelieres, F. P. (2006). A guided tour into subcellular colocalization analysis in light microscopy. *J Microsc, 224*(Pt 3), 213-232. doi: 10.1111/j.1365-2818.2006.01706.x

Bopegamage, S., Kovacova, J., Vargova, A., Motusova, J., Petrovicova, A., Benkovicova, M., . . . Galama, J. M. (2005). Coxsackie B virus infection of mice: inoculation by the oral route protects the pancreas from damage, but not from infection. *J Gen Virol, 86*(Pt 12), 3271-3280. doi: 10.1099/vir.0.81249-0

Bretscher, M. S., & Munro, S. (1993). Cholesterol and the Golgi apparatus. *Science, 261*(5126), 1280-1281.

Bryleva, E. Y., Rogers, M. A., Chang, C. C., Buen, F., Harris, B. T., Rousselet, E., . . . Chang, T. Y. (2010). ACAT1 gene ablation increases 24(S)-hydroxycholesterol content in the brain and ameliorates amyloid pathology in mice with AD. *Proc Natl Acad Sci U S A, 107*(7), 3081-3086. doi:

10.1073/pnas.0913828107
Burke, J. E., Inglis, A. J., Perisic, O., Masson, G. R., McLaughlin, S. H., Rutaganira, F., . . . Williams, R. L. (2014). Structures of PI4KIIIbeta complexes show simultaneous recruitment of Rab11 and its effectors. *Science, 344*(6187), 1035-1038. doi: 10.1126/science.1253397
Cameron, C. E., Oh, H. S., & Moustafa, I. M. (2010). Expanding knowledge of P3 proteins in the poliovirus lifecycle. *Future Microbiol, 5*(6), 867-881. doi: 10.2217/fmb.10.40
Campbell, A. E., Loria, R. M., Madge, G. E., & Kaplan, A. M. (1982). Dietary hepatic cholesterol elevation: effects on coxsackievirus B infection and inflammation. *Infect Immun, 37*(1), 307-317.
Cataldo, A. M., Peterhoff, C. M., Troncoso, J. C., Gomez-Isla, T., Hyman, B. T., & Nixon, R. A. (2000). Endocytic pathway abnormalities precede amyloid beta deposition in sporadic Alzheimer's disease and Down syndrome: differential effects of APOE genotype and presenilin mutations. *Am J Pathol, 157*(1), 277-286.
CDC, Centers for Disease Control and Prevention. (2015). Enterovirus D68 in the United States, 2014. *Non-Polio Enterovirus.* Retrieved Jan. 15, 2015, from http://www.cdc.gov/non-polio-enterovirus/outbreaks/ev-d68-outbreaks.html
CDC, Centers for Disease Control and Prevention. (2015). Overview. *Non-Polio Enterovirus.* Retrieved Jan. 15, 2015, from http://www.cdc.gov/non-polio-enterovirus/about/overview.html
Chang, T. Y., & Chang, C. (2008). Ezetimibe blocks internalization of the NPC1L1/cholesterol complex. *Cell Metab, 7*(6), 469-471. doi: 10.1016/j.cmet.2008.05.001
Chang, T. Y., Chang, C. C., Bryleva, E., Rogers, M. A., & Murphy, S. R. (2010). Neuronal cholesterol esterification by ACAT1 in Alzheimer's disease. *IUBMB Life, 62*(4), 261-267. doi: 10.1002/iub.305
Cherfils, J., & Zeghouf, M. (2013). Regulation of small GTPases by GEFs, GAPs, and GDIs. *Physiol Rev, 93*(1), 269-309. doi: 10.1152/physrev.00003.2012
Cho, M. W., Teterina, N., Egger, D., Bienz, K., & Ehrenfeld, E. (1994). Membrane rearrangement and vesicle induction by recombinant poliovirus 2C and 2BC in human cells. *Virology, 202*(1), 129-145. doi: 10.1006/viro.1994.1329
Christian, A. E., Haynes, M. P., Phillips, M. C., & Rothblat, G. H. (1997). Use of cyclodextrins for manipulating cellular cholesterol content. *J Lipid Res, 38*(11), 2264-2272.
Cornell, C. T., Kiosses, W. B., Harkins, S., & Whitton, J. L. (2006). Inhibition of protein trafficking by coxsackievirus b3: multiple viral proteins target a single organelle. *J Virol, 80*(13), 6637-6647. doi: 10.1128/JVI.02572-05
Cornell, C. T., Kiosses, W. B., Harkins, S., & Whitton, J. L. (2007). Coxsackievirus B3 proteins directionally complement each other to downregulate surface major histocompatibility complex class I. *J Virol, 81*(13), 6785-6797. doi: 10.1128/JVI.00198-07
Cornell, C. T., & Semler, B. L. (2002). Subdomain specific functions of the RNA polymerase region of poliovirus 3CD polypeptide. *Virology, 298*(2), 200-213.

Deitz, S. B., Dodd, D. A., Cooper, S., Parham, P., & Kirkegaard, K. (2000). MHC I-dependent antigen presentation is inhibited by poliovirus protein 3A. *Proc Natl Acad Sci U S A, 97*(25), 13790-13795. doi: 10.1073/pnas.250483097

Deligeorgiev, T., Vasilev, A., Kaloyanova, S., & Vaquero, J. J. (2010). Styryl dyes - synthesis and applications during the last 15 years. *Coloration Technology, 126*(2), 55-80. doi: Doi 10.1111/J.1478-4408.2010.00235.X

Denison, M. R. (2008). Seeking membranes: positive-strand RNA virus replication complexes. *PLoS Biol, 6*(10), e270. doi: 10.1371/journal.pbio.0060270

DeStefano, J. J., & Titilope, O. (2006). Poliovirus protein 3AB displays nucleic acid chaperone and helix-destabilizing activities. *J Virol, 80*(4), 1662-1671. doi: 10.1128/JVI.80.4.1662-1671.2006

Dutta, D., & Donaldson, J. G. (2012). Search for inhibitors of endocytosis: Intended specificity and unintended consequences. *Cell Logist, 2*(4), 203-208. doi: 10.4161/cl.23967

English, A. R., & Voeltz, G. K. (2013). Endoplasmic reticulum structure and interconnections with other organelles. *Cold Spring Harb Perspect Biol, 5*(4), a013227. doi: 10.1101/cshperspect.a013227

Faleck, D. M., Ali, K., Roat, R., Graham, M. J., Crooke, R. M., Battisti, R., . . . Imai, Y. (2010). Adipose differentiation-related protein regulates lipids and insulin in pancreatic islets. *Am J Physiol Endocrinol Metab, 299*(2), E249-257. doi: 10.1152/ajpendo.00646.2009

Fauquet, C. M, Mayo, M. A., Maniloff, J., Desselberger, U., & Ball, L. A. (2005). *Virus Taxonomy: VIIIth Report of the International Commettee on Taxonomy of Viruses*. San Diego, CA: Elsevier Academic Press, Inc.

Flint, S. J., Enquist, L. W., Racaniello, V. R., & Skalka, A. M. (2009). *Principles of Virology: I Molecular Biology* (Vol. 1). Washington, DC: ASM Press.

Garcia-Mata, R., & Sztul, E. (2003). The membrane-tethering protein p115 interacts with GBF1, an ARF guanine-nucleotide-exchange factor. *EMBO Rep, 4*(3), 320-325. doi: 10.1038/sj.embor.embor762

Giachetti, C., & Semler, B. L. (1991). Role of a viral membrane polypeptide in strand-specific initiation of poliovirus RNA synthesis. *J Virol, 65*(5), 2647-2654.

Godi, A., Di Campli, A., Konstantakopoulos, A., Di Tullio, G., Alessi, D. R., Kular, G. S., . . . De Matteis, M. A. (2004). FAPPs control Golgi-to-cell-surface membrane traffic by binding to ARF and PtdIns(4)P. *Nat Cell Biol, 6*(5), 393-404. doi: 10.1038/ncb1119

Godi, A., Pertile, P., Meyers, R., Marra, P., Di Tullio, G., Iurisci, C., . . . De Matteis, M. A. (1999). ARF mediates recruitment of PtdIns-4-OH kinase-beta and stimulates synthesis of PtdIns(4,5)P2 on the Golgi complex. *Nat Cell Biol, 1*(5), 280-287. doi: 10.1038/12993

Goldstein, J. L., & Brown, M. S. (1990). Regulation of the mevalonate pathway. *Nature, 343*(6257), 425-430. doi: 10.1038/343425a0

Goodfellow, I. G., Kerrigan, D., & Evans, D. J. (2003). Structure and function analysis of the poliovirus cis-acting replication element (CRE). *RNA, 9*(1), 124-137.

Greenspan, P., & Fowler, S. D. (1985). Spectrofluorometric studies of the lipid probe, nile red. *J Lipid Res, 26*(7), 781-789.

Greenspan, P., Mayer, E. P., & Fowler, S. D. (1985). Nile red: a selective fluorescent stain for intracellular lipid droplets. *J Cell Biol, 100*(3), 965-973.

Greninger, A. L., Knudsen, G. M., Betegon, M., Burlingame, A. L., & Derisi, J. L. (2012). The 3A protein from multiple picornaviruses utilizes the golgi adaptor protein ACBD3 to recruit PI4KIIIbeta. *J Virol, 86*(7), 3605-3616. doi: 10.1128/JVI.06778-11

Gustafsson, M. G., Shao, L., Carlton, P. M., Wang, C. J., Golubovskaya, I. N., Cande, W. Z., . . . Sedat, J. W. (2008). Three-dimensional resolution doubling in wide-field fluorescence microscopy by structured illumination. *Biophys J, 94*(12), 4957-4970. doi: 10.1529/biophysj.107.120345

He, Y., Mueller, S., Chipman, P. R., Bator, C. M., Peng, X., Bowman, V. D., . . . Rossmann, M. G. (2003). Complexes of poliovirus serotypes with their common cellular receptor, CD155. *J Virol, 77*(8), 4827-4835.

Herold, J., & Andino, R. (2001). Poliovirus RNA replication requires genome circularization through a protein-protein bridge. *Mol Cell, 7*(3), 581-591.

Holland, J. J., Mc, Laren Lc, Hoyer, B. H., & Syverton, J. T. (1960). Enteroviral ribonucleic acid. II. Biological, physical, and chemical studies. *J Exp Med, 112*, 841-864.

Holtta-Vuori, M., Uronen, R. L., Repakova, J., Salonen, E., Vattulainen, I., Panula, P., . . . Ikonen, E. (2008). BODIPY-cholesterol: a new tool to visualize sterol trafficking in living cells and organisms. *Traffic, 9*(11), 1839-1849. doi: 10.1111/j.1600-0854.2008.00801.x

Hsieh, K., Lee, Y. K., Londos, C., Raaka, B. M., Dalen, K. T., & Kimmel, A. R. (2012). Perilipin family members preferentially sequester to either triacylglycerol-specific or cholesteryl-ester-specific intracellular lipid storage droplets. *J Cell Sci, 125*(Pt 17), 4067-4076. doi: 10.1242/jcs.104943

Hsu, N. Y., Ilnytska, O., Belov, G., Santiana, M., Chen, Y. H., Takvorian, P. M., . . . Altan-Bonnet, N. (2010). Viral reorganization of the secretory pathway generates distinct organelles for RNA replication. *Cell, 141*(5), 799-811. doi: 10.1016/j.cell.2010.03.050

Hsu, V. W., Bai, M., & Li, J. (2012). Getting active: protein sorting in endocytic recycling. *Nat Rev Mol Cell Biol, 13*(5), 323-328. doi: 10.1038/nrm3332

Ikonen, E. (2008). Cellular cholesterol trafficking and compartmentalization. *Nat Rev Mol Cell Biol, 9*(2), 125-138. doi: 10.1038/nrm2336

Ilnytska, O., Santiana, M., Hsu, N. Y., Du, W. L., Chen, Y. H., Viktorova, E. G., . . . Altan-Bonnet, N. (2013). Enteroviruses harness the cellular endocytic machinery to remodel the host cell cholesterol landscape for effective viral replication. *Cell Host Microbe, 14*(3), 281-293. doi: 10.1016/j.chom.2013.08.002

Iwasaki, A., Welker, R., Mueller, S., Linehan, M., Nomoto, A., & Wimmer, E. (2002). Immunofluorescence analysis of poliovirus receptor expression in Peyer's patches of humans, primates, and CD155 transgenic mice: implications for poliovirus infection. *J Infect Dis, 186*(5), 585-592. doi:

10.1086/342682
Jansen, M., Ohsaki, Y., Rita Rega, L., Bittman, R., Olkkonen, V. M., & Ikonen, E. (2011). Role of ORPs in sterol transport from plasma membrane to ER and lipid droplets in mammalian cells. *Traffic, 12*(2), 218-231. doi: 10.1111/j.1600-0854.2010.01142.x
Jeong, H. J., Lee, H. S., Kim, K. S., Kim, Y. K., Yoon, D., & Park, S. W. (2008). Sterol-dependent regulation of proprotein convertase subtilisin/kexin type 9 expression by sterol-regulatory element binding protein-2. *J Lipid Res, 49*(2), 399-409. doi: 10.1194/jlr.M700443-JLR200
Jia, L., Betters, J. L., & Yu, L. (2011). Niemann-pick C1-like 1 (NPC1L1) protein in intestinal and hepatic cholesterol transport. *Annu Rev Physiol, 73*, 239-259. doi: 10.1146/annurev-physiol-012110-142233
Jubelt, B., & Lipton, H. L. (2014). Enterovirus/picornavirus infections. *Handb Clin Neurol, 123*, 379-416. doi: 10.1016/B978-0-444-53488-0.00018-3
Karasinska, J. M., & Hayden, M. R. (2011). Cholesterol metabolism in Huntington disease. *Nat Rev Neurol, 7*(10), 561-572. doi: 10.1038/nrneurol.2011.132
Kawamoto, K., Yoshida, Y., Tamaki, H., Torii, S., Shinotsuka, C., Yamashina, S., & Nakayama, K. (2002). GBF1, a guanine nucleotide exchange factor for ADP-ribosylation factors, is localized to the cis-Golgi and involved in membrane association of the COPI coat. *Traffic, 3*(7), 483-495.
Kirchhausen, T., Macia, E., & Pelish, H. E. (2008). Use of dynasore, the small molecule inhibitor of dynamin, in the regulation of endocytosis. *Methods Enzymol, 438*, 77-93. doi: 10.1016/S0076-6879(07)38006-3
Kitamura, N., Semler, B. L., Rothberg, P. G., Larsen, G. R., Adler, C. J., Dorner, A. J., . . . Wimmer, E. (1981). Primary structure, gene organization and polypeptide expression of poliovirus RNA. *Nature, 291*(5816), 547-553.
Krausslich, H. G., Nicklin, M. J., Toyoda, H., Etchison, D., & Wimmer, E. (1987). Poliovirus proteinase 2A induces cleavage of eucaryotic initiation factor 4F polypeptide p220. *J Virol, 61*(9), 2711-2718.
Lange, Y. (1991). Disposition of intracellular cholesterol in human fibroblasts. *J Lipid Res, 32*(2), 329-339.
Lange, Y., Strebel, F., & Steck, T. L. (1993). Role of the plasma membrane in cholesterol esterification in rat hepatoma cells. *J Biol Chem, 268*(19), 13838-13843.
Lange, Y., Ye, J., Rigney, M., & Steck, T. L. (2002). Dynamics of lysosomal cholesterol in Niemann-Pick type C and normal human fibroblasts. *J Lipid Res, 43*(2), 198-204.
Lanke, K. H., van der Schaar, H. M., Belov, G. A., Feng, Q., Duijsings, D., Jackson, C. L., . . . van Kuppeveld, F. J. (2009). GBF1, a guanine nucleotide exchange factor for Arf, is crucial for coxsackievirus B3 RNA replication. *J Virol, 83*(22), 11940-11949. doi: 10.1128/JVI.01244-09
Lee, Y. F., Nomoto, A., Detjen, B. M., & Wimmer, E. (1977). A protein covalently linked to poliovirus genome RNA. *Proc Natl Acad Sci U S A, 74*(1), 59-63.
Li, X., & DiFiglia, M. (2012). The recycling endosome and its role in neurological disorders. *Prog Neurobiol, 97*(2), 127-141. doi:

10.1016/j.pneurobio.2011.10.002
Li, X., Sapp, E., Chase, K., Comer-Tierney, L. A., Masso, N., Alexander, J., . . . Difiglia, M. (2009). Disruption of Rab11 activity in a knock-in mouse model of Huntington's disease. *Neurobiol Dis, 36*(2), 374-383. doi: 10.1016/j.nbd.2009.08.003
Lippincott-Schwartz, J., & Phair, R. D. (2010). Lipids and cholesterol as regulators of traffic in the endomembrane system. *Annu Rev Biophys, 39*, 559-578. doi: 10.1146/annurev.biophys.093008.131357
Macia, E., Ehrlich, M., Massol, R., Boucrot, E., Brunner, C., & Kirchhausen, T. (2006). Dynasore, a cell-permeable inhibitor of dynamin. *Dev Cell, 10*(6), 839-850. doi: 10.1016/j.devcel.2006.04.002
Mackenzie, J. M., Khromykh, A. A., & Parton, R. G. (2007). Cholesterol manipulation by West Nile virus perturbs the cellular immune response. *Cell Host Microbe, 2*(4), 229-239. doi: 10.1016/j.chom.2007.09.003
Magliano, D., Marshall, J. A., Bowden, D. S., Vardaxis, N., Meanger, J., & Lee, J. Y. (1998). Rubella virus replication complexes are virus-modified lysosomes. *Virology, 240*(1), 57-63. doi: 10.1006/viro.1997.8906
Malcolm, B. A. (1995). The picornaviral 3C proteinases: cysteine nucleophiles in serine proteinase folds. *Protein Sci, 4*(8), 1439-1445. doi: 10.1002/pro.5560040801
Martinez-Vicente, M., Talloczy, Z., Wong, E., Tang, G., Koga, H., Kaushik, S., . . . Cuervo, A. M. (2010). Cargo recognition failure is responsible for inefficient autophagy in Huntington's disease. *Nat Neurosci, 13*(5), 567-576. doi: 10.1038/nn.2528
Maxfield, F. R., & Wustner, D. (2002). Intracellular cholesterol transport. *J Clin Invest, 110*(7), 891-898. doi: 10.1172/JCI16500
Mayor, S., & Pagano, R. E. (2007). Pathways of clathrin-independent endocytosis. *Nat Rev Mol Cell Biol, 8*(8), 603-612. doi: 10.1038/nrm2216
Mayor, S., Parton, R. G., & Donaldson, J. G. (2014). Clathrin-independent pathways of endocytosis. *Cold Spring Harb Perspect Biol, 6*(6). doi: 10.1101/cshperspect.a016758
Mercer, J., Schelhaas, M., & Helenius, A. (2010). Virus entry by endocytosis. *Annu Rev Biochem, 79*, 803-833. doi: 10.1146/annurev-biochem-060208-104626
Merrifield, C. J., & Kaksonen, M. (2014). Endocytic Accessory Factors and Regulation of Clathrin-Mediated Endocytosis. *Cold Spring Harb Perspect Biol, 6*(11). doi: 10.1101/cshperspect.a016733
Merrifield, C. J., Perrais, D., & Zenisek, D. (2005). Coupling between clathrin-coated-pit invagination, cortactin recruitment, and membrane scission observed in live cells. *Cell, 121*(4), 593-606. doi: 10.1016/j.cell.2005.03.015
Miesenbock, G., De Angelis, D. A., & Rothman, J. E. (1998). Visualizing secretion and synaptic transmission with pH-sensitive green fluorescent proteins. *Nature, 394*(6689), 192-195. doi: 10.1038/28190
Miller, S., & Krijnse-Locker, J. (2008). Modification of intracellular membrane structures for virus replication. *Nat Rev Microbiol, 6*(5), 363-374. doi:

10.1038/nrmicro1890
Morimoto, K., Janssen, W. J., Fessler, M. B., McPhillips, K. A., Borges, V. M., Bowler, R. P., . . . Vandivier, R. W. (2006). Lovastatin enhances clearance of apoptotic cells (efferocytosis) with implications for chronic obstructive pulmonary disease. *J Immunol, 176*(12), 7657-7665.
Mueller, S., Wimmer, E., & Cello, J. (2005). Poliovirus and poliomyelitis: a tale of guts, brains, and an accidental event. *Virus Res, 111*(2), 175-193. doi: 10.1016/j.virusres.2005.04.008
Mukherjee, S., Zha, X., Tabas, I., & Maxfield, F. R. (1998). Cholesterol distribution in living cells: fluorescence imaging using dehydroergosterol as a fluorescent cholesterol analog. *Biophys J, 75*(4), 1915-1925. doi: 10.1016/S0006-3495(98)77632-5
Nichols, B. J., Kenworthy, A. K., Polishchuk, R. S., Lodge, R., Roberts, T. H., Hirschberg, K., . . . Lippincott-Schwartz, J. (2001). Rapid cycling of lipid raft markers between the cell surface and Golgi complex. *J Cell Biol, 153*(3), 529-541.
Niu, T. K., Pfeifer, A. C., Lippincott-Schwartz, J., & Jackson, C. L. (2005). Dynamics of GBF1, a Brefeldin A-sensitive Arf1 exchange factor at the Golgi. *Mol Biol Cell, 16*(3), 1213-1222. doi: 10.1091/mbc.E04-07-0599
Novak, J. E., & Kirkegaard, K. (1991). Improved method for detecting poliovirus negative strands used to demonstrate specificity of positive-strand encapsidation and the ratio of positive to negative strands in infected cells. *J Virol, 65*(6), 3384-3387.
Palacios, G., & Oberste, M. S. (2005). Enteroviruses as agents of emerging infectious diseases. *J Neurovirol, 11*(5), 424-433. doi: 10.1080/13550280591002531
Palmenberg, A. C. (1987). Picornaviral processing: some new ideas. *J Cell Biochem, 33*(3), 191-198. doi: 10.1002/jcb.240330306
Palmenberg, A. C. (1990). Proteolytic processing of picornaviral polyprotein. *Annu Rev Microbiol, 44*, 603-623. doi: 10.1146/annurev.mi.44.100190.003131
Parsley, T. B., Towner, J. S., Blyn, L. B., Ehrenfeld, E., & Semler, B. L. (1997). Poly (rC) binding protein 2 forms a ternary complex with the 5'-terminal sequences of poliovirus RNA and the viral 3CD proteinase. *RNA, 3*(10), 1124-1134.
Paul, A. V., Rieder, E., Kim, D. W., van Boom, J. H., & Wimmer, E. (2000). Identification of an RNA hairpin in poliovirus RNA that serves as the primary template in the in vitro uridylylation of VPg. *J Virol, 74*(22), 10359-10370.
Paul, A. V., van Boom, J. H., Filippov, D., & Wimmer, E. (1998). Protein-primed RNA synthesis by purified poliovirus RNA polymerase. *Nature, 393*(6682), 280-284. doi: 10.1038/30529
Pelletier, J., Kaplan, G., Racaniello, V. R., & Sonenberg, N. (1988). Cap-independent translation of poliovirus mRNA is conferred by sequence elements within the 5' noncoding region. *Mol Cell Biol, 8*(3), 1103-1112.
Pelletier, J., & Sonenberg, N. (1988). Internal initiation of translation of eukaryotic mRNA directed by a sequence derived from poliovirus RNA. *Nature,*

334(6180), 320-325. doi: 10.1038/334320a0

Plotch, S. J., & Palant, O. (1995). Poliovirus protein 3AB forms a complex with and stimulates the activity of the viral RNA polymerase, 3Dpol. *J Virol, 69*(11), 7169-7179.

Rawson, R. B. (2003). The SREBP pathway--insights from Insigs and insects. *Nat Rev Mol Cell Biol, 4*(8), 631-640. doi: 10.1038/nrm1174

Rosenbaum, A. I., & Maxfield, F. R. (2011). Niemann-Pick type C disease: molecular mechanisms and potential therapeutic approaches. *J Neurochem, 116*(5), 789-795. doi: 10.1111/j.1471-4159.2010.06976.x

Schlegel, A., Giddings, T. H., Jr., Ladinsky, M. S., & Kirkegaard, K. (1996). Cellular origin and ultrastructure of membranes induced during poliovirus infection. *J Virol, 70*(10), 6576-6588.

Sean, P., & Semler, B. L. (2008). Coxsackievirus B RNA replication: lessons from poliovirus. *Curr Top Microbiol Immunol, 323*, 89-121.

Shen, H., Giordano, F., Wu, Y., Chan, J., Zhu, C., Milosevic, I., . . . De Camilli, P. (2014). Coupling between endocytosis and sphingosine kinase 1 recruitment. *Nat Cell Biol, 16*(7), 652-662. doi: 10.1038/ncb2987

Simons, K., & Sampaio, J. L. (2011). Membrane organization and lipid rafts. *Cold Spring Harb Perspect Biol, 3*(10), a004697. doi: 10.1101/cshperspect.a004697

Strating, J. R., van der Linden, L., Albulescu, L., Bigay, J., Arita, M., Delang, L., . . . van Kuppeveld, F. J. (2015). Itraconazole Inhibits Enterovirus Replication by Targeting the Oxysterol-Binding Protein. *Cell Rep*. doi: 10.1016/j.celrep.2014.12.054

Suhy, D. A., Giddings, T. H., Jr., & Kirkegaard, K. (2000). Remodeling the endoplasmic reticulum by poliovirus infection and by individual viral proteins: an autophagy-like origin for virus-induced vesicles. *J Virol, 74*(19), 8953-8965.

Tebruegge, M., & Curtis, N. (2009). Enterovirus infections in neonates. *Semin Fetal Neonatal Med, 14*(4), 222-227. doi: 10.1016/j.siny.2009.02.002

Tobert, J. A. (2003). Lovastatin and beyond: the history of the HMG-CoA reductase inhibitors. *Nat Rev Drug Discov, 2*(7), 517-526. doi: 10.1038/nrd1112

Treusch, S., Hamamichi, S., Goodman, J. L., Matlack, K. E., Chung, C. Y., Baru, V., . . . Lindquist, S. (2011). Functional links between Abeta toxicity, endocytic trafficking, and Alzheimer's disease risk factors in yeast. *Science, 334*(6060), 1241-1245. doi: 10.1126/science.1213210

Trushina, E., Singh, R. D., Dyer, R. B., Cao, S., Shah, V. H., Parton, R. G., . . . McMurray, C. T. (2006). Mutant huntingtin inhibits clathrin-independent endocytosis and causes accumulation of cholesterol in vitro and in vivo. *Hum Mol Genet, 15*(24), 3578-3591. doi: 10.1093/hmg/ddl434

Velier, J., Kim, M., Schwarz, C., Kim, T. W., Sapp, E., Chase, K., . . . DiFiglia, M. (1998). Wild-type and mutant huntingtins function in vesicle trafficking in the secretory and endocytic pathways. *Exp Neurol, 152*(1), 34-40. doi: 10.1006/exnr.1998.6832

Wandinger-Ness, A., & Zerial, M. (2014). Rab Proteins and the

Compartmentalization of the Endosomal System. *Cold Spring Harb Perspect Biol, 6*(11). doi: 10.1101/cshperspect.a022616

Wang, L. J., & Song, B. L. (2012). Niemann-Pick C1-Like 1 and cholesterol uptake. *Biochim Biophys Acta, 1821*(7), 964-972. doi: 10.1016/j.bbalip.2012.03.004

Wassilak, S. G., Oberste, M. S., Tangermann, R. H., Diop, O. M., Jafari, H. S., & Armstrong, G. L. (2014). Progress toward global interruption of wild poliovirus transmission, 2010-2013, and tackling the challenges to complete eradication. *J Infect Dis, 210 Suppl 1*, S5-15. doi: 10.1093/infdis/jiu456

Weigert, R., & Donaldson, J. G. (2005). Fluorescent microscopy-based assays to study the role of Rab22a in clathrin-independent endocytosis. *Methods Enzymol, 403*, 243-253. doi: 10.1016/S0076-6879(05)03020-X

Wessels, E., Duijsings, D., Niu, T. K., Neumann, S., Oorschot, V. M., de Lange, F., . . . van Kuppeveld, F. J. (2006). A viral protein that blocks Arf1-mediated COP-I assembly by inhibiting the guanine nucleotide exchange factor GBF1. *Dev Cell, 11*(2), 191-201. doi: 10.1016/j.devcel.2006.06.005

Whitton, J. L., Cornell, C. T., & Feuer, R. (2005). Host and virus determinants of picornavirus pathogenesis and tropism. *Nat Rev Microbiol, 3*(10), 765-776. doi: 10.1038/nrmicro1284

Wimmer, E., Hellen, C. U., & Cao, X. (1993). Genetics of poliovirus. *Annu Rev Genet, 27*, 353-436. doi: 10.1146/annurev.ge.27.120193.002033

Zhao, X., Lasell, T. K., & Melancon, P. (2002). Localization of large ADP-ribosylation factor-guanine nucleotide exchange factors to different Golgi compartments: evidence for distinct functions in protein traffic. *Mol Biol Cell, 13*(1), 119-133. doi: 10.1091/mbc.01-08-0420

Zhendre, V., Grelard, A., Garnier-Lhomme, M., Buchoux, S., Larijani, B., & Dufourc, E. J. (2011). Key role of polyphosphoinositides in dynamics of fusogenic nuclear membrane vesicles. *PLoS One, 6*(9), e23859. doi: 10.1371/journal.pone.0023859

CURRICULUM VITAE

MARIANITA SANTIANA
Date of Birth: October 25, 1973
Place of Birth: Quito, Ecuador

EDUCATION:

Rutgers University, Newark, New Jersey
Ph.D. in Biological Sciences, Cellular and Molecular, **Sep. 2011 - Present**
M.S. in Biological Sciences, Cellular and Molecular, **Sep. 2006 - May 2011**
B.A. in Biology, **Sep. 2002 to May 2006**

EXPERIENCE:

NIH-NHLBI, Pre-Doctoral IRTA Fellow **Jul. 2013 - Present**
Develop projects, establish protocols, and perform laboratory procedures under Biosafety Level 2+ conditions to study host-virus interactions in cell lines. Perform imaging of samples using confocal and super resolution microscopes. Prepare reports for presentations and publication manuscripts.

Rutgers University, Nwk., N. J., Department of Biology
Grad. Res. Asst., Host-Pathogen Dynamics Group **Sep. 2010 – Jun. 2013**
Develop projects, establish protocols, and perform laboratory procedures under Biosafety Level 2+ conditions to study the host-pathogen interactions in cell lines. Perform imaging of live and fixed cells using fluorescence and confocal microscopes. Prepare reports for presentations and publication manuscripts.

Teaching Assistant **Sep. 2010 – Jun. 2013**
Prepare lessons, teach, and grade the undergraduate Laboratory Parasitology and Microanatomy of the Cell Courses. Assist professor in proctoring and grading of tests and assignments.

Grad. Res. Asst., Parasitology Laboratory **Sep. 2005 – Aug. 2010**
Developed projects with Microsporidian parasites, performed research experiments using molecular techniques, and prepare reports on the progress of treatment of infections in mammalian cells. Apply various microscopic techniques for the analysis of live and fixed cells in fluorescence microscopes.

PUBLICATIONS:

Santiana, M., Pau, C., Takvorian, P. M., & Cali, A. (2015). Analysis of the Beta-Tubulin Gene and Morphological Changes of the Microsporidium *Anncaliia algerae* both Suggest Albendazole Sensitivity. *J Eukaryot Microbiol, 62*(1), 60-68. doi: 10.1111/jeu.12160

Ilnytska, O., **Santiana, M.**, Hsu, N. Y., Du, W. L., Chen, Y. H., Viktorova, E. G., Altan-Bonnet, N. (2013). Enteroviruses harness the cellular endocytic machinery to remodel the host cell cholesterol landscape for effective viral replication. *Cell Host Microbe, 14*(3), 281-293. doi: 10.1016/j.chom.2013.08.002

Hsu, N. Y., Ilnytska, O., Belov, G., **Santiana, M.**, Chen, Y. H., Takvorian, P. M., Altan-Bonnet, N. (2010). Viral reorganization of the secretory pathway generates distinct organelles for RNA replication. *Cell, 141*(5), 799-811. doi: 10.1016/j.cell.2010.03.050